

---

[All ETDs from UAB](#)

[UAB Theses & Dissertations](#)

---

2019

## **BET Bromodomain Inhibition as an Approach for Treatment of Cholangiocarcinoma**

Samuel Charles Fehling  
*University of Alabama at Birmingham*

Follow this and additional works at: <https://digitalcommons.library.uab.edu/etd-collection>

---

### **Recommended Citation**

Fehling, Samuel Charles, "BET Bromodomain Inhibition as an Approach for Treatment of Cholangiocarcinoma" (2019). *All ETDs from UAB*. 1639.  
<https://digitalcommons.library.uab.edu/etd-collection/1639>

This content has been accepted for inclusion by an authorized administrator of the UAB Digital Commons, and is provided as a free open access item. All inquiries regarding this item or the UAB Digital Commons should be directed to the [UAB Libraries Office of Scholarly Communication](#).

BET BROMODOMAIN INHIBITION AS AN APPROACH FOR TREATMENT OF  
CHOLANGIOCARCINOMA

by  
SAMUEL CHARLES FEHLING

KARINA YOON, MENTOR & CHAIR  
SUSAN BELLIS  
DOUGLAS HURST  
RAJEEV SAMANT  
RALPH SANDERSON  
ROBERT VAN WAARDENBURG

A DISSERTATION

Submitted to the graduate faculty of The University of Alabama at Birmingham,  
in partial fulfillment of the requirements for the degree of  
Doctor of Philosophy

BIRMINGHAM, ALABAMA

2019

Copyright by  
Samuel Charles Fehling  
2019

# BET BROMODOMAIN INHIBITION AS AN APPROACH FOR TREATMENT OF CHOLANGIOCARCINOMA

SAMUEL CHARLES FEHLING

CANCER BIOLOGY

## ABSTRACT

Cholangiocarcinoma (CCA) is a highly aggressive neoplasm which arises from the epithelial layer of the biliary tract. It is the second most common primary hepatic malignancy. As CCA is typically diagnosed at late disease stage, the current standard of care, resection followed by gemcitabine with cisplatin, is not effective. Further, up to 90% of CCA patients are ineligible for resection. Of those eligible for resection, postoperative chemotherapy does not prolong overall survival leading to a 5-year survival of ~30%. Previously, mutations have been identified in *KRAS* (17% of CCA cases), *TP53* (44%) and *SMAD4* (17%) but none have been recognized as critical for CCA. This demonstrates an imperative need to identify novel molecular targets to improve CCA patient outcome.

Proto oncogene and transcription factor, c-Myc, is highly expressed in up to 94% of CCA cases while undetectable in normal liver. This suggests c-Myc overexpression may contribute to CCA, however, this hypothesis has not been addressed. The bromodomain and extraterminal domain (BET) family of proteins are epigenetic adapter proteins which promote the transcription of genes including *MYC*. We previously reported that the BET inhibitor JQ1 lead to significant growth reduction and decreased c-Myc expression in a patient-derived xenograft (PDX) model of CCA. Further, downregulation of c-Myc transcriptional target, Chk1, was also observed. This

dissertation details the use of *in vitro* and *in vivo* models of CCA to evaluate the mechanism through which JQ1 leads to reduced tumor growth and c-Myc expression. We report that treatment of CCA *in vitro* models with JQ1 corroborated our CCA PDX results. In addition, downregulation or therapeutic inhibition of DNA damage response (DDR) factor, Chk1, has been reported to sensitize cancer cells to PARP inhibition as well as to gemcitabine. Therefore, we assessed whether treatment with a BET inhibitor lead to enhanced efficacy of these therapeutics in CCA.

We assessed whether JQ1 in combination with PARP inhibition or gemcitabine lead to enhanced therapeutic efficacy in our *in vitro* and *in vivo* CCA models. Our models suggest that these combinations are more effective than when administered as single agents. As our results were completed using chemotherapy-sensitive models, we developed clinically relevant models of gemcitabine resistance including one cell line model and two gemcitabine resistant PDX models. Our *in vitro* gemcitabine resistant model showed greater sensitivity to JQ1 which suggests BET inhibition may potentially overcome gemcitabine resistance. Taken together, these data demonstrate that inhibition of BET proteins in combination with PARP inhibition or gemcitabine are rational approaches for treatment of CCA.

Keywords: Cholangiocarcinoma, BET bromodomain, JQ1, I-BET762, PARP inhibitors, c-Myc, Chk1, RNAi, gemcitabine, cisplatin, combination indices

## DEDICATION

I dedicate this dissertation to my family. This journey would not have been possible without your continuous love and support. Mom and dad, thank you for indulging and fostering my curiosity. Kelly, thank you for being a constant pillar of support as I overcome my anxieties. Minerva, thank you for supporting my passion for science and for standing by my side as I completed this journey. You are both my anchor and my shining light.

## ACKNOWLEDGEMENTS

I would like to thank my mentor, Dr. Karina Yoon. Truthfully, the words, “thank you”, are not nearly enough. Without you, this would not have been possible. When I didn’t have a home, you took me in and gave me shelter. While in the lab transition process, you were the first and only mentor who sat down with me and outlined a plan towards graduation. And for that, I thank you from the bottom of my heart. That act removed the worry, the stress and anxiety from my mind. You have been an excellent mentor and role model over these past three years. You have taught me to think critically, write concisely yet precisely, and, when my c-Myc blots would not work, that I should try-try again! Persistence is key. Thank you for your patience and for treating me with respect. It has truly been my honor to work with you.

Thank you, Dr. Susan Bellis, Dr. Douglas Hurst, Dr. Rajeev Samant, Dr. Ralph Sanderson and Dr. Robert van Waardenburg for serving on my dissertation committee. The time, advice, support and enthusiasm you provided has been vital. And I look forward to discussing with you all about our future successes.

Thank you to past and present Yoon lab members, Dr. Aubrey Miller, Dr. Kelly Kreitzburg, Dr. Patrick Garcia, Becki Vance, Skyler Hendrix and Tracy Gamblin. Your assistance and help on projects are beyond measurable. Dr. Miller and Dr. Garcia, thank you both for your time, expertise and assistance in finishing portions of my manuscript.

You both made the process of manuscript submission coupled with dissertation writing a manageable process. I am indebted to you both. Most importantly, I thank you all for your friendship. It's one thing to be passionate about science, but it's another to be in an environment where friendship and science coincide. When experiments had me down, I could always turn to you to lift my spirits. Thank you. I would also like to thank the cholangiocarcinoma patients who agreed to participate in these studies. Without your contributions, this work would not have been possible.

This work would not have been possible without the love and support from my family. Mom and dad, thank you for supporting my passion for science at such a young age. From building with Legos, to building computers, to cancer research, you have always encouraged my love for learning. When work had me down, you both were always there to remind me that "there's got to be a way." To my sister Kelly, whenever I was anxious about upcoming meetings, experiments or anything in life, you were always there to listen. You helped far more than you know. And lastly, thank you to my girlfriend, Minerva. Thank you for encouraging my ridiculousness, for standing by me, supporting me, for keeping me company as I wrote my dissertation, for cooking while I finished my degree and for reminding me there is more to life than the bench. A simple "thank you" is not enough to express how grateful I am to have you.



## TABLE OF CONTENTS

	<i>Page</i>
ABSTRACT .....	iii
DEDICATION .....	v
ACKNOWLEDGEMENTS .....	vi
LIST OF TABLES .....	x
LIST OF FIGURES .....	xi
LIST OF ABBREVIATIONS .....	xiv
CHAPTER .....	1
1 INTRODUCTION .....	1
Cholangiocarcinoma (CCA) .....	1
Risk factors .....	3
Pathology and clinical presentation of CCA.....	7
Diagnosis and disease staging.....	8
The current treatment options for CCA .....	13
<i>In vitro</i> and <i>in vivo</i> models to study CCA.....	18

	The bromodomain proteins .....	21
	Pharmacological inhibition of BET bromodomain proteins .....	26
	Targeting BET bromodomains in CCA .....	28
	Hypothesis and goals .....	32
2	THE COMBINATION OF BET AND PARP INHIBITORS IS SYNERGISTIC IN MODELS OF CHOLANGIOCARCINOMA.....	33
3	EVALUATING THE COMBINATION OF JQ1 AND GEMCITABINE IN CCA .....	72
4	DEVELOPMENT, CHARACTERIZATION AND TRETMENT OF GEMCITABINE RESISTANT CCA MODELS .....	91
5	DISCUSSION .....	111
6	MATERIALS AND METHODS.....	146
	LIST OF REFERENCES .....	164
	APPENDIX: INSTITUTIONAL ANIMAL CARE AND USE COMMITTEE APPROVAL FORM .....	198

## LIST OF TABLES

<i>Table</i>		<i>Page</i>
1-1	The current AJCC staging system for intrahepatic CCA .....	11
1-2	The current AJCC staging system for perihilar CCA.....	12
1-3	The current AJCC staging system for distal CCA.....	13
S1	Sequences of primers and oligonucleotides used for the study .....	71
6-1	The antibodies used in this dissertation.....	162
6-2	PCR primers .....	163

## LIST OF FIGURES

<i>Figure</i>	<i>Page</i>
1-1 Anatomical location of CCA subtypes .....	3
1-2 Crystal structure of the bromodomain .....	23
1-3 The bromodomain and extraterminal domain (BET) family of proteins display common structural characteristics.....	24
1-4 BRD4 upregulates c-Myc expression .....	26
1 JQ1 decreases the viability and the clonogenic potential of KKU-055 and KKU- 100 CCA cells <i>in vitro</i> .....	55
2 JQ1 decreases the expression of c-Myc and its transcriptional target Chk1 in both KKU-055 and KKU-100 CCA cell lines .....	56
3 A combination of BET and PARP inhibitors are synergistic in KKU-055 and KKU-100 CCA cell lines .....	57
4 Decreased expression of BRD2 (shBRD2) or BRD4 (shBRD4) increased the sensitivity of KKU-055 cells to BET inhibitors (JQ1 or I-BET762) or PARP inhibitors (olaparib or veliparib).....	58
5 shBRD2 and shBRD4 transfectants were more sensitive to combinations of BETi + PARPi than shGFP (control) transfectants .....	59

6	JQ1 + olaparib suppresses tumor growth in an <i>in vivo</i> KKU-055 CCA model.....	61
S1	<i>BRCA1</i> and <i>BRCA2</i> mutational status and primers used.....	66
S2	JQ1 decreases the mRNA expression of <i>BRCA2</i> in KKU-100 cells .....	67
S3	JQ1 + PARP inhibitors (olaparib or veliparib) increased the levels of DNA damage marker $\gamma$ H2AX and apoptotic marker cleaved PARP (Cl. PARP) in KKU- 055 CCA cells .....	68
S4	Cell cycle analysis of JQ1 $\pm$ PARPi .....	69
S5	No compensatory binding of BRD4 (a) or BRD42 (b) to the <i>MYC</i> promoter when BRD2 (a) or BRD4 (b) is downregulated .....	70
3-1	Gemcitabine metabolism & mechanism of action .....	74
3-2	Gemcitabine and cisplatin synergize in CCA cell line, KKU-055 .....	78
3-3	Gemcitabine and cisplatin synergize in CCA cell line, KKU-100.....	79
3-4	The combination of gemcitabine with cisplatin suppresses tumor growth in an <i>in</i> <i>vivo</i> model of CCA .....	81
3-5	The combination of JQ1 with gemcitabine in a 1,000:1 ratio is synergistic in CCA <i>in vitro</i> models .....	84
3-6	The combination of JQ1 with 10 nM gemcitabine is synergistic in CCA <i>in vitro</i> models .....	85
3-7	The combination of JQ1 with 10 nM gemcitabine decreases the expression of c-Myc and Chk1 in CCA <i>in vitro</i> model, KKU-055 .....	86
3-8	Decreased expression of BRD2 or BRD4 does not increase sensitivity of KKU-055	

cells to gemcitabine.....	87
4-1 Mechanisms of gemcitabine resistance .....	94
4-2 KKKU-055 gemcitabine resistant (Gem <sup>R</sup> ) model displays over 500-fold increase in gemcitabine resistance compared to parental .....	97
4-3 KKKU-055 Gem <sup>R</sup> displays no alterations in morphology, cell doubling time nor specific <i>KRAS</i> mutational status compared to parental.....	98
4-4 KKKU-055 Gem <sup>R</sup> is more sensitive to JQ1 .....	99
4-5 Implantation, treatment and dosing timeline for the development of gemcitabine resistant CCA PDX models .....	101
4-6 Generation of CCA1 and CCA2 gemcitabine resistant models .....	102
4-7 CCA1 and CCA2 Gem <sup>R</sup> models display increased cell proliferation <i>in vivo</i> .....	104
4-8 Gemcitabine resistant models of CCA1 & CCA2 display altered expression of gemcitabine metabolic products .....	106

## LIST OF ABBREVIATIONS

AAAALAC	Association for Assessment and Accreditation of Laboratory Animal Care International
AACR	American Association for Cancer Research
AID	Activation-Induced Cytidine Deaminase
AJCC	American Joint Committee on Cancer
AML	Acute Myelogenous Leukemia
ANOVA	Analysis of Variance
AR	Androgen Receptor
ATCC	American Type Culture Collection
ATM	Ataxia Telangiectasia Mutated
ATR	Ataxia Telangiectasia-Rad3-Related
BD	Bromodomain
BET	Bromodomain and Extraterminal Domain
BRD	Bromodomain
CA 19-9	Carbonic Anhydrase 19-9

CAF	Cancer-Associated Fibroblasts
CCA	Cholangiocarcinoma
CD	Cervical Dislocation
CDA	Cytidine Deaminase
CDK	Cyclin Dependent Kinase
CEA	Carcinoembryonic Antigen
ChIP	Chromatin Immunoprecipitation
CI	Combination Index/Indices
CRPC	Castration Resistant Prostate Cancer
CSR	Class Switch Recombination
CT	Computed Tomography
CTD	Carboxyterminal Domain
dCK	Deoxycytidine Kinase
DDR	DNA Damage Response
dFdC	Gemcitabine
dFdCDP	Gemcitabine Diphosphate
dFdCTP	Gemcitabine Triphosphate
DMEM	Dulbecco's Modified Eagle Medium



DMN	Dimethylnitrosamine
DMSO	Dimethyl Sulfoxide
DNA	Deoxyribonucleic Acid
dNTP	Nucleoside Triphosphate
DSB	Double Strand Break
EBRT	External Beam Radiation Therapy
ECL	Enhanced Chemiluminescence
ECM	Extracellular Matrix
EGFR	Epidermal Growth Factor Receptor
EI	Expression Indices
ET	Extra-Terminal
EUS	Endoscopic Ultrasound
FBS	Fetal Bovine Serum
FDA	Food and Drug Administration
FFPE	Formalin Fixed and Paraffin Embedded
FGFR	Fibroblast Growth Factor Receptor
FISH	Fluorescence <i>in situ</i> Hybridization
FXR	Farnesoid X Receptor

GEM	Genetically Engineered Mouse
GEMR	Gemcitabine Resistant
GFP	Green Fluorescent Protein
H&E	Hematoxylin and Eosin
HAT	Histone Acetyl Transferase
HCC	Hepatocellular Carcinoma
hCNT1	Human Concentrative Nucleoside Transporter 1
hENT1	Human Equilibrative Nucleoside Transporter 1
HLA	Human Leukocyte Antigen
HR	Homologous Recombination
IACUC	Animal Care and Use Committee
IB	Immunoblot
IDH	Isocitrate Dehydrogenase
IHC	Immunohistochemistry
IL	Interleukin
IMRT	Intensity-Modulated Radiotherapy
IRB	Institutional Review Board
JCRB	Japanese Cancer Research Resources Bank

KD	Knockdown
KO	Knockout
MDR	Multidrug Resistance
MM	Multiple Myeloma
MMR	Mismatch Repair
MRCP	Magnetic Resonance Cholangiopancreatography
MRI	Magnetic Resonance Imaging
NDPK	Nucleoside diphosphate kinase A
NER	Nucleotide Excision Repair
NHEJ	Non-Homologous Recombination
NMC	NUT Midline Carcinoma
NSLC	Non-Small Lung Cancer
NUT	Nuclear Protein in Testis
PAC	Puromycin N-Acetyl-Transferase
PAGE	Polyacrylamide Gel Electrophoresis
PARP	Poly (ADP-Ribose) Polymerase
PC	Pancreatic Cancer
PCR	Polymerase Chain Reaction

PDAC	Pancreatic Ductal Adenocarcinoma
PDX	Patient-Derived Xenograft
PE	Plating Efficiency
PEI	Polyethylenimine
PET	Positron Emission Tomography
PGFR	Platelet Growth Factor Receptor
PSC	Primary Sclerosing Cholangitis
P-TEFb	Positive Transcription Elongation Factor B
PTEN	Phosphatase and Tensin Homolog
PVDF	Polyvinylidene Difluoride
R0	Margin Negative Resection
RB	Retinoblastoma
RCC	Renal Cell Carcinoma
RNA	Ribonucleic Acid
RR	Ribonucleotide Reductase
RRM1	Ribonucleotide Reductase Catalytic Subunit M1
RRM2	Ribonucleotide Reductase Catalytic Subunit M2
SCID	Severe Combined Immunodeficient

SDS	Sodium Dodecyl Sulfate
SMA	Smooth Muscle Actin
SSB	Single Strand Break
TAA	Thioacetamide
TACE	Transarterial Chemoembolization
TCGA	The Cancer Genome Atlas
TNBC	Triple Negative Breast Cancer
TNM	Tumor-Node-Metastasis
TRS	Tumor Reactive Stroma
TSS	Transcriptional Start Site
UAB	University of Alabama at Birmingham
UDCA	Ursodeoxycholic Acid
VC	Vehicle Control
VEGFR	Vascular Endothelial Growth Factor Receptors
WB	Western Blot
WT	Wild Type
$\gamma$ H2AX	Histone H2AX Phosphorylated at Ser-139

CHAPTER 1  
INTRODUCTION

**Cholangiocarcinoma (CCA)**

During liver development, bipotential progenitor cells, hepatoblasts, establish two cell populations, hepatocytes and cholangiocytes [1, 2]. Cell fate has been hypothesized to be controlled by both cell-extrinsic as well as cell-intrinsic signaling such as expression of MET and albumin for hepatocytes and Notch1, EGFR and IDH1/2 for cholangiocytes [2-4]. Hepatocytes are the major functional units of the liver where they are critical in metabolism, synthesis and detoxification [5]. Cholangiocytes, which represent approximately 5% of the cells in the liver [6], are a dynamic population of epithelial cells which line the three dimension network of extra- and intrahepatic ducts known collectively as the biliary tree [7]. Their primary function lies in the modification of hepatic bile as it progresses from the liver, through the biliary tree and into the duodenum [1, 7]. These modifications occur through transportation of water and various compounds, including chloride and bicarbonate [6], across the cholangiocyte plasma membrane [7]. The biliary tree is composed of two distinct partitions: intrahepatic and extrahepatic ducts [1, 3, 8, 9]. Named based on their anatomical location, intrahepatic ducts are located proximate to the portal veins in the liver whereas the extrahepatic system is located near and extend from the liver [1]. While both systems are in direct

contact with one another, they arise from different origins. For example, extrahepatic systems share an origin with the ventral pancreas [1, 10].

Cholangiocarcinoma (CCA) is a rare, aggressive neoplasm arising from the epithelial layer of the biliary tract [11], and is the second most common primary hepatic malignancy after hepatocellular carcinoma (HCC) [12]. CCA consists of three subtypes, intrahepatic (iCCA), perihilar (pCCA) and distal extrahepatic (dCCA), named based on anatomical location along the biliary tract. iCCA, pCCA and dCCA describe tumors located near the secondary branches of the hepatic duct, between the secondary branches of the hepatic ducts and common hepatic duct, and along the hepatic duct, respectively [12]. Disease etiology has not been established and most cases do not ascribe to known risk factors [11]. Most patients present with pCCA, the most common subtype [12]. Globally, the average age of diagnosis for all CCA subtypes is > 50 with slight male predisposition (ratios of 1:1.2-1.5), though, the reason for this remains unknown [12, 13]. Disease incidence varies by geographical region [13]. As of 2018, iCCA incidences rates in the United States have increased by 11.2% and 13.8% for men and women, respectively [8]. However, not all CCA subtypes are increasing at the same rate worldwide [8, 14]. Primary hepatic malignancies, including both iCCA and HCC, are predicted to become the second leading cause of cancer related death by 2030 [15].

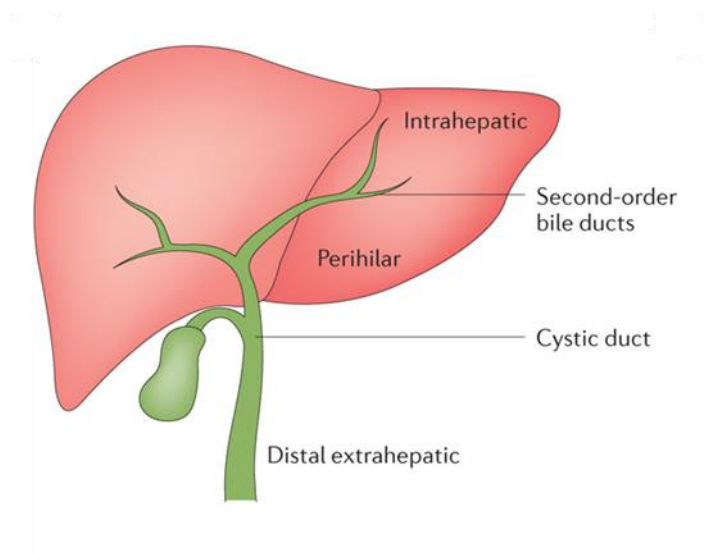


**Figure 1-1. Anatomical location of CCA subtypes.** Cholangiocarcinoma (CCA) is classified into three subtypes, intrahepatic (iCCA), perihilar (pCCA) and distal extrahepatic (dCCA), based on anatomical location along the biliary tract. iCCA describes tumors located near the secondary branches of the hepatic duct, pCCA describes tumors between the secondary branches of the hepatic ducts and common hepatic duct, and dCCA describes tumors along the hepatic duct.

Note: Adapted from “Cholangiocarcinoma: current knowledge and future perspectives consensus statement from the European Network for the Study of Cholangiocarcinoma (ENS-CCA).” by Banales et al. 2016 *Nature Reviews Gastroenterology & Hepatology*. Permission obtained under the Creative Commons Attribution 4.0 International License.

### *Risk factors*

CCA epidemiology differs based on geographical incidence, risk factors associated with that region and genetic variations [8]. Whole genome expression profiling shows increases in proliferative pathways (EGF, RAS, AKT and MET), angiogenesis (vascular endothelial growth factor receptors (VEGFR) and platelet growth factor receptor (PGFR)) as well as inflammation through interleukin-6 (IL-6) [12]. Some of the major tyrosine kinase pathways, including IL-6 receptor, c-MET, EGFR members



ERBB1 and ERBB2, are key players which induce cellular signaling cascades which influence senescence, cell cycle regulation, proliferation and apoptosis [12].

At the genomic level, mutations common in all CCA subtypes include *KRAS* (17%), *TP53* (44%) and *SMAD4* (17%) [16]. However, CCA subtypes display distinct mutational features based on patient disease etiology and anatomical location [12]. iCCA and dCCA contain characteristic isocitrate dehydrogenase 1/2 (IDH1/2) and human epidermal growth factor receptor 2 (HER2) mutations, respectively [16]. Mouse models indicate mutations in IDH1/2 induce iCCA formation by inhibiting hepatocyte, but not biliary, differentiation [12]. Mutant IDH proteins alter the canonical functioning of IDH, converting alpha-ketoglutarate ( $\alpha$ KG) to isocitrate, to instead convert  $\alpha$ KG to 2-hydroxyglutarate (2HG) [17]. This metabolic switch inhibits the function of  $\alpha$ KG-dependent dioxygenases which further impacts cell survival and differentiation [17]. Of note, pCCA does not harbor known characteristic mutations [16]. Canonically, the fibroblast growth factor receptors (FGFR) pathway is involved in cellular proliferation, survival, differentiation and migration [18]. FGFR2 fusions occur in 13% of iCCA cases and have not been observed in dCCA or pCCA [12, 18-20]. Survival of iCCA patients harboring FGFR2 fusions was found to be higher than those harboring wild type (WT) FGFR2 (123 vs. 37 months) which suggests FGFR2 fusion may be a potential prognostic marker [18]. Further, *in vitro* studies utilizing a CCA model harboring FGFR2 fused with MGEA5, a glycosidase which removes O-GlcNAc modifications [21], detailed anti-tumor efficacy utilizing ponatinib, a multi-targeted tyrosine-kinase inhibitor [18, 22]. Additional FGFR2 fusion partners have been reported to include BICC1, AHCYL1, TACC3, KIAA1598, CREB5, KIAA1967, CCDC6, AFF3, CASP7, OFD1, SLC45A3

and ROS1 [18, 23]. However, the exact pathological implications of each FGFR2 fusion is currently unknown [18]. FGFR2 inhibitor, infigratinib, is currently recruiting for phase 2 clinical trials for advanced stage CCA (ClinicalTrials.gov Identifier: NCT02150967) [24].

Categorized as an autoimmune disorder [25], primary sclerosing cholangitis (PSC), caused by blockage of the bile duct due to inflammation and scarring, has been strongly associated with the development of colorectal cancer as well as both iCCA and dCCA [13, 23, 26, 27]. Weismüller et al. reported that up to 10.9% of 7,119 PSC patients were diagnosed with a hepatobiliary malignancy [28]. PSC is observed most in men aged 30 to 40 who present with ulcerative colitis or Crohn's disease [27]. Conflicting theories have emerged describing the development of PSC. Reports detail genetic alterations, particularly in the human leukocyte antigen (HLA) complex, alterations in bile acid homeostasis, gut leakage as well as bile acid toxicity being potential causes [27]. However, the exact origin remains elusive. Populations of T cells, macrophages and neutrophils are prevalent in PSC bile ducts, however, the role of each cell type in PSC has not been established. Research suggests crosstalk between T cells and cholangiocytes results in the recruitment of additional T cells to the portal areas, resulting in a highly inflammatory environment [27]. Inflammation and cholestasis can result in cholangiocyte activation leading to subsequent hepatocellular proliferation, angiogenesis and fibrosis [29]. Treatment options for PSC include liver transplantation, administration of immunosuppressive drugs, bile acid-based therapies utilizing ursodeoxycholic acid (UDCA) and norursodeoxycholic acid [27, 30]. However, efficacy remains limited and disease recurrence has been reported to occur post liver transplantation [27]. It is possible

that limited efficacy could be due to therapeutic administration occurring too late in the course of the disease [27]. Ultimately, the shortcomings in understanding PSC pathogenesis prohibits the development of more efficacious treatment options.

Parasitic infection, occurring primarily in regions of Northeast Thailand, Cambodia, Laos, Southern China, Southeast Asia and South Korea, have been associated with CCA development [14, 31-33]. Reports indicate a high prevalence of CCA cases overlap with liver fluke infection (7 to 85 CCA diagnoses out of 100,000 infections) [31]. *Opisthorchis viverrini* and *Clonorchis sinensis* are hepatobiliary flukes, flatworms, which are ingested through raw, uncooked seafood, dwell in the intrahepatic bile duct and have both been deemed “carcinogenic to humans” by the International Agency for Research on Cancer [13, 33]. Liver flukes are thought to contribute to CCA through three distinct mechanisms [33]. **1)** Mechanical damage results from fluke suckers which hook into the biliary epithelium, causing tissue damage [33]. Additionally, the size of *C. sinensis* is larger than the bile duct lumen, resulting in partial bile obstruction [33]. **2)** Parasite excretory/secretory molecules, such as Ov-GRN-1, a homologue of human granulin, has been reported to induce angiogenesis, decrease apoptosis and promote tumor invasion [33]. **3)** Infection-related inflammation caused by liver fluke increases localized chronic irritation, biliary inflammation and cellular proliferation resulting in hepatobiliary or hepatic abnormalities [13, 33]. Chronic biliary inflammation and an increase in proinflammatory pathways results in downregulation of hepatobiliary transporters and a buildup of bile acids which activate epidermal growth factor receptor (EGFR), apoptotic resistance and cholestasis [12, 34]. Proinflammatory cytokine, IL-6 [33, 35], as well as upregulation of pro-carcinogenic pathways [11], including expression of proto-oncogene,

c-Myc [36], have been further associated with CCA development. Mutational profiles differ between *O. viverrini*-associated and non-*O. viverrini*-associated CCA cases.

Mutations in *TP53* and *SMAD4* are more prevalent in *O. viverrini*-associated CCA while *IDH1/2* mutations are high in non-*O. viverrini*-associated CCA [12, 31]. *KRAS* is commonly mutated in both [31]. Ultimately, most patients develop CCA without any identifiable risk factors other than age [12, 13].

### *Pathology and clinical presentation of CCA*

Correct CCA diagnosis, subtype categorization, monitoring and treatment strategy is dependent on anatomical location of the malignancy. As stated above, CCA is subdivided into three subtypes: pCCA, dCCA and iCCA. pCCA represents ~50% of CCA cases, dCCA ~40% and iCCA less than 10% [16, 37]. Histologically, the majority of CCA cases are tightly enclosed in highly desmoplastic and hypovascular stroma referred to as tumor reactive stroma (TRS) which contains numerous cell populations including inflammatory cells, endothelial cells, myofibroblasts and mesenchymal stem cells [19, 38, 39]. The majority of iCCA cases, defined as well, moderately and poorly differentiated adenocarcinomas [23], are classified as mass forming and present as unencapsulated, solid and white lesions [40]. Both dCCA and pCCA both present as tan-white due to their association with dense TRS [40]. Morphologically, they appear as papillary or scar-like adenocarcinomas featuring cuboidal to columnar shape [40].

iCCA is further divided into three pathological classifications. 1) Intraductal-growing is the most unique subtype (~8-18% of iCCA cases) which manifests as papillary or tubular polypoid lesions. This subtype presents with characteristically slow growth

patterns and good clinical prognosis [19, 40]. **2)** Mass forming tumors are characterized by lobulated margins, no gross vascular invasion and appear as a homogeneous lesion on computed tomography (CT) scans [40]. **3)** Periductal infiltrating tumors (60% of CCA cases) are located near or in the hilar or extrahepatic bile duct [40]. Strictly periductal infiltrating tumors are uncommon and usually occur in combination with mass forming subtypes [40]. Using ultrasound imaging, periductal infiltrating subtypes present as sudden changes in ductal diameter, wall thickening or small masses along the hepatic bile duct [40].

Classically, CCA symptoms include jaundice, fatigue and abdominal pain [12, 27], however, clinical presentation is not specific nor the same for each subtype [12]. Patients diagnosed with iCCA become symptomatic at late disease stage and present with abdominal pain, fatigue, cachexia and night sweats, however, up to 43% of iCCA cases are diagnosed incidentally through routine scans prior to disease symptoms [11, 12]. Both pCCA and dCCA present with painless jaundice (90% of cases), caused by biliary obstruction, subsequent reduction in bile flow and the accumulation of bile contents such as bilirubin and bile acids [41], and acute cholangitis (10% of cases) [12]. Unfortunately, up to 50% of pCCA and dCCA display symptoms of malignancy (anorexia, weight loss and fatigue) upon the initial symptom presentation [12].

### *Diagnosis and disease staging*

The “silent” clinical characteristics at early disease stage presents a diagnostic challenge [8, 19]. Diagnosis requires a high level of disease suspicion and the coordination effort of those in the clinic, lab, endoscopic and radiographic analysis [19].

While medical imaging remains the standard for CCA diagnosis, the exact scan of choice is highly dependent on the suspected CCA subtype. If iCCA is suspected, clinicians must first distinguish HCC from iCCA using CT scans and magnetic resonance imaging (MRI) [16, 19, 40], as most iCCA cases are PET negative with  $^{18}\text{F}$ -fluorodeoxyglucose [16]. Both CT and MRI are non-invasive methods which provide information regarding tumor size and satellite lesions, however, CT scans detail vascular encasement, extrahepatic metastasis and possibility of resection [19, 40]. For CT scans, iCCA features contrast uptake which occurs in both arterial and venous phases while HCC features contrast washout in the venous phase [16, 19]. However, a biopsy is necessary to truly differentiate HCC from iCCA [16]. iCCA diagnosis is further complicated by cellular differentiation [8]. As described above, cholangiocytes and hepatocytes are derived from a common progenitor [1, 3, 42]. As such, liver cancers can contain heterogenous population of hepatocytes and cholangiocytes referred to as hepatocellular-cholangiocellular carcinomas [8, 16]. MRI can confirm the enhanced rim and irregular shape which is characteristic of hepatocellular-cholangiocellular carcinomas [16].

Both pCCA and dCCA are imaged using MRI and CT as well as magnetic resonance cholangiopancreatography (MRCP) and endoscopic ultrasound (EUS) [19]. MRCP is a non-invasive, non-ionizing radiation method to evaluate the liver, gallbladder, bile duct and pancreas for disease. EUS is a minimally invasive method used to pass an ultrasound probe through the mouth and into the digestive tract. The combination of MRI with MRCP has shown to be the most reliable imaging method for pCCA and dCCA [19, 40].

Blood tests can aide in CCA diagnosis, however, the sensitivity of each impacts their utility as diagnostic markers alone. Early diagnostic markers, such as an increase in

carbonic anhydrase 19-9 (CA 19-9) and carcinoembryonic antigen (CEA) serum levels, can correlate with disease progression, but are neither effective nor specific to CCA [11, 12, 27, 43]. While CA 19-9 concentration is significantly higher in CCA patients compared to benign disease/healthy individuals, levels can also be elevated in patients experiencing cholestasis, cholangitis, benign PSC or other cancers [4, 16, 43]. Additionally, CA 19-9 specificity was found to be less specific for pCCA than for iCCA (63%) [19]. Further, patients who are Lewis antigen negative (7% of the general population) have low to undetectable CA 19-9 serum concentration [16].

In addition to blood biomarkers, a molecular cytogenetic technique, fluorescence *in situ* hybridization (FISH) can detect aneuploidy particularly in pCCA and dCCA [12, 19, 40]. Further, immunohistochemical (IHC) staining for cholangiocyte markers, cytokeratin 7 (CK7) and cytokeratin 19 (CK19), can be utilized to detect CCA. While CK7 (90% of cases) and CK19 (84% of cases) are characteristic markers of CCA, both are expressed on hepatocellular carcinoma (HCC) as well as metastatic adenocarcinomas [12, 19, 40]. More specific diagnostic markers are needed.

If a mass is confirmed to be CCA, the diagnostic information is used to stage the tumor. The American Joint Committee on Cancer (AJCC) and the College of American Pathologists grade CCA into stages based on the tumor-node-metastasis (TNM) system which is defined by the extent of the primary tumor (T), regional lymph node metastasis (N) and the presence or absence of distant metastasis (M) [44]. Proper diagnosis and subsequent CCA treatment options depend upon anatomical location. As such, AJCC assigned independent TNM classifications for iCCA (**Table 1-1**), and pCCA (**Table 1-2**)

dCCA (**Table 1-3**) [45-47]. These diagnostic criteria precede the treatment options available to the patient.

Table 1-1. The current AJCC staging system for intrahepatic CCA

<b>TMN</b>	<b>Description</b>		
T1a	Solitary tumor $\leq$ 5 cm without vascular invasion		
T1b	Solitary tumor $>$ 5 cm without vascular invasion		
T2	Solitary tumor with intrahepatic vascular invasion or multiple tumors, with or without vascular invasion		
T3	Tumor perforating the visceral peritoneum		
T4	Tumor involving the local extrahepatic structures by direct invasion		
N0	No regional lymph node metastasis		
N1	Regional lymph node metastasis present		
M0	No distant metastasis		
M1	Distant metastasis present		
<b>Stage</b>	<b>T</b>	<b>N</b>	<b>M</b>
Ia	T1a	N0	M0
Ib	T1b	N0	M0
II	T2	N0	M0
IIIa	T3	N0	M0
IIIb	T4	N0	M0
	Any T	N1	M0
IV	Any T	Any N	M1



Table 1-2. The current AJCC staging system for perihilar CCA

<b>TMN</b>	<b>Description</b>		
T1	Tumor confined to the bile duct, with extension up to the muscle layer or fibrous tissue		
T2a	Tumor invades beyond the wall of the bile duct to surrounding adipose tissue		
T2b	Tumor invades adjacent hepatic parenchyma		
T3	Tumor invades unilateral branches of the PV or HA		
T4	Tumor invades main PV or its branches bilaterally, or the common hepatic artery, or unilateral second-order biliary radicals with contralateral portal vein or hepatic artery involvement		
N0	No regional lymph node metastasis		
N1	Metastasis in 1-3 regional lymph nodes		
M0	No distant metastasis		
M1	Distant Metastasis		
<b>Stage</b>	<b>T</b>	<b>N</b>	<b>M</b>
I	T1	N0	M0
II	T2a-b	N0	M0
IIIa	T3	N0	M0
IIIb	T4	N0	M0
IIIc	Any T	N1	M0
IVa	Any T	N2	M0
IVb	Any T	Any	M1

Table 1-3. The current AJCC staging system for distal CCA

<b>TMN</b>	<b>Description</b>		
T1	Depth of invasion < 5 mm		
T2	Depth of invasion 5-12 mm		
T3	Depth of invasion > 12 mm		
T4	Tumor involves the celiac axis or the superior mesenteric artery		
N0	No regional lymph node metastasis		
N1	Metastasis in 1-3 regional lymph nodes		
M0	No distant metastasis		
M1	Distant Metastasis		
<b>Stage</b>	<b>T</b>	<b>N</b>	<b>M</b>
I	T1	N0	M0
IIa	T1-2	N0-1	M0
IIb	T2-3	N0-1	M0
IIIa	T1-3	N2	M0
IIIb	T4	Any N	M0
IV	Any T	Any N	M1

*The current treatment options for CCA*

As with most cancers, the primary course of treatment is resection and systemic chemotherapy. With varying degrees of success, surgery remains the only cure for all CCA subtypes, however, only 10% are eligible for resection [8, 48]. Of those eligible, 10% to 45% present with bilateral, multifocal disease or distant metastasis found during explorative laparotomy, marking it unresectable [12, 40]. However, up to 15% of “suspicious” biliary strictures are found to be benign post operation [12]. Margin-negative (R0) surgical resections display the most prominent outcomes [40]. Surgical resection is the most efficacious option for iCCA which prolongs disease-free survival by an additional 12-36 months and resection of pCCA is potentially curative for those without exclusion criteria such as bilateral involvement of the second-order bile duct or PSC [8, 49, 50]. For iCCA, the most pronounced efficacy was reported by DeOliveira et

al. in which median survival of a R0 iCCA case was reported to be 80 months [51]. Further, improvements to vascular reconstruction and techniques to increase liver volume have made conventionally unresectable pCCA tumors resectable [8]. Comparatively, resection of dCCA involves a pancreaticoduodenectomy [8, 12, 40]. A pancreaticoduodenectomy, also known as the Whipple procedure, was popularized by and named after Dr. Allen Whipple and is used in surgical treatment for cancers of the pancreas, bile duct, duodenum and ampulla [52]. The classic yet extensive procedure removes the head of the pancreas, distal bile duct, gallbladder, duodenum, the first few centimeters of the jejunum and the distal stomach [52].

For those who are not eligible for resection, liver transplantation prolongs survival. Liver transplantation following neoadjuvant chemoradiation promotes the greatest survival benefit for unresectable pCCA [8]. Unfortunately, most are not eligible for this procedure. Nevertheless, pCCA arising in individuals suffering from PSC undergo liver transplantation regardless of CCA status [8, 12]. Liver transplantation for iCCA patients is controversial as there is a high risk of disease recurrence [8, 40]. Of iCCA patients who underwent liver transplantation and reported 1-, 2-, and 5-year survival rates of 72%, 48% and 23%, respectively, with 50% experiencing disease recurrence within 2 years [40]. However, in contrast to the controversy, Sapisochin et al. reported a 5-year survival of 73% for 8 patients who received “very early” (tumor < 2 cm in diameter) liver transplantation [53]. In the event iCCA is both unresectable and patients are ineligible for liver transplantation, transarterial chemoembolization (TACE) is a safe treatment which promotes a median overall survival of 12-15 months [8, 12, 40]. TACE is a minimally-invasive procedure which injects embolic particles coated with chemotherapeutic drugs

through a catheter into an artery directly to the site of the tumor [54]. Additionally, cases where both resection and liver transplantation are not possible, enrollment in clinical trials utilizing targeted therapeutic, such as those targeting mutant IDH1 (NCT02989857) or FGFR fusions (NCT03773302), is strongly recommended [8].

In general, treatment with gemcitabine (dFdC) in combination with cisplatin remains the current standard of care for CCA [8]. Gemcitabine, a nucleoside analog, is imported through equilibrative and concentrative nucleoside transporters, human equilibrative nucleoside transporter (hENT) and human concentrative nucleoside transporter (hCNT), with the majority imported through hENT1 [55]. Once through the plasma membrane, gemcitabine is phosphorylated in the cytoplasm by deoxycytidine kinase (dCK) to form the monophosphate (dFdCMP) which is subsequently phosphorylated by pyrimidine nucleoside monophosphate kinase (UMP-CMP kinase) to gemcitabine diphosphate (dFdCDP) [55]. Nucleoside diphosphate kinase A (NDPK) is responsible for the final phosphorylation step where dFdCDP is phosphorylated once more to dFdCTP. Gemcitabine promotes its cytotoxicity through incorporation of dFdCTP into DNA during DNA synthesis [55]. Only a single deoxynucleotide can be incorporated following incorporation of dFdCTP resulting in “masked chain termination”. dFdCTP masks removal of gemcitabine by DNA repair [55]. Further, dFdCDP inhibits the production of deoxyribonucleotides through inhibition of ribonucleotide reductase (RR) which results in a reduced deoxyribonucleotide (dNTP) pool [55]. With the reduction in the dNTP pool and the inability to remove gemcitabine from DNA, replicating cells succumb to replication fork stalling and subsequent replication fork collapse leading to cell death [55]. Additionally, treatment with cisplatin, a heavy metal complex containing a central

platinum ion bound to two chloride atoms, exerts its cytotoxicity through the formation of intra-strand and inter-strand links in genomic DNA, particularly through N7 on purines, as well as mitochondrial DNA [56]. Cisplatin is hydrolyzed in the cytoplasm where the chloride atoms are displaced by water molecules, forming a potent electrophile [57]. Intra-strand DNA crosslinks by cisplatin is repaired through nucleotide excision repair (NER) [58]. Mismatch repair (MMR) does recognize cisplatin-mediated DNA damage, however, MMR reportedly is critical to cisplatin cytotoxicity [56]. Cancer cells harboring mutations in *MSH1* or *MLH1* of the MMR system experienced cisplatin-resistance and those which were *MLH1*-proficient displayed increased sensitivity to cisplatin [58].

Unfortunately, chemotherapy does not markedly improve survival in those harboring resected or unresected CCA [12, 16, 40]. Valle et al. reported a median survival of 11.7 months following treatment with gemcitabine in combination with cisplatin over 8.1 months in those receiving gemcitabine alone [59]. As clinical CCA symptoms present at late disease stage, patients experience rampant chemoresistance [48, 60, 61]. Normal, nonmalignant cholangiocytes display intrinsic resistance to the toxic compounds found in bile and hepatic blood through downregulation of nucleoside transporters or upregulation of multidrug resistance (MDR) genes through activation of farnesoid X receptor by bile acids [6, 61]. Further, low levels of gemcitabine transporters, such as hENT1, are associated with shorter survival and gemcitabine resistance (Gem<sup>R</sup>) [55]. Though, reduced expression does not always correlate with Gem<sup>R</sup> [62]. Additionally, Gem<sup>R</sup> populations can inactivate gemcitabine through deamination by cytidine deaminase (CDA) as well as deoxycytidylate deaminase when in the monophosphate form (dFdCMP) [55]. Another marker of resistance is an increase in the subunits of RR, RRM1

and RRM2, which results in an increase in the dNTP pool [55]. Additionally, TRS further enhance drug resistance [39, 61]. Cancer-associated fibroblasts (CAFs) play a major role in tumor progression, metastasis and chemoresistance with the extent of CAFs infiltration determined through staining for alpha-smooth muscle actin ( $\alpha$ -SMA) [16]. In a preclinical model of CCA, treatment with navitoclax, a BH3 mimetic, resulted in targeted apoptosis in CAFs [63]. However, the impact on gemcitabine sensitivity was not addressed.

In addition to chemotherapeutic regimens, improvements to imaging techniques have permitted greater radiation precision for CCA [8]. External beam radiation therapy (EBRT) techniques, such as 3D conformal radiotherapy and intensity-modulated radiotherapy (IMRT), allow the targeting of cancer cells while not affecting nonmalignant tissues [8]. Patients with R0 resectable iCCA experienced greater overall survival with surgical intervention in combination with IMRT compared to those who underwent R0 surgery alone (21.8 months vs. 15.0 months) [64]. Radiation treatment does not strictly benefit those undergoing R0 resection. Tao et al. reported that patients with unresectable iCCA experienced a median survival of 30 months post EBRT [65]. This study built the foundation for a phase III clinical trial utilizing EBRT post chemotherapy for unresectable iCCA (NCT02200042) [8]. Similar studies have been performed for patients diagnosed with pCCA and dCCA, however, the results are not conclusive [8]. Even with treatment, the 5-year survival for patients with iCCA, pCCA and dCCA remains 32%, 28% and 34%, respectively [12, 38]. Further, relapse occurs within 2-3 years following resection [12].

### *In vitro and in vivo models to study CCA*

In cancer research, biological model systems are utilized to recreate tumor characteristics to further our understanding of the disease as well as develop and test therapeutics for patients. Depending on the specific question, a host of biological systems, from *in vitro* cell lines to patient derived xenograft (PDX) models and genetically modified mouse (GEM) models are available. Each with their own discrete set of advantages and disadvantages for CCA research.

Immortalized cell lines – a staple of cancer research in labs across the country – are invaluable tools to assess the role of cellular and molecular alterations in the development, progression and treatment of cancer. Due to underlying mutations, immortalized cell lines divide infinitely [66]. Cell lines offer many advantages for studying CCA. They are cost effective, easy to maintain and offer no mouse nor human ethical concerns [67]. Manipulations, including gain/loss-of-function mutations, genetic knockout/knockdown as well as gene overexpression models can be generated to answer critical questions. However, cell lines have been reported to change at both the genetic and transcriptional level following decades of *in vitro* culturing [66]. Compounding this issue, decades of culturing leads to loss of tumor heterogeneity as well as relevant components of the desmoplastic tumor microenvironment, immune populations and vasculature [66]. The earliest documented CCA cell line was reported by Yamaguchi et al. in 1985, HChol-Y1, which expressed characteristically high levels of CEA and CA 19-9 [68]. Since this time, relatively few human CCA *in vitro* models have been reported. The American Type Culture Collection (ATCC) does not carry any human CCA cell line models and the Japanese Cancer Research Resources Bank (JCRB) offers 9 human CCA

*in vitro* models for purchase. This scarcity of CCA cell lines drastically hinders the development of additional therapeutics options.

While *in vitro* models provide valuable insight into the cellular and molecular alterations of CCA, they do not fully represent the disease. Preclinical *in vivo* models provide further insight into disease onset, progression and response to treatment. Carcinogen-based CCA models recapitulate tumor microenvironment, TRS, immune system and disease progression, however, they are not widely reported. Most common methods of carcinogen-based CCA result from the administration of dimethylnitrosamine (DMN), thioacetamide (TAA) or furan to induce DNA mutations, structural changes or enhance tumor formation [69]. First reported in 1978, the combination of parasitic infection *O. viverrini* or *C. sinensis* with exposure to DMN was shown to induce iCCA, other gastrointestinal tumors as well as skin, lung and hematopoietic tumors in mice [69]. Further, a 1984 report detailed that the administration of TAA induced liver fibrosis, cirrhosis and iCCA in rodents, however, the mechanism through which this occurs is unknown. Additionally, treatment with furan, a compound found in manufacturing and herbicides, shows a 98% iCCA take rate and induction of CK19. Disease histology strongly resembles human disease as well as disease progression. However, rodents developed malignant mesothelioma and mononuclear cell leukemia in addition to iCCA [69].

GEM models provide disease onset, progression and therapeutic response similar to carcinogen-based CCA with the benefit of controlled mutational characteristics. To date, multiple CCA GEM models have been established. As discussed earlier, *SMAD4* is one of the most prevalent mutations in CCA (17% of cases). Conditional knockout (KO)



of both *Smad4* as well as phosphatase and tensin homolog (*Pten*), utilizing flanked loxP (floxed) sites surrounding *Smad4* and *Pten*, results in the generation of iCCA in 4-7-month-old mice [69]. A second CCA GEM model utilizes activating *Kras* mutation (LSL-*Kras*<sup>G12D</sup>) in combination with conditional *Pten* KO (*Pten*<sup>fllox</sup>) [69]. These tumors display histology similar to iCCA and have not been reported to metastasize [69]. A third CCA GEM model utilizes activating *Kras* mutation (LSL-*Kras*<sup>G12D</sup>) in combination with mutant *IDH2* (LSL-*IDH2*<sup>R172K</sup>). The *Kras*<sup>G12D</sup> and *IDH2*<sup>R172K</sup> driven CCA GEM model displays similar histology and location to iCCA with positive staining for CK19 [69]. One disadvantage to the discussed GEM models is the use of albumin-Cre. Albumin is expressed in both hepatocytes and cholangiocytes during embryogenesis which limits the cell type specificity of the genetic KO and/or mutation [69].

A third preclinical model of CCA used in cancer research is the PDX model. Initial implantation of PDX models displayed strong promise in evaluation of drug candidates and combination therapies [66]. PDX models are generated by implantation of patient tumor tissue orthotopically or subcutaneously into immunocompromised mice [70]. Orthotopic implantation, implantation into the anatomical organ, represents the most physiologically relevant model, however, specialized surgical techniques may be required and dependent on cancer type [70]. Additionally, monitoring of tumor growth requires the use of imaging systems. Implanting tumors subcutaneously does not require the same surgical expertise as orthotopic implantation and tumor volume can be measured using calipers. PDX models contain tumor cells as well as the desmoplastic tumor microenvironment, preserving cell-cell interactions. Human stroma is maintained through low passages; however, replacement with mouse stroma occurs over recurring

passages [66, 70]. Disadvantages of PDX models are their low engraftment rates and slow growing nature, requiring up to 6 months to generate a PDX model [66]. Together this makes working with PDX models more difficult, time consuming and costly. Further, implantation of human tissue into mouse requires an immunocompromised host to avoid tumor rejection, therefore, studying the role of immune populations on tumor progression is not possible. While no model system is perfect, PDX model provide vital information as preclinical models to assess drug efficacy, establish potential biomarkers and are utilized in co-clinical trials [70]. Unfortunately, the number of resectable CCA severely limits the potential number of CCA PDX models. Despite this disadvantage in generation of CCA PDX models, in collaboration with surgeons at the University of Alabama at Birmingham (UAB), we have developed the first five CCA patient derived xenograft (PDX) models representing dCCA (4) and metastatic iCCA (1) with a 100% take rate [71].

Models utilized in this dissertation include established CCA cell lines as well as CCA PDX models developed in our lab.

### **The bromodomain proteins**

First described in 1942, Waddington defined ‘epigenetics’ as alterations in gene expression patterns without changes to the underlying genome [72]. Epigenetic modifications are a dynamic and reversible process in which DNA methylation, histone modifications and noncoding RNA mediate gene expression [72, 73]. Epigenetic regulators are categorized into three classes: writers, erasers and readers. As their

classifications suggest, writers catalyze the addition of molecular modifications to DNA and histones through acetylation, methylation, phosphorylation and ubiquitination [74]. Erasers remove these modifications and readers recognize and bind these specific DNA or histone modifications. Of the epigenetic regulators, the bromodomain (BRD) containing proteins are the most well studied and characterized and specifically recognize acetylated lysine (K-Ac) residues [74, 75]. Histones and additional nuclear proteins are acetylated on the  $\epsilon$ -amino terminus of lysine residues [76]. Since the first BRD discovery in the early 1990's, the human genome has been found to code for 46 BRD containing proteins which consists of a total of 61 BRD components [75, 77, 78]. Each bromodomain consists of 4 alpha helices,  $\alpha_Z$ ,  $\alpha_A$ ,  $\alpha_B$  and  $\alpha_C$ , with one loop connecting  $\alpha_Z$  and  $\alpha_A$  (ZA loop) and another connecting  $\alpha_B$  and  $\alpha_C$  (BC loop) (**Figure 1-1**) [79]. An evolutionarily conserved asparagine residue in the BC loop hydrogen bonds with K-Ac, stabilizing the interaction and allowing BRD containing proteins to recognize and bind their targets [80, 81].

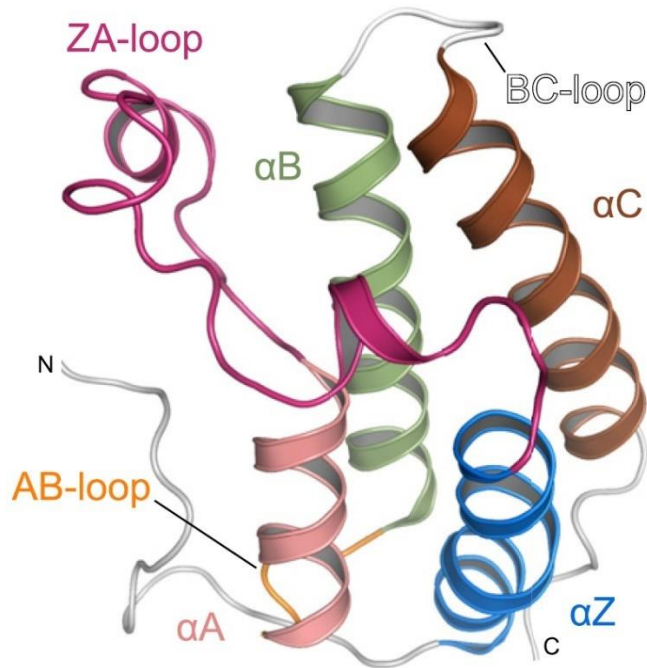


**Figure 1-2. Crystal structure of the bromodomain.** The crystal structure of the bromodomain (BRD) of BRD4. Four alpha helices,  $\alpha Z$ ,  $\alpha A$ ,  $\alpha B$  and  $\alpha C$ , with one loop connecting  $\alpha Z$  and  $\alpha A$  (ZA loop) and another connecting  $\alpha B$  and  $\alpha C$  (BC loop) for the hydrophobic binding pocket. An asparagine residue located in the BC loop hydrogen binds with K-Ac which stabilizes the interaction.

Note: Adapted from “Histone recognition and large-scale structural analysis of the human bromodomain family.” by Filippakopoulos et al. 2012 *Cell*. Permission obtained under the Creative Commons Attribution License (CC BY).

BRD domains bind to mono-acetylated lysine residues, however, reports of di-acetylated substrates binding to a single BRD have been reported [82, 83]. The BET family, encompassing BRD2, BRD3, BRD4 and BRDT, are epigenetic adaptor proteins which recognize and bind acetylated lysine (K-Ac) residues on the carboxyterminal domain (CTD) of histones 3 and 4 as well as other nuclear proteins [78]. Structurally, each member of the BET family contains two N-terminal hydrophobic K-Ac binding

BRD domains (BD1 and BD2) followed by an extra-terminal (ET) domain (**Figure 1-2**) [80].

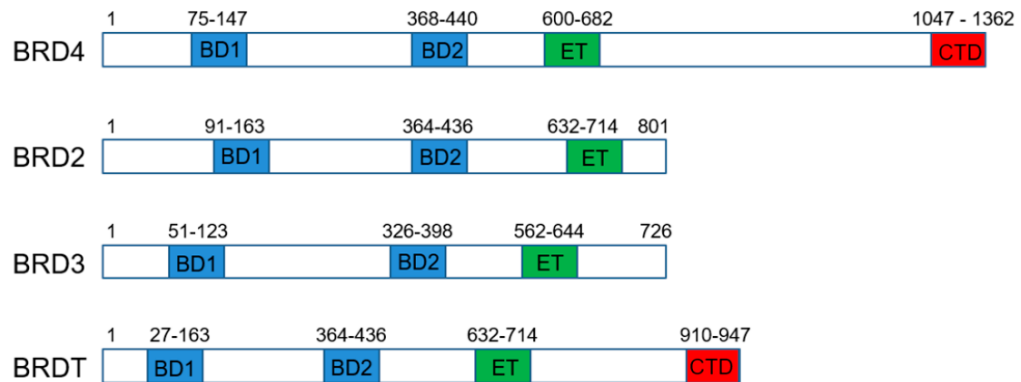


**Figure 1-3. The bromodomain and extraterminal domain (BET) family of proteins display common structural characteristics.** Each BET family member contains two N-terminal bromodomains (BD1 and BD2) and a conserved extraterminal (ET) domain.

Note: Adapted from “BET Family Protein BRD4: An Emerging Actor in NF $\kappa$ B Signaling in Inflammation and Cancer” by Hajmirza et al. 2018 *Biomedicines*. Permission obtained under the Creative Commons Attribution License (CC BY 4.0).

Of the BET family of proteins, BRD2, BRD3 and BRD4, are all ubiquitously expressed in mammalian tissues whereas BRDT expression is constrained to the testis [84, 85]. BRDT gene expression is silent during spermatogonia, but becomes expressed during spermatogenesis [86]. Interestingly, the K-Ac histone binding capacity of BRDT BD1 is dependent on the binding of two neighboring K-Ac residues whereas BD2 does not share this same characteristic [86]. While BRD3 is the least characterized BET family member, it has been reported to negatively regulate myogenic differentiation and bind to erythroid transcription factor GATA1 through BD1 [87, 88]. Additionally, BRD3 was reported to be essential for interleukin-1 $\beta$  (IL-1 $\beta$ ) or tumor necrosis factor- $\alpha$  (TNF- $\alpha$ )-induced matrix-degrading gene transcription in human chondrosarcoma cells [89].

BRD2, which primarily associates with acetylated H4K5 and H4K12 residues, is reported to stimulate E2F activity, promote E2F-dependent G1/S transition cell cycle progression and is involved in the production of proinflammatory cytokines [84, 88, 90]. In addition, BRD2 was found to associate with the *MYC* gene locus in H23 cells *in vitro* [91]. Generation of BRD2 null mice results in abnormalities in neural tube formation and is embryonic lethal whereas BRD2 heterozygotes display decreased number of GABAergic neurons and increased frequency of seizures [88, 92].

BRD4 is the most well-studied and characterized member of the BET family. Similar to BRD2 KO mice, BRD4 null mice are embryonic lethal [92]. BRD4 recognizes and binds K-Ac residues on the tails of histones 3 and 4 and promotes gene transcription by recruiting positive transcription elongation factor b (P-TEFb) [78, 93-95]. BRD4 then stimulates P-TEFb-mediated phosphorylation of RNA Polymerase II C-terminal domain (CTD) on Ser-2 to induce transcription elongation [78] (**Figure 1-3**). BRD4 binds to over 300 super-enhancer regions [85], including those in the *MYC* locus [96]. Further, BRD4 has been reported to remain associated with chromatin during mitosis indicating potential involvement in gene bookmarking and transcription acceleration post-mitosis [97]. BRD4 insulates chromatin from DNA damage signaling [98], is involved in telomere maintenance [93] and it contains an extraterminal domain which is involved in transcriptional regulation through interactions with many proteins such as lysine methyltransferase NSD3 and the chromosome remodeling complex SWIF/SNF [93]. Additionally, BRD4 has been reported to associate with numerous transcription factors (TFs) including p53, YY1, AP2, c-JUN, C/EBP $\alpha/\beta$  and the heterodimer c-MYC/MAX in a bromodomain (BD) independent manner [93]. Further, BRD4 has been shown to

contain a histone acetyltransferase (HAT) domain which acetylates histones H3 and H4 in patterns distinct from those catalyzed by established HATs [99]. BRD4 acetylates H3K122 which promotes nucleosome eviction, chromatin decompaction and increased transcription [93]. Additionally, BRD4 functions in Ig class switching as a repair complex adaptor of nonhomologous end joining (NHEJ) [100].

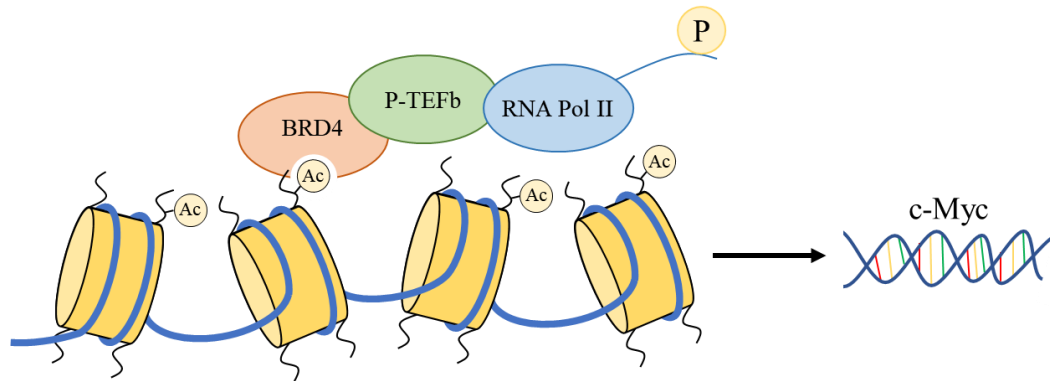


**Figure 1-4. BRD4 Upregulates c-Myc Expression.** BET protein BRD4 upregulates c-Myc through recruitment of positive transcription elongation factor b (P-TEFb). BRD4 then stimulates P-TEFb-mediated phosphorylation of RNA Polymerase II CTD on Ser-2 to induce transcription elongation of genes including c-Myc.

#### *Pharmacological inhibition of BET bromodomain proteins*

Collectively, the BET family of proteins regulate cell differentiation, cell cycle progression and growth. It is unsurprising that aberrant activity of these family members results in the development of cancer or other diseases [101]. The first indication that BET proteins were involved in cancer was the identification of a chromosomal translocation where BRD3 or BRD4 were fused with nuclear protein in testis (NUT) in NUT midline carcinoma (NMC) [81, 102]. Importantly, RNA interference (RNAi) of BRD2 and BRD4 in NMC arrests proliferation and induces differentiation, prompting investigation into BET bromodomain inhibition [81].

BET inhibitors (BETi) JQ1 and I-BET, developed in the laboratories of Dr. James Bradner and Dr. Alexander Tarakhovskiy, respectively, were first reported in 2010 [81, 103]. These structurally similar small molecule inhibitors of the BET family function as acetylated lysine (K-Ac) mimetics that bind to the K-Ac binding pocket of BET protein family members. JQ1 and I-BET are both pan-BET inhibitors and affect all three BET proteins simultaneously [104], though with varying binding affinities [81]. Binding of these compounds competitively inhibit the association of BET proteins with K-Ac residues of chromatin-associated histones and nuclear proteins, inhibiting recruitment of transcriptional complexes to genomic loci that mediate expression of multiple proteins [81, 85, 96, 105, 106]. As the specific substrates for each BRD containing protein is unknown, chromatin immunoprecipitation (ChIP) and binding assays were utilized to confirm BET family specificity of both JQ1 and I-BET [81, 103].

Since the initial report, JQ1 has displayed efficacy across a range of hematological malignancies driven by the BET-dependent oncogene, c-Myc [107]. JQ1 treatment reduces c-Myc expression which coincides with decreased tumor growth in xenograft models of leukemia and lymphoma while inducing cell cycle arrest and senescence in an *in vitro* model of multiple myeloma [96, 108]. In addition, JQ1 has shown efficacy in multiple solid tumor models including pancreatic cancer [109, 110], thyroid cancer [111] and renal cell carcinoma [112]. However, BET-dependent protein expression reportedly varies among tumor types [78, 81, 93, 113]. As such, BETi mechanism of action and subsequent therapeutic efficacy may be cancer or cell type dependent as treatment with BETi has shown therapeutic efficacy via downregulation of c-Myc, CDC25B, n-Myc and FOSL1 in multiple myeloma (MM), pancreatic ductal



adenocarcinoma (PDAC), neuroblastoma and non-small lung cancers, respectively [85, 110, 114, 115].

### *Targeting BET bromodomains in CCA*

There are several reasons why CCA could display sensitivity to BET bromodomain inhibition. First, biliary tract cancer tissue data from The Cancer Genome Atlas (TCGA) state that up to 40% of CCA cases display alterations in histone acetylation patterns [116]. Second, up to 94% of all CCA cases express elevated c-Myc protein [36]. Elevated c-Myc expression could be due to numerous factors including insertional mutagenesis, chromosomal translocations and gene amplifications, however, the mechanism through which c-Myc protein expression is elevated in CCA has not been established [117]. c-Myc upregulation or amplification results in cellular transformation, differentiation, cell growth, cell cycle progression and stem cell self-renewal [117-120]. c-Myc is a basic helix-loop-helix zipper transcription factor which heterodimerizes with binding partner, MAX, to bind to E-box enhancer sequences and regulate ~15% of the human genome [121]. During normal liver development, c-Myc protein expression is observed from 18 weeks gestation up to 5 years' postnatal [36]. TCGA data suggests high c-Myc protein expression in CCA (z-score threshold =  $\pm 2$ ) correlates with significantly shorter overall survival (30.3 months vs. 5.58 months) [122]. Third, in a CCA cell line model, Li et al. identified that downregulation of c-Myc through RNA interference (RNAi) significantly decreased invasiveness *in vitro*, however, the impact on cellular viability was not assessed [123]. Direct therapeutic inhibition of c-Myc is difficult as c-Myc is rarely mutated in cancer and the interaction between c-Myc and MAX lacks

recognizable and druggable motifs or clefts [124]. As discussed above, the BET family of proteins, particularly BRD2 and BRD4, have been reported to facilitate c-Myc transcription and treatment with a BETi, such as JQ1, decreases c-Myc expression in hematological malignancies and solid tumors [96, 108, 111, 125]. Knowing the majority of CCA cases express elevated c-Myc protein expression, this suggests the use of BETi may prove efficacious.

Given that the scarcity of available *in vitro* and *in vivo* CCA models hinder therapeutic development, we have developed five CCA PDX models comprising 4 dCCA (CCA1, CCA2, CCA3 and CCA4) and 1 iCCA (CCA5). Briefly, within 1-6 hours' post resection, primary tumor tissue was collected and subcutaneously (s.c.) implanted into the flank of SCID mice. Tumor pathology, assessed by Hematoxylin and Eosin (H&E) staining and the specific mutational status of *KRAS* codon 12, mutated in 17% of all CCA cases [16], were retained between primary tumor (F0) and first generation PDX models (F1). As stated above, c-Myc is expressed in ~94% of CCA patients, but is undetectable in normal tissue [36]. We observed relatively high c-Myc expression in three CCA PDX models (CCA1, CCA2 and CCA4) by immunohistochemistry (IHC) suggesting BETi may prove efficacious in these models [71].

To determine whether BETi inhibits c-Myc expression and tumor growth, we utilized two dCCA models, CCA1 and CCA2. Both models display similar growth patterns and express comparable levels of proto-oncogene, c-Myc. These models were s.c. implanted into the flank of SCID mice. Once tumors reached 200 mm<sup>3</sup>, mice were randomized into two groups where they were treated with either vehicle control (VC) or the non-toxic regimen of 50 mg/kg JQ1 via intraperitoneal (i.p.) injection once a day for

20 days. Tumors were measured non-invasively using calipers three times a week and tumor volume was calculated using the formula [126]:  $(Length \times Width \times Width) \times \left(\frac{\pi}{6}\right)$ . Post JQ1 treatment, CCA2 tumor volume was significantly decreased on day 20 (>50% reduction in volume compared to VC), the final day of treatment, whereas CCA1 tumor volume was not affected over the course of the study. At the end of the study and within 24 hours of final treatment, CCA1 and CCA2 mRNA/protein samples were snap frozen and tumor tissues were formalin fixed and paraffin embedded (FFPE). We wanted to assess whether this decrease in tumor volume was due to a decrease in tumor cell proliferation. Proliferation, assessed via IHC staining of proliferative marker, Ki67, was found to be significantly reduced in CCA2 post JQ1 treatment (~70% reduction in the percentage of Ki67 positive tumor cells), whereas no significant reduction was observed in CCA1 [71].

BET proteins regulate countless genes including Fos, JunB and c-Myc [93]. To assess the transcriptional impact of post JQ1 treatment in CCA2, we utilized NanoString nCounter analysis to investigate the expression of 230 PanCancer genes and to determine whether downregulation of specific targets, such as c-Myc, correspond to decreased tumor growth. NanoString analysis of CCA2 mRNA identified a  $\geq 2.4$ -fold down-regulation in cell cycle regulator genes *WEE1*, *CDK4*, *CDK6*, *E2F1*, *TP53* and *MYC*, potentially responsible for decreased proliferation. In addition, we observed down-regulation in c-Myc transcriptional targets *BRCA2*, *CHEK1* and *MSH2* and corroborated these results using IHC. This suggests that JQ1-mediated cytotoxicity in CCA2 may be potentiated through inhibition of c-Myc and c-Myc transcriptional targets. JQ1-insensitive model, CCA1, did not display a reduction in c-Myc protein nor its

downstream targets. JQ1 did not alter BRD4 protein expression in either CCA model, which is consistent with the literature [71, 109].

Additionally, we made the novel observation that JQ1 significantly increased the percentage of  $\gamma$ H2AX positive cells in CCA2. Phosphorylation of the histone H2A subtype, H2AX on residue Ser-139, forming  $\gamma$ H2AX, plays a central role in the assembly of DDR proteins at sites of single-strand breaks (SSBs) as well as double-strand DNA breaks (DSBs) [127]. Increased  $\gamma$ H2AX and cleaved caspase-3, indicative of apoptosis, was observed in our JQ1-sensitive model, CCA2, but not our JQ1-insensitive model, CCA1. Together, these data suggest that JQ1 may potentiate DNA damage and decrease tumor growth through downregulation of c-Myc and its gene targets involved in DDR including *BRCA2*, *CHEK1* and *MSH2* [71].

## Hypothesis and goals

CCA disease etiology is poorly understood and late stage detection along with rampant chemoresistance limits available therapeutic options. The current standard of care, resection followed by postoperative chemotherapy with gemcitabine and cisplatin, only prolongs survival by an additional 3-6 months over resection alone. In addition, the scarcity of available CCA models further hinder therapeutic development. There is an imperative need to develop additional therapeutic strategies for CCA. Based on our findings, we propose that JQ1 merits further investigation to study the efficacy of single and combination therapy for treatment of CCA. Our previous findings suggest JQ1-mediated increases in DNA damage, as observed as increases in  $\gamma$ H2AX positive cells, suggests JQ1 might further enhance the efficacy of additional therapeutics such as PARP inhibitors (PARPi) as cells harboring relatively high levels of DNA damage display increased PARPi sensitivity. We further hypothesized that JQ1-mediated reduction of c-Myc and its transcriptional target, Chk1, will sensitize CCA to gemcitabine. These studies pave the way for unique therapeutic intervention for CCA patients.

Chapter 2 will provide a comprehensive investigation into the novel combination of BETi with PARPi for use in CCA. Chapter 3 will provide insight into the combination of BETi with the current standard of care, gemcitabine. Chapter 4 will describe the development and characterization of *in vitro* and *in vivo* gemcitabine resistant (Gem<sup>R</sup>) models of CCA. Further, we will address BETi sensitivity in these resistant model systems. Using the methods described in this section, we can develop additional drug resistance models.

## CHAPTER 2

# THE COMBINATION OF BET AND PARP INHIBITORS IS SYNERGISTIC IN MODELS OF CHOLANGIOCARCINOMA

### Introduction

Cholangiocarcinoma (CCA) is an aggressive neoplasm arising from the epithelial layer of the biliary tract. It is predicted that primary hepatic malignancies, including hepatocellular carcinoma (HCC) and CCA, will become the second leading cause of cancer related deaths by 2030 [15]. CCA is diagnosed at late disease stage where the current standard of care, resection followed by postoperative chemotherapy with gemcitabine and cisplatin, is the primary therapeutic option. However, up to 90% of cases are ineligible for resection and postoperative chemotherapy only prolongs survival by an additional 3-6 months [11] which demonstrates the vital need to develop additional therapeutic options. Whole genome expression profiling has identified mutations in *IDH1/2* as well as *FGFR2* fusion proteins in CCA and clinical trials are currently ongoing to assess the efficacy of therapeutics targeting these alterations (NCT02989857 and NCT02150967, respectively). Unfortunately, *IDH1/2* mutations and *FGFR2* fusion proteins account for only 20% and 13% of iCCA cases, respectively, suggesting a minority of CCA patients would benefit from these targeted therapies [18, 128].

Upregulation of proto-oncogene c-Myc has been identified in up to 94% of CCA cases with no observed expression differences existing between CCA subtypes suggesting c-Myc inhibition could benefit the majority of CCA patients irrespective of subtype diagnosis [36].

Previously, we have investigated whether therapeutic inhibition of the BET family of proteins suppresses CCA growth *in vivo*. The BET family of proteins, including BRD2, BRD3, BRD4 and BRDT, are epigenetic readers which recognize and bind K-Ac residues on histone tails and other nuclear proteins [78]. Interactions of BET family members with K-Ac residues recruit transcriptional activators and repressors which influence transcriptional regulation and gene expression. Specifically, BET proteins BRD2 and BRD4 have been reported to associate with the *MYC* gene locus [91, 96]. The BET inhibitor JQ1 binds to the K-Ac binding pocket of the BET family of proteins preventing their interactions with nuclear proteins and indirectly reducing c-Myc transcription. JQ1 has shown efficacy in multiple solid tumor models including pancreatic cancer [105, 109, 110], thyroid cancer [111] and renal cell carcinoma [112], though, not strictly through c-Myc downregulation.

Initial results by our lab indicated that BET inhibition by JQ1 significantly decreased CCA PDX tumor volume and the expression of c-Myc as well as its transcriptional targets, specifically Chk1, while significantly increasing the percentage of cells positive for markers of apoptosis and DNA damage. However, tumor regression was not observed. The current literature suggests that cells harboring DNA repair deficiency or relatively high levels of DNA damage display increased sensitivity to PARP inhibitors [129-134] and Chk1 inhibition has been reported to potentiate the efficacy of PARPi in

gastric cancer [135]. Chk1 is a DNA damage response (DDR) factor involved in homologous recombination (HR) and plays a role in G2/M cell cycle progression. Upon DNA damage, ataxia telangiectasia and Rad3-related (ATR) phosphorylates Chk1 on Ser-317 and Ser-345 leading to its activation. Activated Chk1 subsequently phosphorylates cell cycle regulator, Cdc25a, resulting in its proteasomal-mediated degradation and subsequent slow or stalled DNA replication. Chk1 further phosphorylates and activates Wee1 kinase which phosphorylates and inhibits cell cycle regulator, Cdk1, preventing entry into mitosis. Chk1-deficient cells exhibit a decrease in the rate of DNA replication, may become stuck in S-phase with incomplete DNA replication and subsequently enter mitosis prematurely due to the lack of a Chk1-controlled G2/M checkpoint. As the cell continues to divide, they experience mitotic catastrophe [136].

Tumors deficient in cell cycle regulators and DDR factors are sensitive to PARPi [135, 137]. Inhibition of these factors in combination with PARPi can induce synthetic lethality, where the perturbation of two genes in combination, but not individually, result in cell death [138]. The first drug used to induce synthetic lethality was olaparib [139]. Breast cancer patients receive FDA-approved PARP1/2 inhibitor, olaparib, to induce synthetic lethality in tumors deficient or containing mutations in *BRCA1* or *BRCA2* [140, 141]. Under normal conditions, PARP1 is rapidly recruited to both single and double strand breaks where it catalyzes the addition of branched poly-ADP-ribose (pADPr) residues to acceptor proteins including histones and PARP1 [137]. These branches recruit hundreds of proteins to DNA break lesions which assist in DNA repair [137]. Olaparib and veliparib inhibit the catalytic activity of PARP1 and PARP2, trapping PARP on



DNA, unable to recruit additional DDR factors [139]. This results in stalled or collapsed replication forks and the generation of double-strand breaks (DSBs) [139] which are not repaired via HR due to the deficiencies or mutations in *BRCA1/2* [138]. These reports as well as our observation that JQ1 induces DNA damage and decreases Chk1 expression in our CCA PDX model, led us to investigate whether PARPi in combination with BETi could prove efficacious in CCA.

In this chapter, we address the effect of BETi on cell viability, colony forming potential, DNA damage and the expression of DNA repair protein, Chk1, using CCA *in vitro* models. Second, we assess the efficacy of BETi in combination with PARPi *in vitro*. Third, we investigate whether the efficacy of BETi with a PARPi is through inhibition of a single BET family member through development of stable KKU-055 knockdown (KD) models of BRD2 and BRD4. Each model was exposed to BETi and PARPi both as single agents and in combination. Finally, we assessed the efficacy of JQ1 in combination with olaparib using a cell line-derived xenograft model of KKU-055 implanted into SCID mice.

## **The combination of BET and PARP inhibitors is synergistic in models of cholangiocarcinoma [142]**

Note: Adapted from “The combination of BET and PARP inhibitors is synergistic in models of cholangiocarcinoma.” by Fehling et al. 2019 Cancer Letters. Permission obtained under the Creative Commons Attribution License (CC BY).

DOI: 10.1016/j.canlet.2019.10.011

Samuel C. Fehling,<sup>1,#</sup> Aubrey L. Miller,<sup>1,#</sup> Patrick L. Garcia,<sup>1</sup> Rebecca B. Vance,<sup>1</sup> and  
Karina J. Yoon<sup>1,\*</sup>

<sup>1</sup>Department of Pharmacology and Toxicology, University of Alabama at Birmingham, Birmingham, AL, USA

<sup>#</sup>Contributed equally to the project

**Running Title:** BETi + PARPi induces synergistic cytotoxicity in cholangiocarcinoma

**Key Words:** cholangiocarcinoma, BET inhibitors, PARP inhibitors, c-Myc, RNAi, combination indices

**\*Corresponding author:** Karina J. Yoon, Department of Pharmacology and Toxicology, University of Alabama at Birmingham, VH 241, 1670 University Blvd, Birmingham, AL 35294

Email: [kyoon@uab.edu](mailto:kyoon@uab.edu)

**Conflicts of Interest:** The authors declare no potential conflict of interest.

**Grant Support:** This work was supported by the National Institutes of Health (National Cancer Institute) grants R21CA205501 and R01CA208272 (K.J.Y).

Word count: 4,017 (excluding abstract, references and figure legends)

Abstract: 176/185

Figures: 6 Figures, 1 Supplemental Table, 5 Supplemental Figures

## **ABSTRACT**

Our previous finding that the BET inhibitor (BETi) JQ1 increases levels of the DNA damage marker  $\gamma$ H2AX suggested that JQ1 might enhance the sensitivity of tumor cells to PARP inhibitors (PARPi), which are selectively toxic to cells that harbor relatively high levels of DNA damage. To address this hypothesis, we evaluated the effect of a BETi (JQ1 or I-BET762) combined with a PARPi (olaparib or veliparib) in KKU-055 and KKU-100 cholangiocarcinoma (CCA) cell lines and of JQ1 with olaparib in a xenograft model of CCA.

Each combination was more effective than any of the four drugs as single agents. Combination indices ranged from 0.1 to 0.8 at the ED50 for all combinations, indicating synergy and demonstrating that synergy was not limited to a specific combination. Mechanistically, downregulation of BETi molecular targets BRD2 or BRD4 by shRNA sensitized CCA cells to BETi as single agents as well as to the combination of a BETi + a PARPi.

Our data indicate that combinations of a BETi with a PARPi merit further evaluation as a promising strategy for CCA.

## **Highlights**

- BETi + PARPi exerts synergistic cytotoxicity in cholangiocarcinoma *in vitro*.
- JQ1 + olaparib inhibits growth of cholangiocarcinoma tumors in a preclinical model.
- shRNA-mediated decrease in BETi molecular targets BRD2 or BRD4 increases the sensitivity of cholangiocarcinoma cells to BETi  $\pm$  PARPi.

## 1. Introduction

Cholangiocarcinoma (CCA) is a rare, aggressive neoplasm arising from the epithelial layer of the biliary tract [11], and is the second most common primary hepatic malignancy after hepatocellular carcinoma [12]. CCA is usually diagnosed at late disease stage and present with symptoms including jaundice, fatigue and abdominal pain [12]. Patients who receive the current standard of care, resection followed by gemcitabine with or without cisplatin, see the greatest survival benefit [11]. However, 90% of patients are ineligible for resection [48]. The 5-year survival for patients with CCA is ~30% [12], with relapse occurring 2-3 years following resection [12] and development of chemoresistance [48, 60, 61]. This study focuses on identifying a novel combination of agents with synergistic cytotoxicity *in vitro* and anti-tumor activity *in vivo* in CCA.

BET inhibitors (BETi) such as JQ1 and I-BET762 function as acetylated lysine (K-Ac) mimetics that bind to the K-Ac binding pocket of BET protein family members (BRD2, BRD3, BRD4 and BRDT) to competitively inhibit the association of BET proteins with K-Ac residues of chromatin-associated histones, thereby inhibiting recruitment of transcriptional complexes to genomic loci that mediate expression of multiple proteins. Proteins whose expression is BET-dependent reportedly vary among tumor types [78, 81, 93, 113].

We recently reported the efficacy of the BETi JQ1, with two patient-derived xenograft (PDX) models of CCA [71]. We observed that 50 mg/kg JQ1 administered daily to mice bearing CCA2 tumors suppressed tumor growth ( $P < 0.001$ ). We also observed a concomitant decrease in expression of c-Myc and its transcriptional target Chk1. Further, we made the novel observation that JQ1 increased levels of the DNA

damage marker  $\gamma$ H2AX and induced apoptosis as reflected by increases in cleaved caspase-3 and cleaved PARP. Because PARP inhibitors (PARPi) are known to be selectively toxic to cells deficient in DNA double strand break repair [129-134] and with elevated levels of DNA damage, we hypothesized that BETi + PARPi would exert synergistic cytotoxicity. The current study evaluates the potency of the BETi (JQ1 or I-BET762) with the PARPi (olaparib or veliparib) in CCA cell lines and efficacy of JQ1 + olaparib in a xenograft model of CCA. This study also determines the effect of level of expression of BETi targets BRD2 or BRD4 on the potency of BETi  $\pm$  PARPi in CCA cells.

## **2. Materials and Methods**

### **2.1 Ethics statement**

Animal protocols were approved by the University of Alabama at Birmingham Animal Care and Use Committee.

### **2.2 Cell Culture and Compounds**

KKU-055 (JCRB1551) and KKU-100 (JCRB1568) cholangiocarcinoma cell lines were purchased from the Japanese Cancer Research Resources Bank (JCRB) (National Institute of Biomedical Innovation, Japan). Cells were cultured in DMEM (Fisher Scientific, Waltham, MA, USA) supplemented with 10% fetal bovine serum (Atlanta Biologicals, Flowery Branch, GA, USA) and 2 mM L-glutamine (Fisher Scientific). Both CCA cell lines were tested for mycoplasma using MycoAlert<sup>TM</sup> PLUS Mycoplasma Detection Kit (Lonza, Walkersville, MD, USA) and were negative. JQ1 (HY-13030, MedChem Express, Monmouth Junction, NJ, USA), I-BET762 (HY-13032, MedChem

Express), olaparib (HY-10162, MedChem Express) and veliparib (ABT-888, Enzo Life Sciences, Farmingdale, NY, USA) were prepared as solutions in DMSO. Final concentrations of DMSO in *in vitro* experiments were <0.3%.

### **2.3 In Vitro Cell Viability Assay**

Cell viability assays were carried out as described previously [105, 143]. Briefly, cells were seeded in 96-well plates and allowed to adhere for 24 hours. Serial dilutions of BET inhibitors (JQ1 or I-BET762) and/or PARPi (olaparib or veliparib) were added to the culture medium for 96 hours. AlamarBlue (Fisher Scientific) was added in accordance with manufacturer instructions. Fluorescence was read on a PerkinElmer Victor X5 microplate reader at 560nm excitation and 590nm emission wavelengths. IC<sub>50</sub> values were calculated using GraphPad Prism 7.0 (San Diego, CA, USA). Combination indices (CI) were calculated using CompuSyn 1.0 software with values <1.0 indicating synergism [144]. Three independent experiments were performed with quadruplicated wells.

### **2.4 Clonogenic Assay**

**Survival Fraction (Fig.1):** Cells were plated in a confluency between 50 to 150 cells and 100 to 1,500 cells into 6-well plates for KKU-055 and KKU-100, respectively, and allowed to adhere overnight. Cells were exposed to drug for 72 hours, washed with PBS, given fresh non-drug containing media and allowed to grow for an additional 14 days (total of 18 days in culture). Cells were then formalin fixed and stained with 0.025% crystal violet. Colonies of greater than 50 cells were counted. Control (DMSO) plating efficiency (PE) was calculated using:  $(PE = \frac{\# \text{ colonies formed}}{\# \text{ of cells seeded}} \times 100)$ . Percent clonogenic

survival, the number of colonies that formed after treatment, was calculated using the equation: (% *Clonogenic Survival* =  $\frac{\# \text{ of colonies formed after treatment}}{\# \text{ of cells seeded} \times PE} \times 100$ ) [145].

**Colony formation (Fig.3):** Two thousand K KU-055 or K KU-100 cells were plated per well in 24-well plates and allowed to adhere overnight. Cells were exposed to DMSO (<0.3%) or various concentrations of JQ1 (0.1  $\mu$ M, 1  $\mu$ M or 10  $\mu$ M), olaparib (0.1  $\mu$ M, 1  $\mu$ M or 10  $\mu$ M), or JQ1 + olaparib (1:1) for 72 hours, washed with PBS, and grown in drug-free media for an additional 14 days. Cells were then formalin fixed and stained with 0.025% crystal violet. Plates were imaged using an Epson scanner. Three independent experiments were performed.

## 2.5. qRT-PCR Assay

Trizol-chloroform extraction was used to isolate total RNA. qRT-PCR was performed as previously described [105, 110]. Three independent experiments were performed.

Primers used are listed in **Table S1**.

## 2.6 Immunoblotting Analysis

Cell lysates were prepared in NP-40 (Fisher Scientific) or RIPA buffer (MilliporeSigma, St. Louis, MO, USA) containing protease inhibitors (Fisher Scientific). Primary antibodies used were: c-Myc (5606S, Cell Signaling, 1:1,000), GAPDH (2118S, Cell Signaling, 1:1,000), vinculin (v4505, MilliporeSigma, 1:10,000), Chk1 (A300-298AT, Bethyl, 1:5,000), BRD2 (5848, Cell Signaling, 1:1,000), BRD4 (13440, Cell Signaling, 1:1,000), cleaved PARP (5625, Cell Signaling, 1:1,000) and  $\gamma$ H2AX (9718S, Cell Signaling, 1:1,000). Secondary antibodies used were: HRP goat anti-rabbit IgG (6721, Abcam, 1:50,000) and HRP anti-mouse IgG (7076, Cell Signaling, 1:5,000).

Immunoblots were quantitated using ImageStudio Lite 5.2. Data were first normalized to respective loading controls and then to DMSO control.

## **2.7 Cell Cycle Analysis**

KKU-055 cells were exposed to JQ1 (30  $\mu$ M), olaparib (5  $\mu$ M), veliparib (10  $\mu$ M), JQ1 (30  $\mu$ M) + olaparib (5  $\mu$ M) or JQ1 (30  $\mu$ M) + veliparib (10  $\mu$ M) for 48 hours. Cells were harvested, centrifuged and added drop-wise into ice-cold 70% ethanol while vortexing. The cells were incubated at 4°C overnight. The next day, cells were centrifuged, and the precipitate was incubated with propidium iodide-Triton X-100 resuspension buffer in PBS (0.1% Triton X-100, 200  $\mu$ g/ml RNAase A, and 20  $\mu$ g/ml propidium iodide) for a minimum of an hour prior to running flow cytometry [146]. Flow cytometry was carried out at the UAB flow cytometry core using a FACSCalibur (BD Biosciences, San Jose, CA, USA) flow cytometry machine. Twenty-thousand cells were analyzed using FlowJo™ (v10.6.1, BD Biosciences) and the Dean-Jett-Fox univariate model.

## **2.8 Chromatin Immunoprecipitation (ChIP)**

ChIP was performed as previously described [105]. Briefly, digested cellular chromatin was immunoprecipitated with a ChIP grade anti-BRD4 or anti-BRD2 antibody (Cell Signaling) or normal rabbit IgG (Cell Signaling) as a negative control. DNA coprecipitated with BRD4 or BRD2 was quantitated using qRT-PCR with primers that bind to a locus in the promoter region of the *MYC* gene. Data were analyzed relative to the percent input (2%). Two independent experiments were performed. Primers used are listed in **Table S1**.



## 2.9 Generation of Stable shRNA-Transfected Cell Lines

Stable shRNA gene knockdown was performed as previously described [105]. K KU-055 cells were plated at low confluency (10%) in 6-well plates and transfected with MISSION shRNA targeted for BRD2, BRD4 (MilliporeSigma) or the control shRNA for GFP (Addgene, Watertown, MA, USA) using PEI (Polysciences Inc., Warrington, PA, USA) for 8 hours. Cells were then washed with PBS and grown in fresh media for 72 hours. Transfected cell populations were selected using puromycin (7.5  $\mu\text{g/ml}$ ) (BML-GR312, Enzo Life). The sequences of shRNA oligonucleotides are listed in **Table S1**.

## 2.10 *In Vivo* Drug Efficacy Studies

CB17<sup>-/-</sup> female SCID mice (4-week-old) were purchased from Taconic Farms (Newton, MA, USA) and housed in the AAALAC accredited vivarium at University of Alabama at Birmingham Research Support Building. K KU-055 cells ( $5 \times 10^6$ ) in 100  $\mu\text{L}$  PBS were injected into each flank via subcutaneous injection. Mice bearing bilateral tumors were randomized into four groups of 5 mice/group when tumors reached  $\sim 200 \text{ mm}^3$  [105, 110, 143]. Tumor numbers were VC = 6, JQ1 = 8, olaparib = 7 and JQ1 + olaparib = 9. Intraperitoneal injections of JQ1, olaparib or the combination was given daily for 21 days. Drug solutions were prepared in DMSO and diluted 1:10 into 10%  $\beta$ -cyclodextrin (MilliporeSigma). 10%  $\beta$ -cyclodextrin dissolved in sterile water was utilized for JQ1 and sterile PBS was used for olaparib [105]. Olaparib was administered 30 minutes prior to JQ1 [105]. Tumor volumes were measured three times a week using digital calipers, and tumor volume calculated using the formula  $v = (\pi/6) \times d^3$ . Results were normalized to Day 0 of drug treatment, and data are expressed as normalized tumor volume. Average mouse body weight (g) was assessed three times a week using a scale throughout the study. Data

are presented as mean  $\pm$  S.E.M. Statistics were done using two-way analysis of variance (ANOVA) using GraphPad Prism 7.

### 2.11 Statistical Analysis

All statistical analyses were performed using GraphPad Prism 7 software (SanDiego, CA, USA) [105, 110]. Statistical significance was calculated using one-way or two-way ANOVA.  $P \leq 0.05$  was considered significant.

## 3. Results

### 3.1 JQ1 inhibits CCA cell viability and clonogenic potential.

Human cholangiocarcinoma (CCA) cell lines KKU-055 and KKU-100 represent the CCA subtypes intrahepatic and hilar, respectively [147]. Both cell lines have epithelial-like morphology and proliferate *in vitro* in discrete patches. Cell doubling time was ~24 hours and ~42 hours for KKU-055 and KKU-100 cells, respectively. KKU-100 cells express mutant *KRAS*<sup>G12D</sup>, while KKU-055 cells express wild type *KRAS* (**Fig.1a**). Neither KKU-055 nor KKU-100 cells harbored mutations in six previously characterized hot spots for *BRCA1* mutations or in four hotspots for *BRCA2* mutations (**Fig.1a, Fig.S1**) [148]. Because the overall goal of this study was to use CCA models to evaluate the efficacy of BET inhibitors as single agents and in combination, we compared the potency of the BET inhibitors JQ1 and I-BET762 in cell viability and clonogenic assays *in vitro*, assessed efficacy *in vivo*, and determined the effect of these agents on c-Myc expression and function, using CCA cell lines and a xenograft model.

To assess the potency of JQ1 *in vitro*, we exposed CCA cell lines to a range of JQ1 concentrations for 72 to 120 hours and assessed cell viability using alamarBlue assays (**Figs.1b, 1c**). JQ1 decreased cell viability in a dose-dependent manner, and IC<sub>50</sub>s

depended on duration of exposure (**Fig. 1d**). To also assess the effect of JQ1 on clonogenic potential, we exposed cells to JQ1 for 72 hours, and then propagated them in drug-free medium for an additional 14 days, as detailed in Materials and Methods (**Figs. 1e, 1f**). Under these conditions, JQ1 decreased the clonogenic potential at micromolar concentrations ( $P < 0.0001$ ) (**Fig. 1g**). Representative images are shown in **Figs. 1h and 1i**.

### **3.2 JQ1 decreases expression of c-Myc and its downstream target Chk1.**

Published studies suggest that c-Myc expression depends, at least in part, on BET protein function [107]. Therefore, we evaluated the effect of JQ1 on c-Myc expression. Further, because Chk1 expression was downregulated by JQ1 in an *in vivo* model of CCA [71] and is regulated by c-Myc [149, 150], we assessed the effect of JQ1 on Chk1 expression, as a measure of c-Myc function.

qRT-PCR assays showed that exposure to  $10^{-6}$  -  $10^{-4.5}$  M JQ1 for 72 hours decreased expression of *MYC* mRNA by >50% ( $P < 0.01$ ) in both cell lines, compared to DMSO controls (**Figs. 2a, 2b**). JQ1 decreased expression of the c-Myc transcriptional target *CHEK1* mRNA up to ~60% ( $P < 0.05$ ) and by >80% ( $P < 0.001$ ) in KKU-055 and KKU-100 cells, respectively (**Figs. 2a, 2b**). We corroborated qRT-PCR results by performing immunoblots (IB) to assess expression of c-Myc and Chk1 protein. JQ1 decreased c-Myc and Chk1 expression in a dose dependent manner, with >50% inhibition of both proteins in both cell lines following exposure to  $10^{-6}$  -  $10^{-4.4}$  M JQ1 for 72 hours (**Figs. 2c-2f**). As we previously reported that JQ1 inhibited the expression of BRCA2 [71], we evaluated the effect of JQ1 on the expression of *BRCA2* in KKU-055 and KKU-100 cell lines *in vitro*. We found that JQ1 (1-32 $\mu$ M for 72 hours) inhibited the expression of *BRCA2* mRNA in KKU-100 cells >90% ( $P < 0.0001$ ), and JQ1 (32 $\mu$ M for 72 hours)

inhibited the expression of *BRCA2* mRNA in KKU-055 cells by ~50% ( $P < 0.01$ ) (**Fig. S2**).

Based on our previous finding that JQ1 also increases levels of the DNA damage marker  $\gamma$ H2AX in pancreatic cancer models and a PDX model of CCA [71, 105], we next assessed the effect of JQ1 on levels of this DNA damage marker, using assay conditions similar to those under which we observed decreases in c-Myc and Chk1. We exposed CCA cells to  $10^{-6}$  -  $10^{-4.4}$  M JQ1 for 48-72h and determined levels of expression of  $\gamma$ H2AX by immunoblot. JQ1 increased the levels of  $\gamma$ H2AX in a dose-dependent manner (**Figs. 2g-2j**). In light of reports in the literature documenting that DNA repair deficiency or relatively high levels of DNA damage sensitize tumor cells to PARP inhibitors [105, 135, 138, 140, 141], we next assessed the potency of BET inhibitors in combination with PARP inhibitors.

### **3.3 BETi + PARPi exerts synergistic cytotoxicity in CCA cell lines.**

We assessed the potency of the BET inhibitors JQ1 or I-BET762 in combination with PARP inhibitors olaparib or veliparib in alamarBlue cell viability assays. We exposed KKU-055 and KKU-100 cells to a range of BETi + PARPi ( $10^{-7}$  M to  $10^{-4}$  M) as single agents or the combination at a 1:1 ratio for 96 hours (**Figs. 3a, 3b**). JQ1 or olaparib as a single agent was more potent than I-BET762 or veliparib in both CCA cell lines. We also calculated combination indices (CI) using CompuSyn (1.0) software, based on Chou and Talalay methodology (**Figs. 3c, 3d**). Combination indices (CI) ranged from 0.03106 to 0.48820 for KKU-055 cells (**Fig. 3c**) and from 0.03511 to 0.83408 for KKU-100 cells (**Fig. 3d**). All indices indicate synergy for all four combinations evaluated. Using clonogenic assays, we observed that the combination of JQ1 + olaparib was more

effective than either drug alone in both CCA cell lines (**Figs. 3e, 3f**). Further, we evaluated the impact of JQ1 ± olaparib or veliparib on levels of protein markers for DNA damage ( $\gamma$ H2AX) and apoptosis (cleaved PARP). As shown in **Fig.S3**, the combinations increased the levels of cleaved PARP >100-fold compared to DMSO controls. We also performed cell cycle analysis using JQ1 ± olaparib or veliparib (**Fig.S4**). Results agree with data in the literature demonstrating that JQ1 arrests cells in G1; olaparib arrests cells in G2; and veliparib has little, if any, effect on cell cycle distribution [151, 152]. Interestingly, the combination of JQ1 + olaparib arrests cells in G2- similar to olaparib as a single agent and in contrast to JQ1 as a single agent. JQ1 + veliparib had little effect on cell cycle distribution.

Together, the data demonstrate that combinations of a BETi with a PARPi are synergistic in K KU-055 and K KU-100 CCA cells, and that observed synergy was seen with multiple combinations of these classes of agents.

### **3.4 c-Myc expression was BET-dependent.**

Studies in the literature report that BRD4 and BRD2 contribute to regulation of c-Myc expression in multiple cancer types including lung cancer cells, acute leukemia cells, and multiple myeloma cells [91, 107, 153]. We hypothesized that down-regulation of either of these BET proteins would decrease c-Myc expression. To downregulate BRD2 or BRD4 expression, we transfected CCA cells with a shRNA plasmid targeting BRD2 (shBRD2), BRD4 (shBRD4) or GFP (shGFP, negative control). When BRD2 expression was decreased by >95%, we observed a concomitant >95% decrease in c-Myc expression (**Fig. 4a**). When BRD4 was decreased by >98%, c-Myc expression is also

down-regulated by ~50% (**Fig. 4b**). Our data indicate that c-Myc expression is BRD2- or BRD4-dependent in CCA tumor cells, a novel finding in CCA cells.

### **3.5 Decreased expression of BRD2 or BRD4 increased the sensitivity of CCA cells to BET inhibitors.**

To assess whether contrasting levels of expression of JQ1 targets BRD2 or BRD4 affected the sensitivity of CCA cells to JQ1, we exposed shBRD2 and shBRD4 transfectants to a range of JQ1 concentrations ( $10^{-7}$  M to  $10^{-4}$  M) for 96 hours and compared the viability of shBRD2 and shBRD4 transfectants to control shGFP transfectants (**Fig. 4c**). We observed that shRNA-transfected KKU-055 cells with lower levels of BRD2 or BRD4 were ~18- to 29-fold more sensitive to JQ1 than shGFP control transfectants (**Figs. 4c, 4e**). Similar results were observed with the BET inhibitor I-BET762 (**Figs. 4c, 4e**). BET inhibitors target BET family members BRD2, BRD3, BRD4 and BRDT, with each protein likely contributing to the expression of a different subset of gene products. When one protein is downregulated, the others still comprise molecular targets for BET inhibitors. We interpret the data to indicate that cells with low level BET protein expression are more sensitive to BET inhibitors than cells with high level BET expression. We also observed that shBRD2 transfectants showed less than 3-fold increase in sensitivity to olaparib and veliparib, and shBRD4 transfectants less than 1.5-fold increase in sensitivity to these PARPi (**Figs. 4d, 4f**). When combined with PARPi, neither shBRD2 nor shBRD4 transfectants reflect the synergistic cytotoxicity we observed with BETi + PARPi in parental CCA cells. Another question we asked was whether BRD2 and BRD4 can complement each other to induce c-Myc expression. We performed chromatin immunoprecipitation (ChIP) assays to examine whether

downregulation of one BET protein would alter the binding between the other BET protein and the promoter region of *MYC*. As shown in Supplemental **Fig.S5**, we observed no compensatory binding of BRD2 to the *MYC* promoter when BRD4 is downregulated and no compensatory binding of BRD4 to the *MYC* promoter when BRD2 is downregulated.

### **3.6 shBRD2 and shBRD4 transfectants were more sensitive to BETi + PARPi combinations than control transfectants.**

Results with JQ1 in shBRD2 and in shBRD4 transfectants predicted that a combination of BETi+ PARPi might be more effective than either drug alone. Data assessing the effect of JQ1 + olaparib, JQ1 + veliparib, I-BET762 + olaparib and I-BET762 + veliparib on cell viability in shBRD2 (**Fig. 5a**) and shBRD4 (**Fig. 5b**) were consistent with this hypothesis. We calculated CI values and shown in **Figs. 5c, 5d**. CI values indicated synergy for all combinations (**Figs. 5c, 5d**). We also evaluated the impact of JQ1 ± PARPi (olaparib or veliparib) on levels of cleaved PARP, a marker for apoptosis, in shBRD4 and shBRD2 cells (**Figs. 5e, 5f**). The data show that in both shBRD4 and shBRD2 transfected cells, JQ1 increased the levels of the apoptosis marker cleaved PARP. Further, JQ1 + olaparib or veliparib increased levels of this apoptotic marker more than JQ1 as a single agent. We concluded that CCA cells expressing relatively low levels of BRD2 or BRD4 were more sensitive to the effects of a BETi + PARPi than cells expressing higher levels of these BET proteins, as reflected by induction of increased levels of cleaved PARP.

### **3.7 JQ1 + olaparib suppresses tumor growth in an *in vivo* KKV-055 CCA model.**

Data above indicate that, of the combinations evaluated, K KU-055-derived tumors would be predicted to be sensitive to the combination of JQ1 + olaparib. We addressed this hypothesis directly by injecting 5 million K KU-055 cells, suspended in PBS, into the flanks of SCID mice (Taconic Farms), and allowed tumors of ~200mm<sup>3</sup> volume to develop. Tumor-bearing mice were injected intraperitoneally with vehicle control (VC), 50 mg/kg JQ1, 50 mg/kg olaparib or the combination once a day for 21 days. We observed significant differences between each treatment group and the VC group (P<0.001). Importantly, we also observed that JQ1 + olaparib was more effective than JQ1 or olaparib as a single agent (P≤0.05) (**Fig.6a**), with the nontoxic regimen used for the study (**Fig.6b**). We also verified that, consistent with *in vitro* data, JQ1 and the combination of JQ1 + olaparib decreased *MYC* expression compared to VC (P<0.0001) (**Fig. 6c**). Interestingly, olaparib reduced the expression of *MYC* mRNA compared to vehicle control. This finding is consistent with previous reports [154, 155]. Potential explanations for this observation include: 1) PARP-1 could bind directly to the promoter region of *MYC* to regulate *MYC* expression; or 2) PARP-1 could interact with E2F-1, and this interaction increases promoter activity of E2F-1 and expression of E2F-1 responsive genes such as *MYC*.

*In vitro* and *in vivo* data indicate that the combination of BETi + PARPi merits further investigation as potentially effective treatment for patients with CCA tumors.

#### **4. Discussion**

This study assesses the anti-proliferative effects of BET bromodomain inhibitors (JQ1 or I-BET762) in combination with PARP inhibitors (veliparib or olaparib) in CCA models *in vitro* and the efficacy of JQ1 + olaparib in a CCA xenograft model. Each



combination of a BETi + PARPi induced synergistic cytotoxicity ( $CI < 1$ ) in both KKU-055 and KKU-100 CCA cell line models. Further, the combination of JQ1 + olaparib had a greater effect than either drug alone in the *in vivo* model. Mechanistically, JQ1 reduced expression of c-Myc and Chk1 in dose and time dependent manners *in vitro*. The data demonstrate that BRD2 and BRD4 contribute to the regulation of c-Myc expression in CCA cells, a novel finding in CCA tumor models, and that JQ1 + olaparib have efficacy in preclinical models of this tumor type.

The likely mechanism by which JQ1 decreases c-Myc expression has been postulated to involve competitive inhibition of the K-Ac binding function of the BET protein BRD4 [96, 104, 111]. It follows that inhibition of Chk1 expression would be due to inhibition of c-Myc expression, since *CHEK1* is a c-Myc transcriptional target. Relevant to these findings, data in the Cancer Genome Atlas (TCGA) suggest that a relatively high c-Myc expression (z-score threshold =  $\pm 2$ ) in CCA tumors correlates with shorter overall survival in CCA ( $P < 0.001$ ) [122], suggesting c-Myc as a potential therapeutic target. Our data demonstrate that JQ1 decreased c-Myc expression, and we propose that BETi may have utility for treatment of this tumor type.

Of particular interest was our finding that shRNA transfectants expressing relatively low levels of BRD2 or BRD4 were relatively sensitive to JQ1 or I-BET762. These data suggest that tumor cells with lower BRD2 or BRD4 expression may be more sensitive to BET inhibitors than cells expressing relatively high levels of these BETi molecular targets. Notably, JQ1 and I-BET762 inhibit all four BET protein family members (BRD2, BRD3, BRD4, BRDT) [104], with varying binding affinities [81]. We postulate that the efficacy of JQ1 depends on simultaneous inhibition of BRD2 and

BRD4 in CCA tumors. We further observed that shBRD2 model shows a <3-fold increase in sensitivity to olaparib and veliparib, while shBRD4 model shows <1.5-fold increase in sensitivity to these PARPi. However, when exposed to PARPi neither shBRD2 nor shBRD4 transfectants recapitulate the synergistic cytotoxicity like phenotype observed in parental KKU-055 when exposed to the combinations of BETi with PARPi. Generation of a model with decreased expression of all BET targets, BRD2, BRD3 and BRD4, simultaneously may address our current hypothesis that the observed potency of BETi and synergy between BETi and PARPi depends upon inhibition of multiple members of the BET family as opposed to a single member.

Our data demonstrate that JQ1 decreased c-Myc and increased the levels of DNA damage and apoptosis, and that BETi JQ1 sensitized CCA tumor cells to PARPi olaparib. Further, in addition to inhibiting expression of c-Myc and Chk1, BETi also decreases levels of multiple genes including Ku80, RAD51, BRCA1, WEE1, CDC25B or TOPBP1, that contribute to the DNA damage repair and response [71, 105, 110, 156]. The resulting increase in the levels of DNA damage and apoptosis would be anticipated to sensitize tumor cells to PARPi. Our data indicate that BETi in combination with PARPi may be a promising strategy for CCA.

**Acknowledgement**

This work was supported by the National Institutes of Health (National Cancer Institute) grants R21CA205501 and R01CA208272 (K.J.Y). We thank Dr. Banchob Spira (Khon Kaen University) for establishment of both KKU-055 and KKU-100 CCA cell lines.

Fig 1

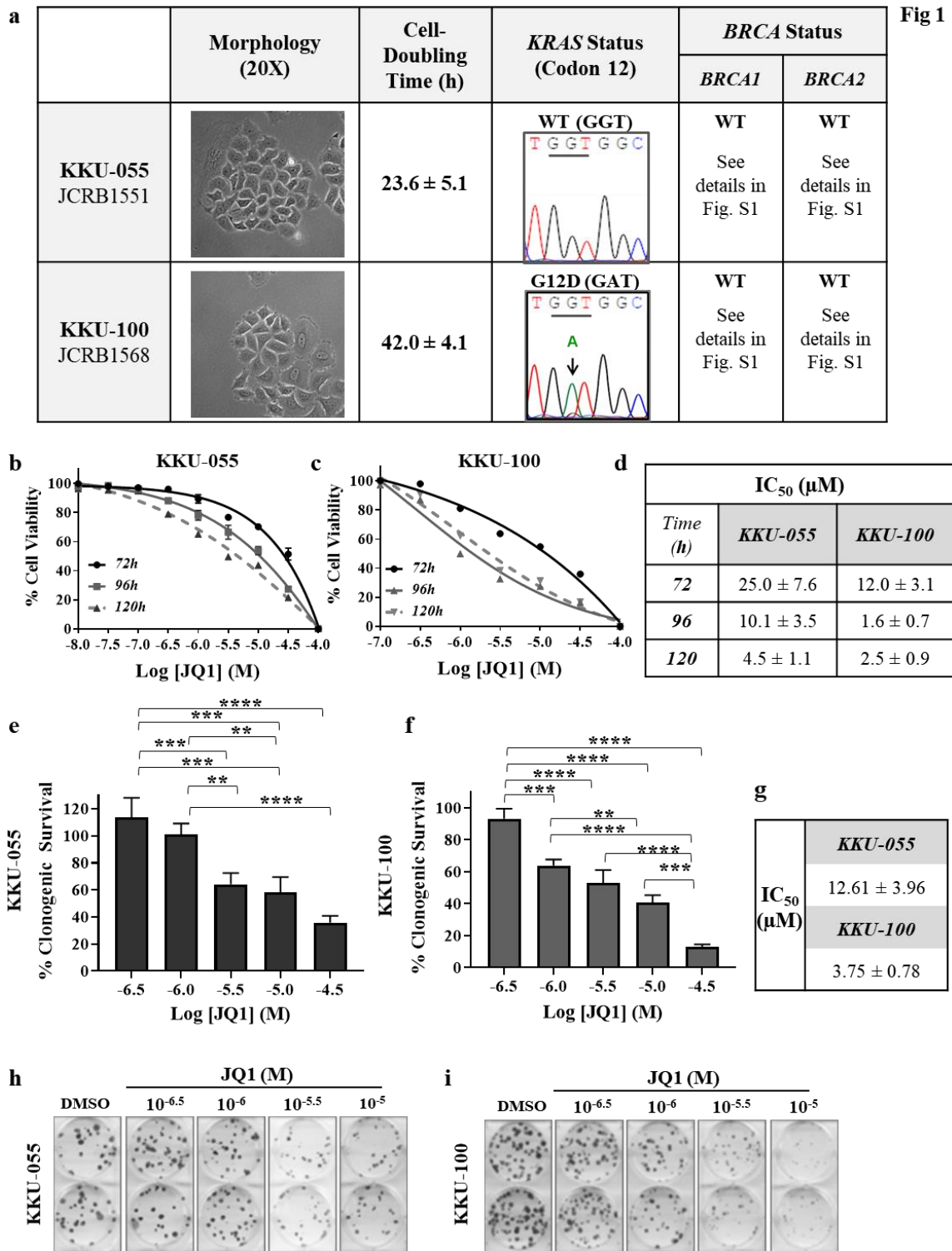


Figure 2

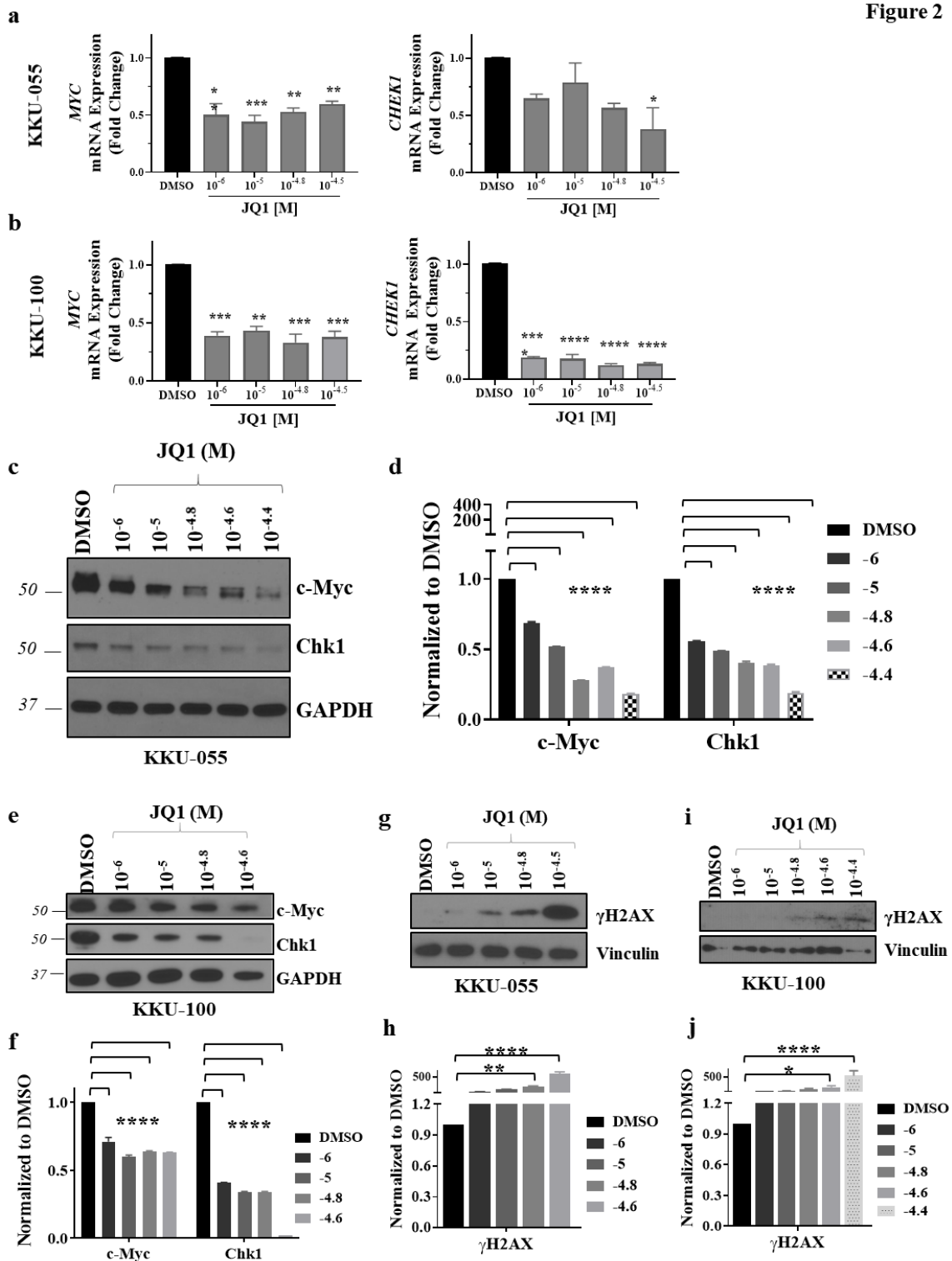


Figure 3

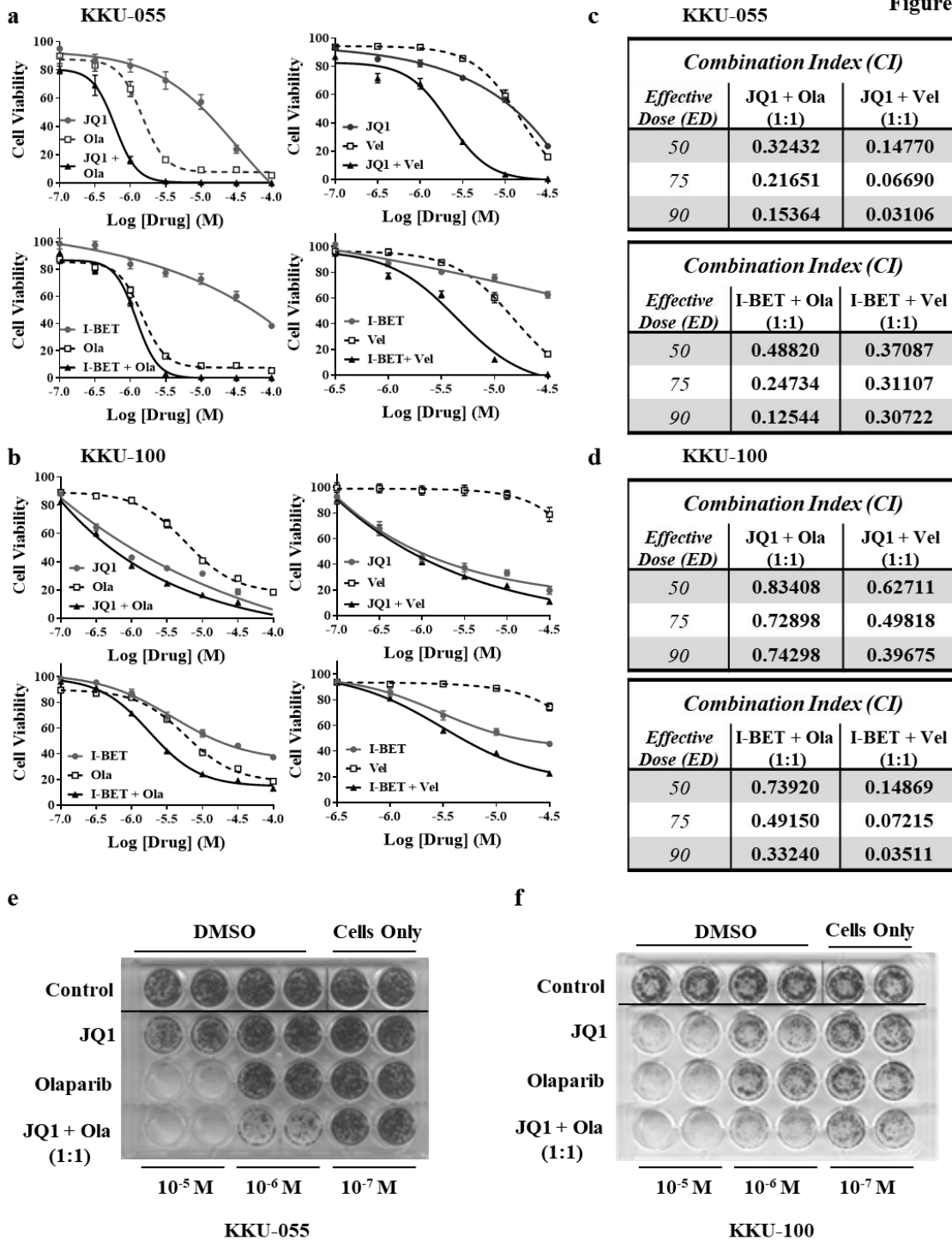


Figure 4

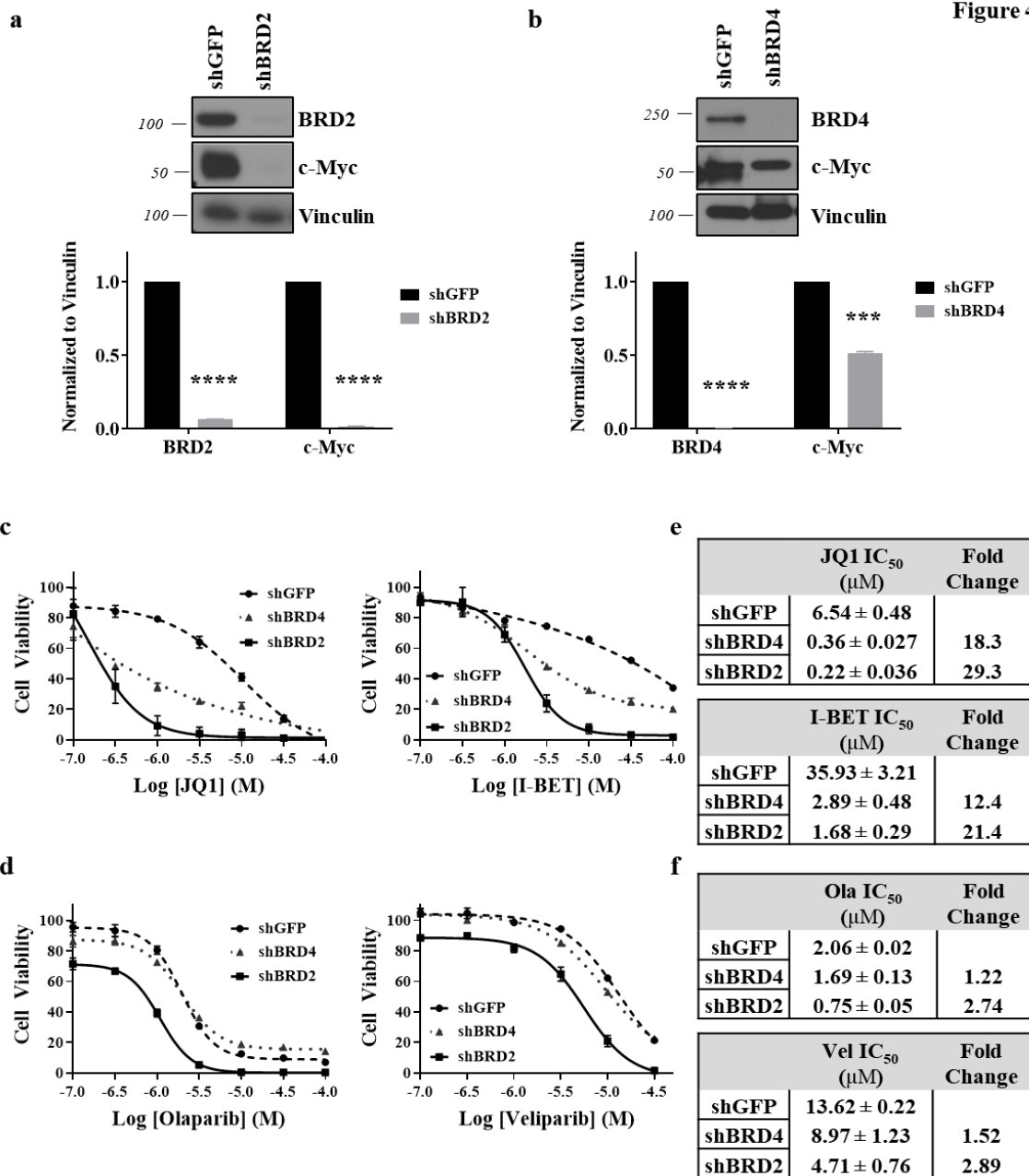


Figure 5

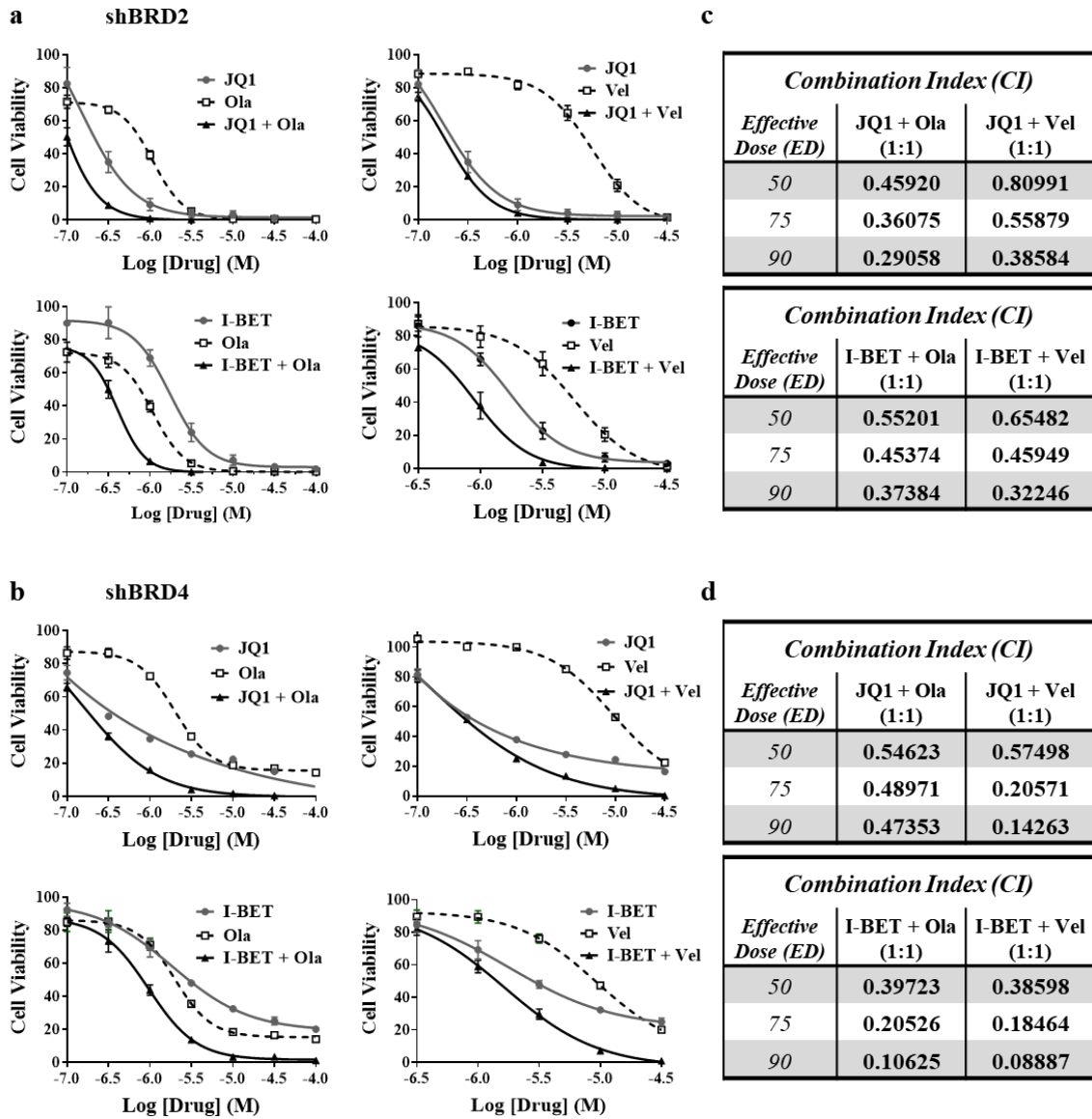
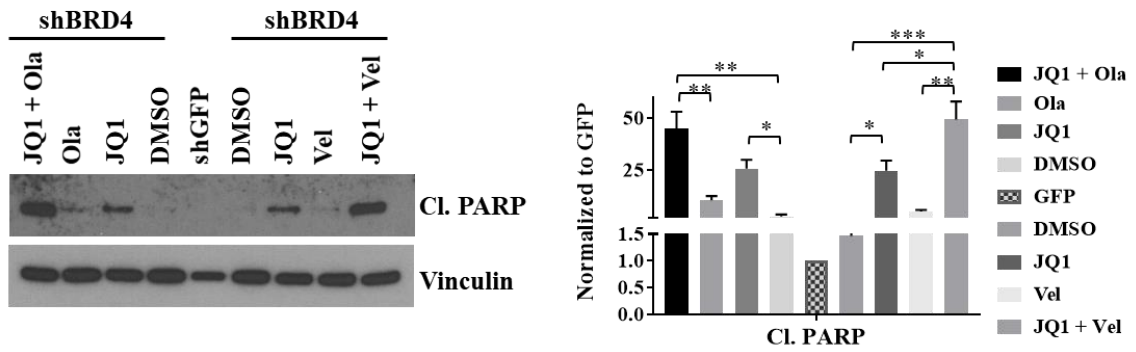




Figure 5

e



f

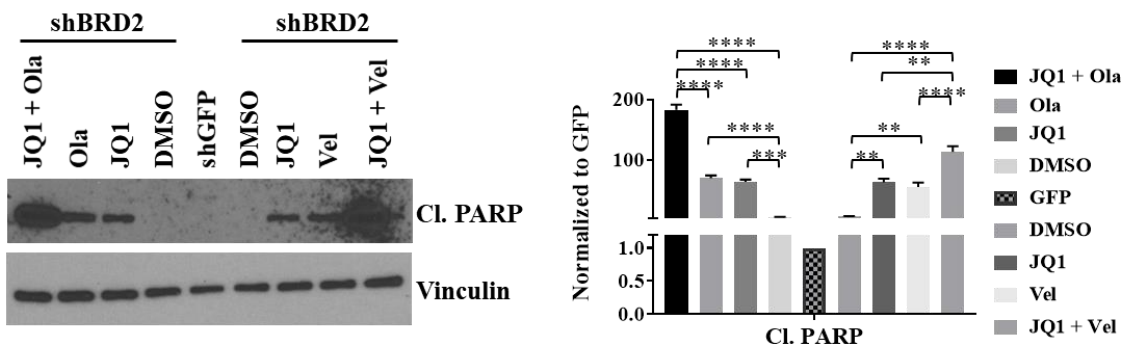
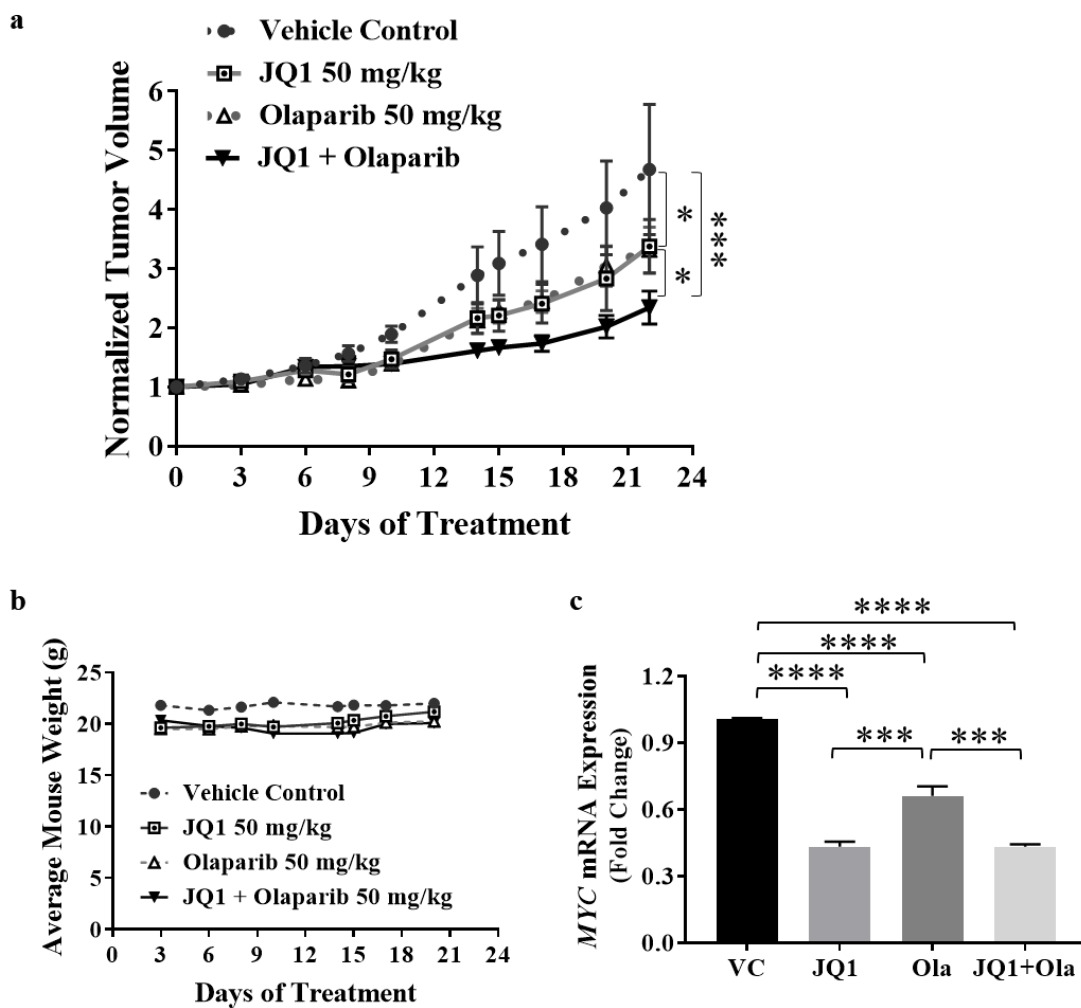


Figure 6



## Figure Legends

**Figure 1. JQ1 decreases the viability and the clonogenic potential of KKKU-055 and KKKU-100 CCA cells *in vitro*.** (a) Morphology, cell-doubling time, *KRAS* codon 12 status and *BRCA1/2* mutational status of KKKU-055 and KKKU-100 CCA cell lines. KKKU-055 (b) or KKKU-100 (c) cells were exposed to the indicated concentrations of JQ1 for 72, 96, or 120 hours. Cell viability was assessed by alamarBlue assays and data are presented as mean  $\pm$  S.E.M. A minimum of three independent experiments were performed. (d) A table with JQ1 concentration required to inhibit cell viability by 50% ( $IC_{50}$ ) from **Fig.1b** and **Fig.1c**. (e - i) JQ1 inhibited the growth of colony in clonogenic assays. Between 20 and 150 KKKU-055 cells (e) or 100 and 1,500 KKKU-100 cells (f) were plated, exposed to various concentrations of JQ1 or DMSO for 72 hours, washed with PBS and fresh media added. Cells were incubated in drug-free media for another 14 days. Colonies of >50 cells were counted and quantitated using DMSO as 100%. Three independent experiments were performed.  $IC_{50}$  values were calculated and shown in (g). Representative images of clonogenic assays for KKKU-055 (plating cell number = 50) (h) and KKKU-100 (plating cell number = 200) (i) cell lines are shown.

**Figure 2. JQ1 decreases the expression of c-Myc and its transcriptional target Chk1 in both KKKU-055 and KKKU-100 CCA cell lines.** qRT-PCR shows that JQ1 inhibited the mRNA expression of *MYC* and *CHEK1* in KKKU-055 (a) and KKKU-100 (b) cell lines. (c) & (e) JQ1 inhibited expression of c-Myc and Chk1 protein in KKKU-055 (c) and KKKU-100 (e) cell lines. (d) & (f) Immunoblot data in (c) and (e) were quantitated as percent DMSO using ImageStudio Lite (LI-COR Biosciences) and are reported as bar graphs

mean  $\pm$  S.E.M. **(g-j)** JQ1 increased the level of  $\gamma$ H2AX, a marker of DNA damage, in KKU-055 **(g)** and KKU-100 **(i)** cell lines. **(h) & (j)** Immunoblot data in **(g)** and **(i)** were quantitated as described above and are reported as bar graphs (mean  $\pm$  S.E.M.). Analysis was done by one-way ANOVA (\*P<0.05, \*\*P<0.01, \*\*\*P<0.001, \*\*\*\*P<0.0001).

**Figure 3. A combination of BET and PARP inhibitors are synergistic in KKU-055 and KKU-100 CCA cell lines.** KKU-055 **(a)** and KKU-100 **(b)** CCA cell lines were exposed to 1:1 concentration ratio of BET inhibitors (JQ1 or I-BET762)  $\pm$  PARP inhibitors (olaparib or veliparib) for 96 hours. Cell viability was assessed by alamarBlue as described in Materials and Methods. Data are presented as mean  $\pm$  S.E.M, in a minimum of three independent experiments with quadruplicated wells. Combination indices (CI) were calculated for **(a)** and **(b)** using CompuSyn and presented at ED50, ED75 and ED90 in **(c)** for KKU-055 and **(d)** for KKU-100 cell lines. Clonogenic assays for KKU-055 **(e)** and KKU-100 **(f)** cell lines were done as described in Materials and Methods, and representative images are shown. Three independent experiments were performed.

**Figure 4. Decreased expression of BRD2 (shBRD2) or BRD4 (shBRD4) increased the sensitivity of KKU-055 cells to BET inhibitors (JQ1 or I-BET762) or PARP inhibitors (olaparib or veliparib).** Expression of c-Myc was BRD2 **(a)** or BRD4 **(b)** dependent. Quantitation of immunoblots (IB) were done and presented as bar graphs below each IB blots. We used shRNA (see details in Materials and Methods and Table S1 for sequences) to decrease expression of BRD2 (shBRD2) or BRD4 (shBRD4) in KKU-

055 cells. (c) Decreased expression of BRD2 or BRD4 increased the sensitivity of KKU-055 cells to JQ1 (left panel) or I-BET762 (right panel). IC<sub>50</sub> values were calculated using GraphPad Prism 7 and shown in (e). (d) Decreased expression of BRD2 or BRD4 increased the sensitivity of KKU-055 cells to olaparib (left panel) or veliparib (right panel). IC<sub>50</sub> values were calculated using GraphPad Prism 7 and shown in (f). A minimum of three independent experiments were performed and IC<sub>50</sub> values presented as mean ± S.E.M.

**Figure 5. shBRD2 and shBRD4 transfectants were more sensitive to combinations of BETi + PARPi than shGFP (control) transfectants.** Simultaneous exposure of BET inhibitors (JQ1 or I-BET762) + PARP inhibitors (olaparib or veliparib) induced synergistic cytotoxicity in BRD2 downregulated (shBRD2) (a) or BRD4 downregulated (shBRD4) (b) KKU-055 cells. Cells were exposed to the indicated concentrations of BETi ± PARPi (1:1 ratio) for 96 hours, alamarBlue solution was added, and fluorescence read. Data were normalized to DMSO controls at each time point, with control values = 100%. Each point represents the mean of quadruplicated wells from a minimum of three independent assays. Data are presented as mean ± S.E.M. Combination indices (CI) were calculated for (a) and (b) using CompuSyn and presented at ED50, ED75 and ED90 in (c) for shBRD2 and (d) for shBRD4 KKU-055 cells. (e) shBRD4 or (f) shBRD2 transfectants were exposed to the IC<sub>50</sub> values (listed in Figs.4e and 4f) of JQ1, olaparib, veliparib, JQ1 + olaparib or JQ1 + veliparib for 48 hours. Cell lysates were harvested and immunoblots performed. Quantitation and statistics are shown on the right side of the panel. The values presented as mean ± S.E.M analyzed using Prism (one-way ANOVA).

\*P<0.05, \*\*P<0.01. \*\*\*P<0.001, \*\*\*\*P<0.0001.

**Figure 6. JQ1 + olaparib suppresses tumor growth in an *in vivo* K KU-055 CCA**

**model. (a)** Tumor-bearing mice were treated with JQ1 (50 mg/kg daily, i.p.), olaparib (50 mg/kg daily, i.p.), or JQ1 + olaparib, or vehicle (VC daily) for 21 days. Tumor volumes were measured three times per week. Tumor volumes (mm<sup>3</sup>) were normalized to tumor volumes on Day 0 for each tumor. P values were calculated by two-way ANOVA followed by Tukey posttest. \*P≤0.05, \*\*\*P<0.001. **(b)** Average body weight per mouse per each treatment group during the treatment period was within 13% for all treatment groups. Average mouse weight was calculated by weighing each cage of mice and dividing by the number of mice per cage. **(c)** qRT-PCR shows that JQ1 as well as JQ1 + olaparib inhibited the mRNA expression of *MYC* in an *in vivo* K KU-055 CCA model. A minimum of three biological experiments were performed and values presented as mean ± S.E.M. \*\*\*P<0.001, \*\*\*\*P<0.0001.

(a)

	Site	Sequence	KKU-055	KKU-100
			Mutation	Mutation
<b>BRCA1</b>	BRCA1 c.68-69delAG	TCTTAGAGTGTCC	WT	WT
	BRCA1 c.4188 (p.Q1396H)	TGAAGCAGAGGGA	WT	WT
	BRCA1 c.1630 C>G (p.Q544E)	ATGGTCAAGTGAT	WT	WT
	BRCA1 c.4810 C>T (p.Q1604*)	TTCCCCAATTGAA	WT	WT
	BRCA1 c.4186 C>T (p.Q1396*)	TGAAGCAGAGGGA	WT	WT
	BRCA1 c.5266 C>T (p.Q1756*)	AATCCCAGGACAG	WT	WT
<b>BRCA2</b>	BRCA2 c.2808-2811delACAA	GATAAACAAGCAAC	WT	WT
	BRCA2 c.2830 A>T (p.K944*)	CAATTAAAAAAGA	WT	WT
	BRCA2 c.9154 C>T (R3052W)	AGCCACGGGAGCC	WT	WT
	BRCA2 c.9976 A>T (K3326*)	CATTAAAAAATT	WT	WT

(b)

Gene	Primer Sequence	Product Size
<b>BRCA1 c.68-69delAG</b>	Fwd 5'-GAAGTTGTCATTTTATAAACCTTT-3'	258 bp
	Rev 5'-TGCTTTTCTTCCCTAGTATGT-3'	
<b>BRCA1 c.4188 (p.Q1396H)</b>	Fwd 5'-CACCAAGTCTTTGAAATGTGCC-3'	540 bp
	Rev 5'-TCTGGATTTTCGAGGTCCTC-3'	
<b>BRCA1 c.1630 C&gt;G (p.Q544E)</b>	Fwd 5'-ACAAGAGCGTCCCCTCACAA-3'	390 bp
	Rev 5'-AGCGCATGAATATGCCTGGTA-3'	
<b>BRCA1 c.4810 C&gt;T (p.Q1604*)</b>	Fwd 5'-GAGGGAACCCCTTACCTGGA-3'	242 bp
	Rev 5'-AATTCTGGCTTCTCCCTGCTC-3'	
<b>BRCA1 c.4186 C&gt;T (p.Q1396*)</b>	Fwd 5'-CACCAAGTCTTTGAAATGTGCC-3'	540 bp
	Rev 5'-TCTGGATTTTCGAGGTCCTC-3'	
<b>BRCA1 c.5266 C&gt;T (p.Q1756*)</b>	Fwd 5'-AAATATGACGTGTCTGCTCCACT-3'	259 bp
	Rev 5'-TCTTACAAAATGAAGCGGCC-3'	
<b>BRCA2 c.2808-2811delACAA</b>	Fwd 5'-TGAGCTGTTGCCACCTGAAA-3'	505 bp
	Rev 5'-TGGACCTAAGAGTCCTGCCC-3'	
<b>BRCA2 c.2830 A&gt;T (p.K944*)</b>	Fwd 5'-TGAGCTGTTGCCACCTGAAA-3'	505 bp
	Rev 5'-TGGACCTAAGAGTCCTGCCC-3'	
<b>BRCA2 c.9154 C&gt;T (R3052W)</b>	Fwd 5'-TCAACAACCTACCGGTACAAACCT-3'	337 bp
	Rev 5'-CCAAGTGGTAGCTCCAATAA-3'	
<b>BRCA2 c.9976 A&gt;T (K3326*)</b>	Fwd 5'-ACATTTGTTTCTCCGGTGC-3'	349 bp
	Rev 5'-ATTCTTCCGTAAGGCTGG-3'	

\* Indicates stop codon

**Figure S1. BRCA1 and BRCA2 mutational status and primers used.** (a) *BRCA1* and *BRCA2* mutational status of KKU-055 and KKU-100 cells are shown. Six mutational hot spots for *BRCA1* and four for *BRCA2* were assessed using DNA isolated from these two CCA cell lines. (b) Primer sets we used to detect the total of 10 hot spots of *BRCA1/2* mutations are listed. These hot spots were determined from data available in the COSMIC database (*J.G. Tate et al., COSMIC: the Catalogue Of Somatic Mutations In Cancer, Nucleic Acids Res, 47 (2019) D941-D947.*) and correlated with known pathogenic mutations identified in breast-ovarian cancer documented in the literature (*R. Janavičius, Founder BRCA1/2 mutations in the Europe: implications for hereditary breast-ovarian cancer prevention and control, EPMA J, 1 (2010) 397-412.*).

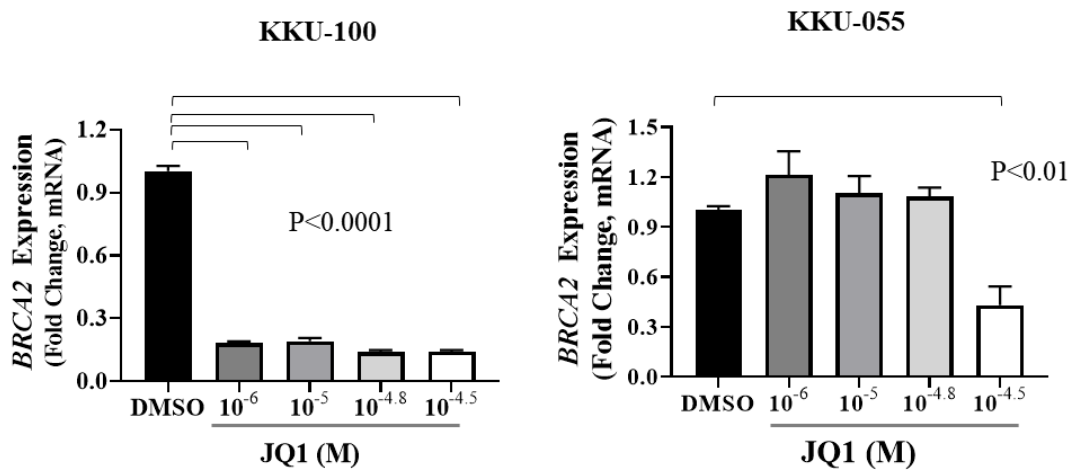


**Figure S2. JQ1 decreases the mRNA expression of *BRCA2* in KKU-100 cells.** KKU-100 or KKU-055 cells were exposed to DMSO (control) or various concentrations of JQ1 ( $10^{-6}$  –  $10^{-4.5}$  M) for 72 hours. RNA extracted and qRT-PCR performed to assess mRNA expression of *BRCA2*. qRT-PCR data show that JQ1 inhibited the mRNA expression of *BRCA2* in KKU-100 cells ( $P < 0.0001$ ). JQ1 inhibited the mRNA expression of *BRCA2* only at the highest concentration ( $10^{-4.5}$  M) of JQ1 ( $P < 0.01$ ). Experiments were performed a minimum of two independent experiments. Analysis was done by one-way ANOVA.



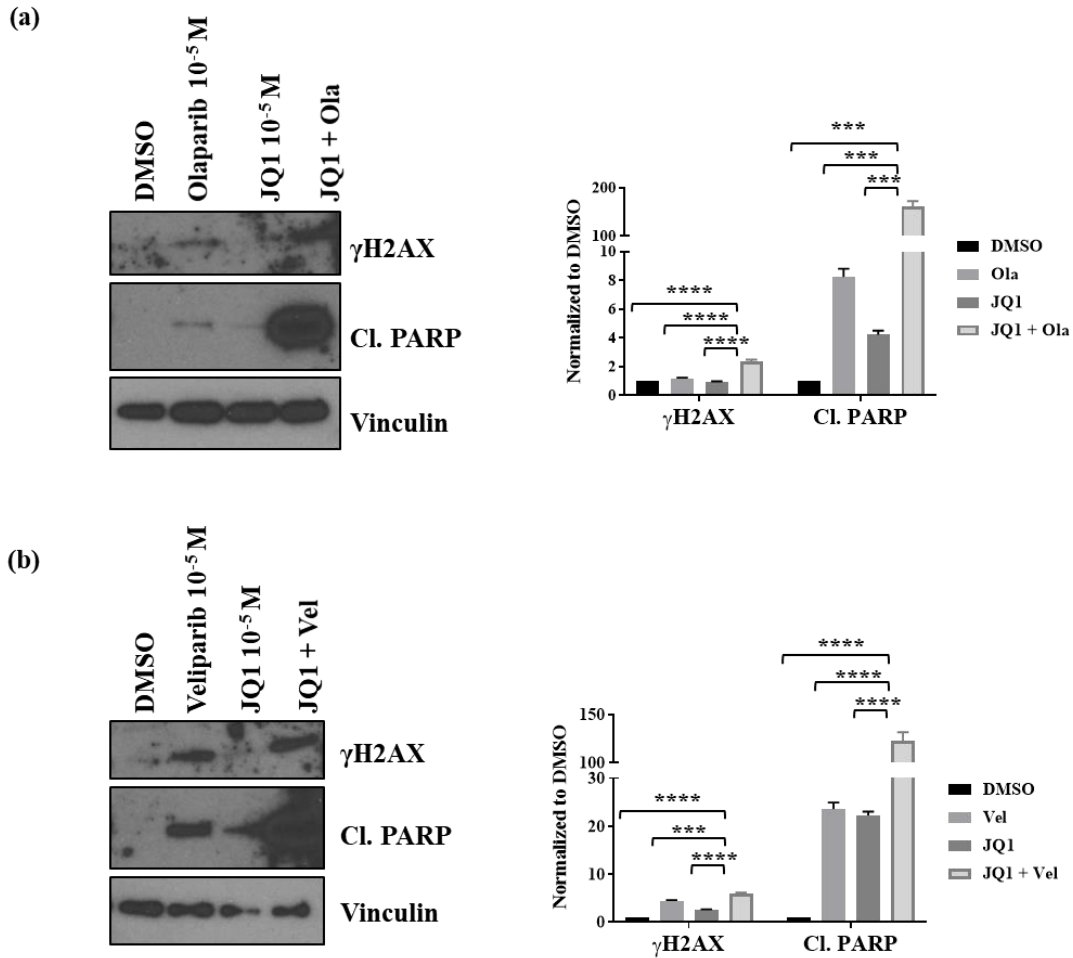


**Figure S3. JQ1 + PARP inhibitors (olaparib or veliparib) increased the levels of DNA damage marker  $\gamma$ H2AX and apoptotic marker cleaved PARP (Cl. PARP) in K KU-055 CCA cells.** (a) Cells were exposed to DMSO, JQ1 ( $10^{-5}$  M), olaparib ( $10^{-5}$  M) or JQ1 + olaparib for 48 hours or (b) to DMSO, JQ1 ( $10^{-5}$  M), veliparib ( $10^{-5}$  M) or JQ1 + veliparib for 24 hours. Cell lysates were collected and immunoblotted to detect  $\gamma$ H2AX and cleaved PARP. Vinculin was used as loading control. Analysis was done by one-way ANOVA using Prism 7. \*\*\* $P < 0.001$ , \*\*\*\* $P < 0.0001$ .

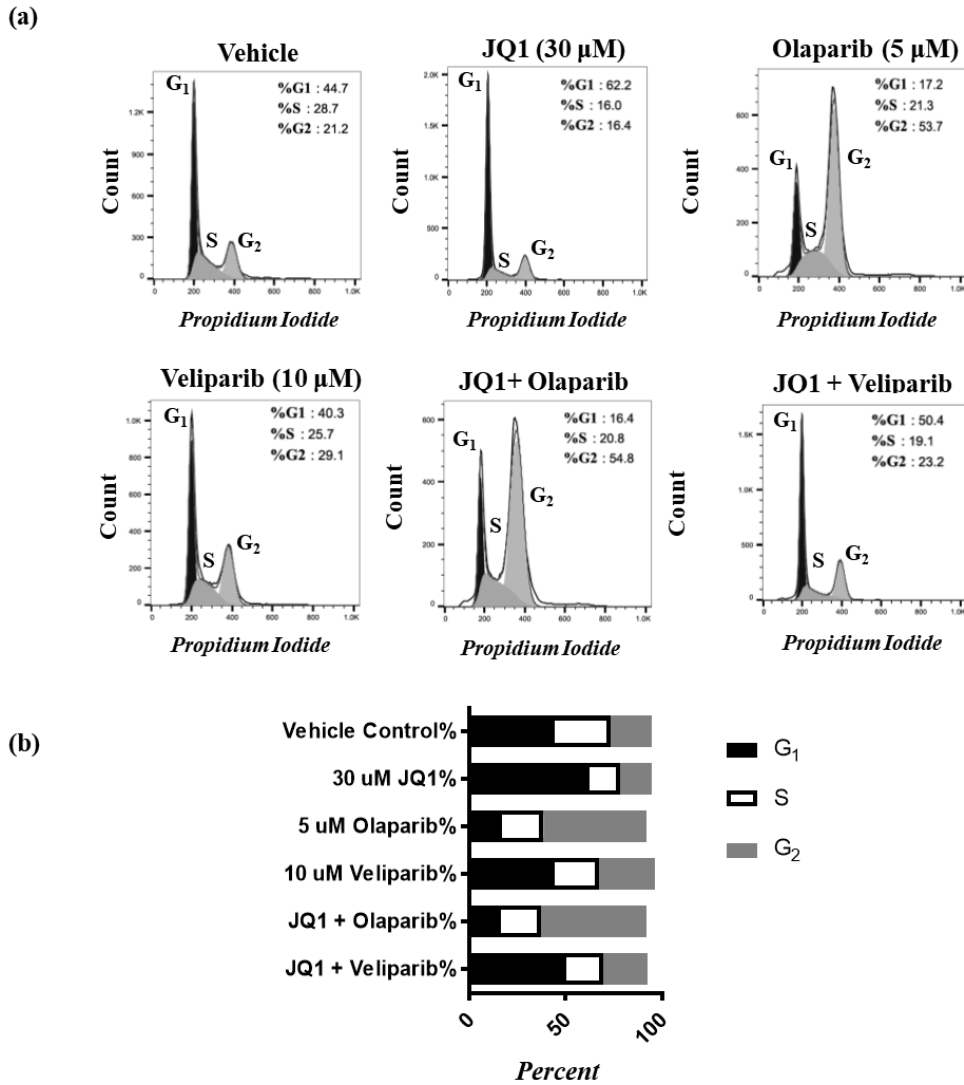


**Figure S4. Cell cycle analysis of JQ1 ± PARPi.** (a) KKU-055 (300,000 cells/well) were plated in 6-well plates and allowed to adhere overnight. The following day cells were treated with JQ1 (30 μM), olaparib (5 μM), veliparib (10 μM) or JQ1+olaparib or JQ1+veliparib for 48 hours. The cells were trypsinized and harvested for cell cycle analysis (C. Riccardi, I. Nicoletti, *Analysis of apoptosis by propidium iodide staining and flow cytometry*, *Nat Protoc*, 1 (2006) 1458-1461). Flow cytometry was carried out at the UAB flow cytometry core using a FACSCalibur (BD Biosciences, San Jose, CA) flow cytometry machine and 20,000 cells were collected for analysis. Cell cycle analysis was performed using FlowJo™ (v10.6.1, BD Biosciences) using the Dean-Jett-Fox model. (b) Percent of each stages of cell cycle is compared as bar graph. The graph was generated using GraphPad Prism (version 7).

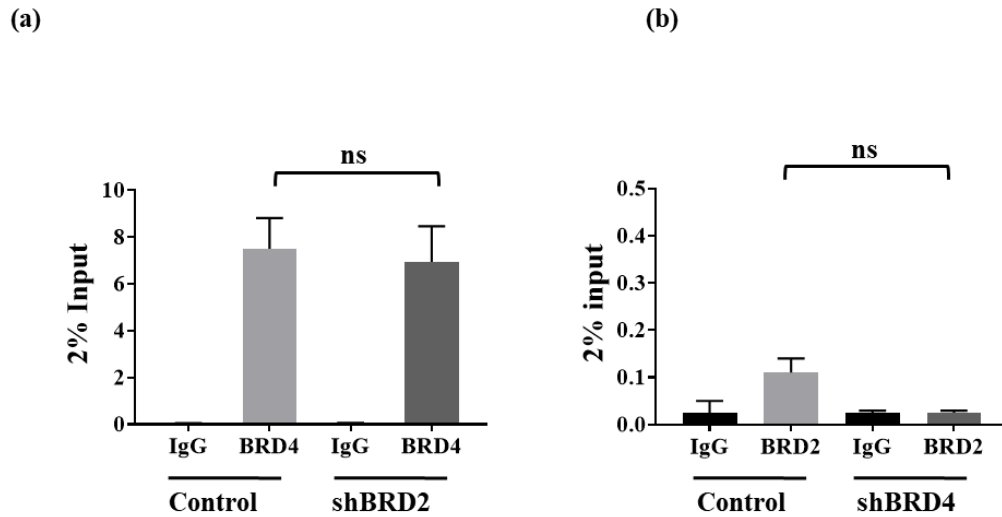


**Figure S5. No compensatory binding of BRD4 (a) or BRD42 (b) to the *MYC* promoter when BRD2 (a) or BRD4 (b) is downregulated.** ChIP assays were performed to determine whether BRD2 and BRD4 can complement each other, to induce *MYC* expression at the promoter. The experiments were done using shBRD2, shBRD4 transfectants, the parental KKU-055 cells (control), and a *MYC* primer set designed to bind to the promoter region of the *MYC* gene. Detailed methods are in the Materials and Methods section. Two independent experiments were performed, and 2% input values presented as mean  $\pm$  S.E.M. analyzed using Prism (one-way ANOVA). ns: not statistically significant.

**Table S1. Sequences of primers and oligonucleotides used for the study.**

Gene	Forward (5' to 3')	Reverse (5' to 3')
<i>MYC</i>	CGACTCTGAGGAGGAACAAG	GTGATCCAGACTCTGACCTTT
<i>CHEK1</i>	ATATGAAGCGTGCCGTAGACT	TGCCTATGTCTGGCTCTATTCTG
<i>GAPDH</i>	AACATCATCCCTGCTTCCAC	GACCACCTGGTCCTCAGTGT

shRNA Oligo	Sequence (5' to 3')
shGFP	GCAAGCTGACCCTGAAGTTCAT
shBRD2	CCGGCCGGAAGCCCTACACCATTAACCTCGAGTTAATGGTGTAGGGCTCCGGTTTTTG
shBRD4	CCGGCAGTGACAGTTCGACTGATGACTCGAGTCATCAGTCGAACTGTCACTGTTTTTTG

Primer Set Utilized for ChIP Assays		
Gene	Forward (5' to 3')	Reverse (5' to 3')
<i>MYC Promoter P2</i> <sup>a</sup>	CTTGCGGGAAAAAGAACGG	CTGCCTCTCGCTGGAATTACT

<sup>a</sup>*MYC* is most often transcribed through transcription factor (TF) binding to the promoter, P2.

## CHAPTER 3

### EVALUATING THE COMBINATION OF JQ1 AND GEMCITABINE IN CCA

#### Introduction

Cholangiocarcinoma (CCA) is an aggressive disease which is diagnosed at late stage. The current standard of care, resection followed by gemcitabine with cisplatin is the only potential curable option for patients. However, up to 90% of patients are ineligible for resection and, of those eligible, postoperative chemotherapy only prolongs survival by an additional 3-6 months over resection alone [11, 12, 48]. Further, relapse occurs within 2-3 years. Although new therapeutic targets, including IDH1/2 and FGFR2 are being investigated in clinical trials, IDH1/2 mutations and FGFR2 fusions account for only 20% and 13% of iCCA cases, respectively. Further, iCCA only accounts for up to 8% of all CCA cases thoroughly limiting the number of eligible patients. For these reasons, gemcitabine with cisplatin has remained the current standard for CCA patients.

Gemcitabine (dFdC) is a nucleoside analogue and prodrug which must be metabolized to exert its cytotoxic function (**Figure 3-1**). dFdC is transported into the cytoplasm primarily by human nucleoside transporter, hENT1, and to lesser extents by hENT2, hCNT1 and hCNT3. Once transported into the cytoplasm, dFdC undergoes multiple phosphorylation events. First, dFdC is phosphorylated to its monophosphate

form by deoxycytidine kinase (dCK) to form dFdCMP. dFdCMP is then subsequently phosphorylated by pyrimidine nucleoside monophosphate kinase (UMP-CMP kinase) to gemcitabine diphosphate (dFdCDP). dFdCDP is phosphorylated a third and final time by nucleoside diphosphate kinase A (NDPK) to gemcitabine triphosphate (dFdCTP). Depending on phosphorylation status, gemcitabine promotes cytotoxicity through multiple mechanisms. Gemcitabine triphosphate (dFdCTP) incorporates into replicating DNA followed by an additional nucleotide. This single nucleotide addition masks gemcitabine incorporation from DNA repair enzymes resulting in “masked chain termination” and the stalling on the replication fork. Further, gemcitabine diphosphate (dFdCDP) covalently binds to the active site of ribonucleotide reductase (RR), an enzyme which replenishes the deoxyribonucleotide (dNTP) pool. Covalent interaction of dFdCDP and RR depletes the available dNTP pool further increasing the probability of dFdCTP incorporation into the DNA [55].

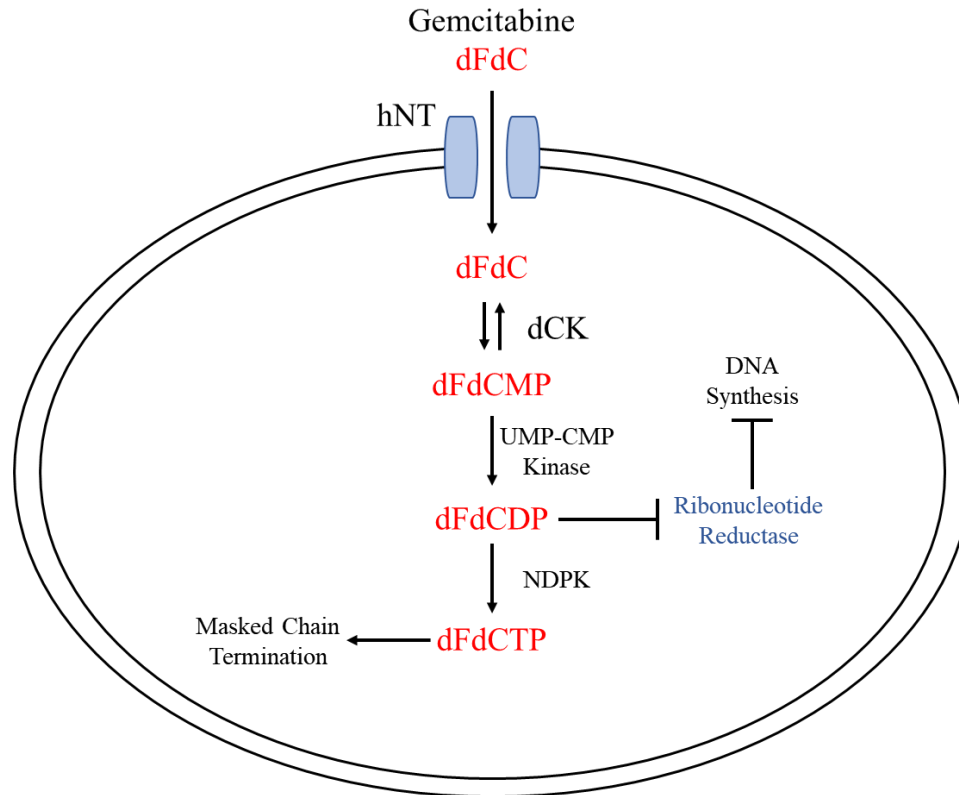


**Figure 3-1. Gemcitabine metabolism & mechanism of action.** Gemcitabine (dFdC) must be imported into the cell by human nucleoside transporters (hNTs) and metabolized. Once inside, gemcitabine is phosphorylated by dCK to its monophosphate form (dFdCMP) and further to its diphosphate (dFdCDP) and triphosphate (dFdCTP) forms by pyrimidine nucleoside monophosphate kinase (UMP-CMP kinase) and nucleoside diphosphate kinase A (NDPK). dFdCTP is incorporated into the DNA followed by one additional nucleotide which inhibits DNA synthesis through masked chain termination. dFdCDP covalently interacts with ribonucleotide reductase (RR) to deplete the endogenous dNTP pool and increase the potential for gemcitabine incorporation during DNA synthesis.

Additionally, cisplatin promotes its cytotoxicity through the formation of inter-strand and intra-strand links in genomic and mitochondrial DNA. Cisplatin, a heavy metal complex containing platinum bound to two chloride atoms, is hydrolyzed in the cytoplasm where the chloride atoms are displaced by water molecules, forming a reactive electrophile. Cisplatin-mediated intra-strand DNA crosslinks are repaired through

nucleotide excision repair (NER) with mismatch repair (MMR) recognizing cisplatin-mediated damage. However, cells harboring intact MMR are reportedly more sensitive to cisplatin than those harboring mutations in MMR components, *MSH1* or *MLH1* [58].

While gemcitabine with cisplatin remains the standard of care for CCA, the combination only improves overall survival by an additional 3-6 months over resection alone. This is thought to be due to intrinsic and/or acquired chemoresistance in CCA. Combining standard chemotherapy with novel therapeutic targets, especially those which cause dysregulation in DDR, may prove efficacious in CCA. The literature suggests that tumors deficient in cell cycle regulators and DDR factors are sensitive to gemcitabine [157-159]. Inhibition of the Ser/Thr protein kinase, Chk1, reportedly increases the sensitivity of pancreatic and colon cancer cell lines to gemcitabine [157, 158, 160]. Chk1 is a DNA damage response (DDR) factor involved in homologous recombination (HR). Upon DNA damage, ATR phosphorylates Chk1 on Ser-317 and Ser-345, inducing its activation. Chk1 phosphorylates Cdc25a, leading to its proteasomal-mediated degradation and slowed or stalled DNA replication. Further, Chk1 phosphorylates and activates Wee1 kinase which subsequently phosphorylates and inhibits Cdk1, ultimately preventing entry into mitosis [136]. Additionally, Farrell et al. demonstrated that RNAi-mediated reduction of proto oncogene, c-Myc, increased the sensitivity of PDAC cell lines, MiaPaca2, Panc1 and Capan1, to gemcitabine [161]. Using a patient derived xenograft (PDX) model of CCA, we reported downregulation of c-Myc and its transcriptional target, Chk1, following once a day treatment with the BET inhibitor, JQ1. In Chapter 2, we established that JQ1 reduces the expression of c-Myc and Chk1 in *in vitro* models of



CCA (**Figures 2C & 2E**). These data provide a strong rationale for use of a BET inhibitor JQ1 in sensitizing CCA models to gemcitabine.

In this chapter, we investigate the efficacy of gemcitabine in combination with cisplatin utilizing two CCA *in vitro* models, KKU-055 and KKU-100, as well as an *in vivo* CCA PDX model, CCA1. Second, we investigate the potency of JQ1 in combination with gemcitabine using cell viability and colony formation assays in two CCA *in vitro* models and compare the results to the combination of gemcitabine with cisplatin. Finally, we utilize our BRD2 and BRD4 knockdown (KD) models of KKU-055 to assess whether reduction in either of these BET family members increases sensitivity to gemcitabine.

## Results

### *Gemcitabine and cisplatin synergize in in vitro models of CCA*

Through a randomized phase 2 clinical trial, Valle et al. began the pioneering work to investigate the combination of gemcitabine with cisplatin for use in CCA [59]. This small 86 patient clinical trial identified an improvement in progression-free survival over a 6-month duration and was further extended to a phase 3 study (ABC-02) [59]. Their chemotherapeutic regimen, gemcitabine and cisplatin administered at 1,000 mg/m<sup>2</sup> and 25 mg/m<sup>2</sup>, respectively, every 3 weeks for eight cycles, extended median survival from 8.1 months with gemcitabine alone to 11.7 months with the combination [59]. Further, therapeutic efficacy was achieved regardless of CCA subtype, disease stage or geographical region [59, 162]. Based on this clinical trial, gemcitabine in combination with cisplatin quickly became the current standard of care for CCA patients.

Therefore, we assessed the potency of gemcitabine in combination with cisplatin using CCA *in vitro* models, KKU-055 and KKU-100. The combination of gemcitabine with cisplatin has not been reported using these model systems previously. We hypothesized that gemcitabine will synergize with cisplatin and will prove more efficacious than either drug alone in our model systems. To characterize the effects of drug synergy, we utilized the Chou-Talay method to calculate combination index (CI) values using CompuSyn 1.0. Briefly, CI values greater than 1 indicate drug antagonism, values equal to 1 indicate additive effects and values less than 1 indicate drug synergy. CI values less than 0.5 indicate strong drug synergy [144]. As the therapeutic dose between gemcitabine and cisplatin represent a 40-fold difference (1,000 mg/m<sup>2</sup> vs. 25 mg/m<sup>2</sup>, respectively), we assessed drug combination potency of gemcitabine with cisplatin at ratios including 50:1 as well as 1:50 and 1:10. Both *in vitro* models were exposed to gemcitabine and cisplatin alone (100 nM to 100 pM) or in combination for 120 hours with cell viability assessed using alamarBlue. Cell viability curves for KKU-055 and KKU-100 are shown in **Figure 3-2A** and **Figure 3-3A**, respectively. The CI values at the indicated fraction of cells affected are plotted in **Figure 3-2B** and **Figure 3-3B**, respectively. Data indicate that gemcitabine and cisplatin as single agents reduce cell viability in a dose-dependent manner with both models displaying strong drug synergy when combined in ratios of 1:10 and 50:1. No synergy was observed when KKU-055 cells were exposed to gemcitabine with cisplatin in a ratio of 1:50 whereas KKU-100 displayed synergy at a ratio of 1:50 for fraction of cells affected at 0.1 to 0.2 but not greater.

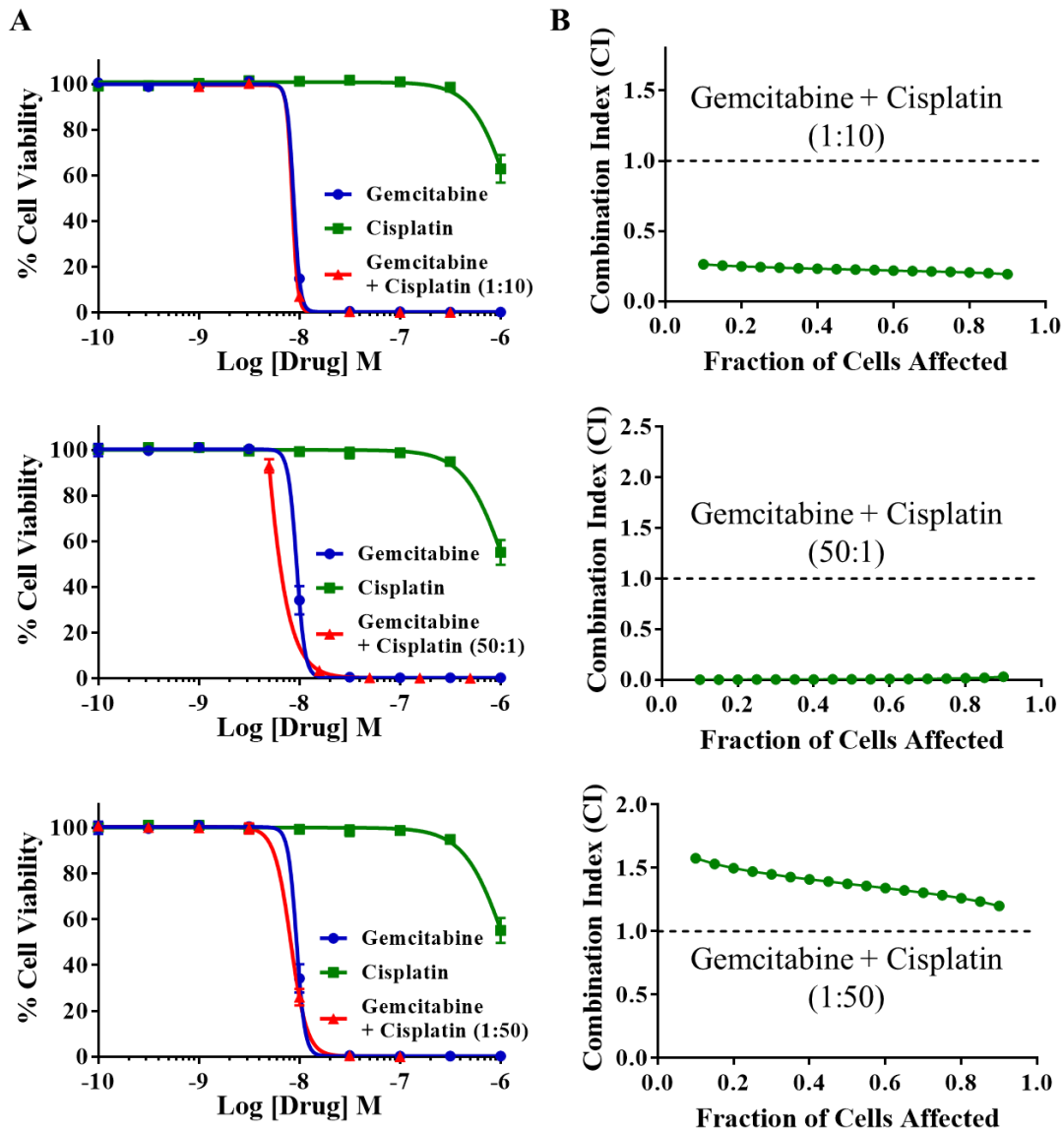


**Figure 3-2. Gemcitabine and cisplatin synergize in CCA cell line, KKU-055.** KKU-055 cells were treated with the indicated concentrations of gemcitabine, cisplatin or the combination in ratios of 1:10, 50:1 or 1:50 for 120 hours. **A)** At the end of drug treatment, alamarBlue was added and cell viability was assessed. Data represent the mean of quadruplet wells  $\pm$  SD for each dose. GraphPad Prism 7 was used to generate each graph. **B)** Combination index (CI) values were plotted against the fraction of cells affected. CI values less than 1 indicate drug synergy between gemcitabine and cisplatin at ratios of 1:10 and 50:1 in KKU-055.

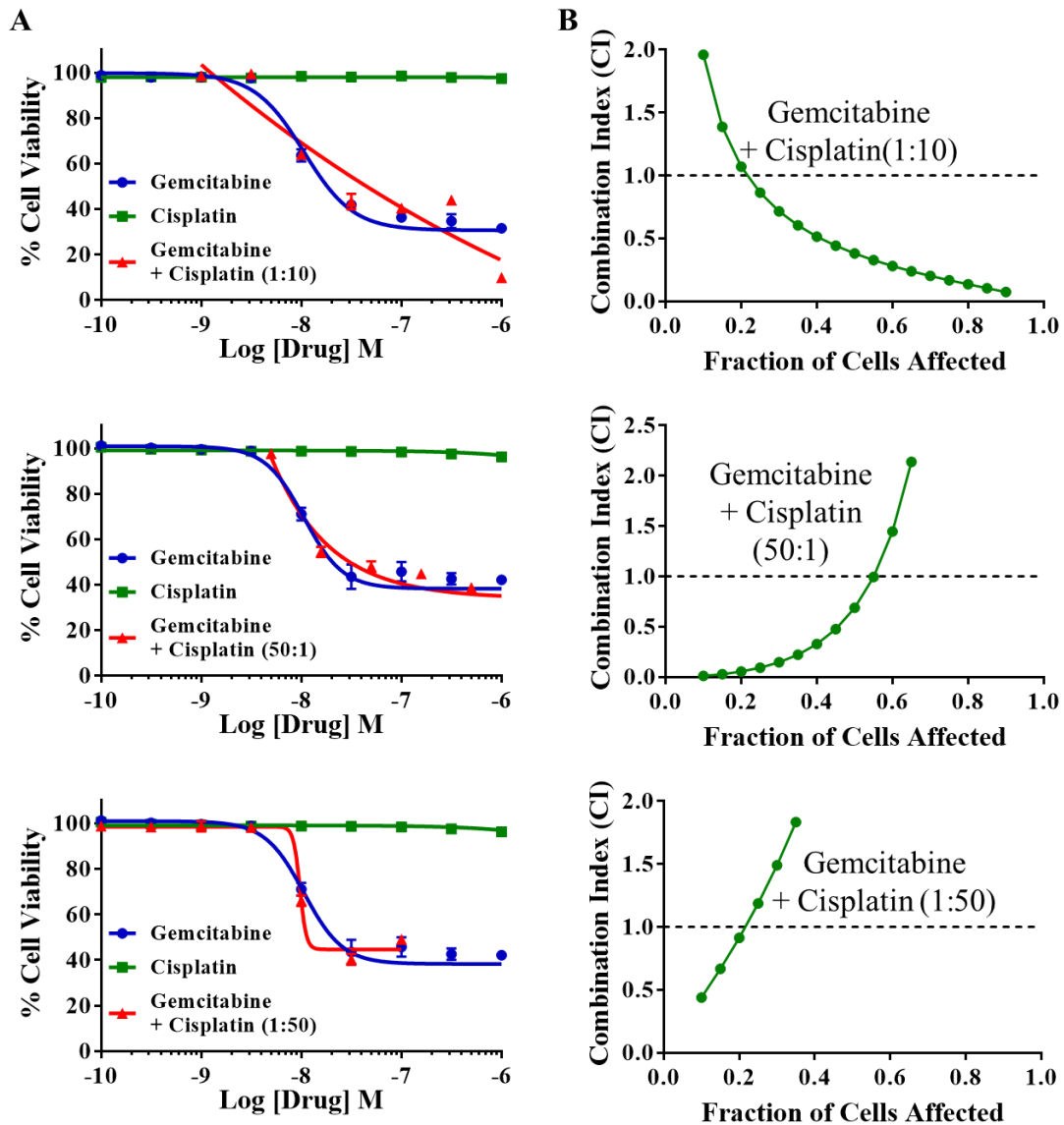


**Figure 3-3. Gemcitabine and cisplatin synergize in CCA cell line, KKU-100.** KKU-100 cells were treated with the indicated concentrations of gemcitabine, cisplatin or the combination in ratios of 1:10, 50:1 or 1:50 for 120 hours. **A)** At the end of drug treatment, alamarBlue was added and cell viability was assessed. Data represent the mean of quadruplet wells  $\pm$  SD for each dose. GraphPad Prism 7 was used to generate each graph. **B)** Combination index (CI) values were plotted against the fraction of cells affected. CI values less than 1 indicate drug synergy between gemcitabine and cisplatin at ratios of 1:10 and 50:1 in KKU-100.

*Gemcitabine in combination with cisplatin suppresses tumor growth in CCA PDX model*

Following the observation that gemcitabine in combination with cisplatin is synergistic in *in vitro* models of CCA, we assessed the efficacy of this combination in our CCA PDX model, CCA1. Mice bearing CCA1 tumors were randomized into four treatment groups to receive the saline vehicle control (VC) (n=6), gemcitabine (n=8), cisplatin (n=8) or gemcitabine with cisplatin (n=8). Gemcitabine and cisplatin were administered at doses of 60 mg/kg and 2.5 mg/kg via intraperitoneal injection (i.p.) once a week, consistent with previous reports utilizing this combination [163]. Tumor volumes were measured every other day over the 28-day study. The growth curve over the 28-day treatment duration are displayed in **Figure 3-4A** and represent the normalized tumor volume which has been normalized to day 0, one day prior to the beginning of treatment.

Treatment with either gemcitabine or cisplatin alone suppressed tumor volume compared to VC, with the combination displaying a more pronounced effect beginning on day 12. Following the 28-day treatment, mice were taken off treatment and placed on observation. Tumor measurements were continuously assessed every other day with results displayed in **Figure 3-4B**. Gemcitabine treated tumors began growing 32 days after the last day of treatment (day 60 of the study). Further, cisplatin treated tumors began to grow 92 days after the last day of treatment (day 120 of the study). Over the course of the study, up to day 130, tumors treated with gemcitabine in combination with cisplatin did not regrow.

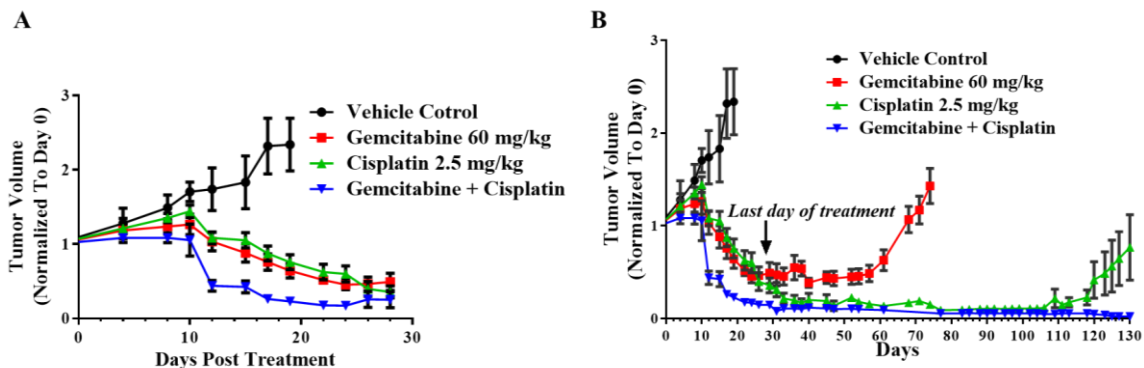


**Figure 3-4. The combination of gemcitabine with cisplatin suppresses tumor growth in an *in vivo* model of CCA.** **A)** Mice bearing CCA PDX model, CCA1, were treated with 60 mg/kg gemcitabine, 2.5 mg/kg cisplatin or the combination once a week for 28 days. Both gemcitabine and cisplatin as single agents suppressed tumor volume with the combination decreasing tumor volume more prominently beginning on day 12 of the study. **B)** At the end of the 28-day study, mice were placed on observation and no longer received treatment. Tumor measurements were assessed every other day for tumor regrowth. Gemcitabine treated tumors began growing 32 days after the last day of treatment (day 60 of the study). Further, cisplatin treated tumors began to grow 92 days after the last day of treatment (day 120 of the study). Over the course of the study, up to day 130, tumors treated with gemcitabine in combination with cisplatin did not regrow.

#### *JQ1 synergizes with gemcitabine in *in vitro* models of CCA*

Gemcitabine efficacy relies upon its incorporation into replicating DNA which results in “masked chain termination” and the stalling of the replication fork. The literature suggests that tumors deficient in cell cycle regulators and DDR factors display increased gemcitabine sensitivity [157-159]. Chk1, involved in homologous recombination repair, has been reported to be both a direct and indirect c-Myc transcriptional target [150, 164]. We previously reported a significant reduction in Chk1 post JQ1 treatment in our CCA PDX model, CCA2 [71]. Further, we reported significantly reduced Chk1 protein and mRNA expression in CCA *in vitro* models, KKU-055 and KKU-100, post JQ1 treatment (**Figures 2A, 2B 2C & 2E**).

Therefore, we hypothesized that JQ1-induced downregulation of c-Myc transcriptional target, Chk1, would sensitize CCA *in vitro* models to gemcitabine. To address this, we utilized two CCA *in vitro* models, KKU-055 and KKU-100, which represent the subtypes iCCA and pCCA, respectively. CCA *in vitro* models were exposed to increasing concentrations of JQ1 ( $10^{-4}$  to  $10^{-7}$  M), gemcitabine ( $10^{-7}$  to  $10^{-10}$  M) or the combination in a 1,000:1 ratio for 96 hours with cell proliferation assessed using alamarBlue. Cell viability curves for KKU-055 and KKU-100 are displayed in **Figure 3-5A & 3-5B**, respectively, with CI values for the fraction of cells affected displayed below each respective curve. Data indicate that JQ1 and gemcitabine as single agents reduce cell viability in a dose-dependent manner with both models displaying strong drug synergy when combining JQ1 with gemcitabine in a ratio of 1,000:1.

Next, we assessed whether JQ1 increased each *in vitro* models' sensitivity to a single dose of gemcitabine. To address this, both *in vitro* models were exposed to a range of JQ1 concentrations ( $10^{-4}$  to  $10^{-7}$  M), gemcitabine ( $10^{-7}$  to  $10^{-10}$  M) or JQ1 in combination with their gemcitabine  $IC_{50}$  of 10 nM for 96 hours. Cell viability curves for KKU-055 and KKU-100 are displayed in **Figure 3-6A & 3-6B**, respectively. CI values for each dose of JQ1 in combination with 10 nM gemcitabine is displayed below each respective curve. Favorable CI values were obtained when cells were exposed to 10 nM gemcitabine in combination with both high and low concentrations of JQ1. Using clonogenic assays, we observed that the combination of JQ1 with 10 nM gemcitabine was more effective than either drug alone in both CCA cell lines. Results of clonogenic studies are depicted in **Figures 3-6C & 3-6D**. We further assessed the effect of 10  $\mu$ M JQ1 in combination with 10 nM gemcitabine on the expression of c-Myc and its

transcriptional target, Chk1. We exposed KKU-055 to DMSO, 10  $\mu$ M JQ1, 10 nM gemcitabine or the combination of 10  $\mu$ M JQ1 with 10 nM gemcitabine for 72 hours. We observed that treatment with 10  $\mu$ M JQ1 significantly inhibited the expression of c-Myc and Chk1 protein in KKU-055, similar to results shown in **Figure 4a**. In addition, the combination of JQ1 with gemcitabine similarly display downregulation of c-Myc with more pronounced Chk1 downregulation (**Figure 3-7**).



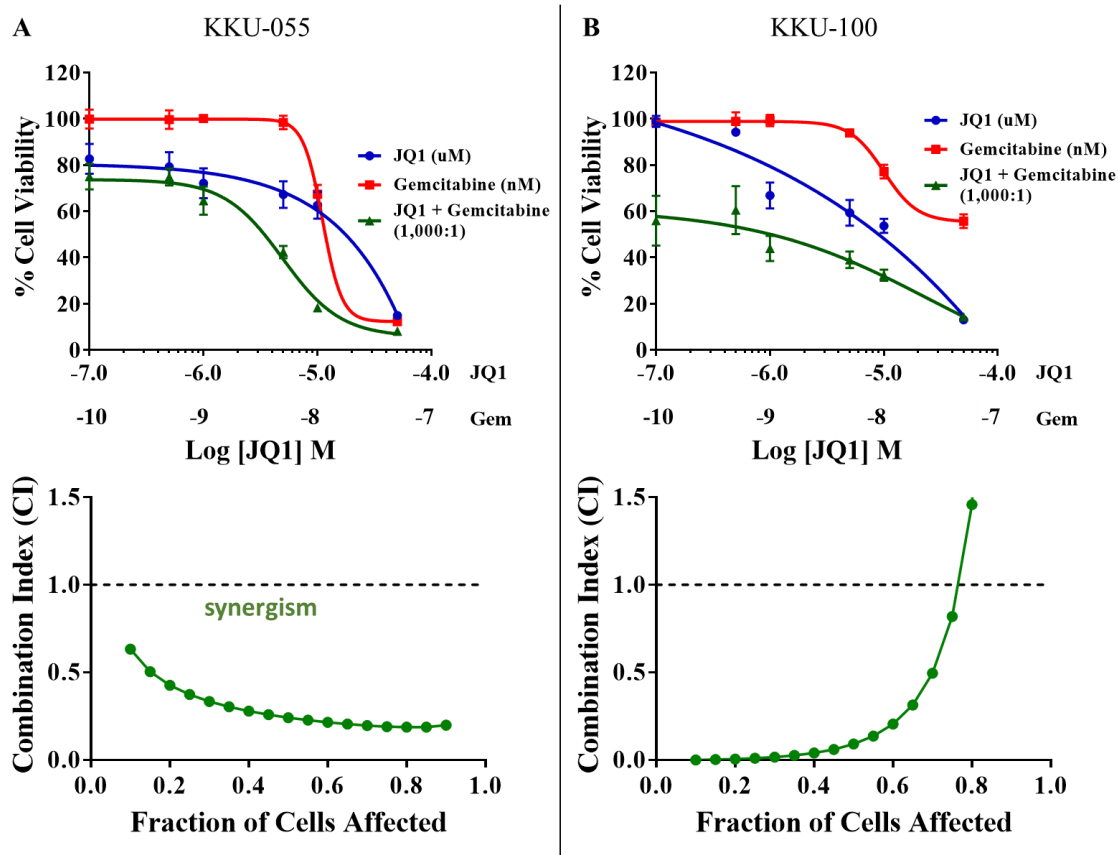


**Figure 3-5. The combination of JQ1 with gemcitabine in a 1,000:1 ratio is synergistic in CCA *in vitro* models. A) KKU-055 and B) KKU-100 cells were treated with the indicated concentrations of JQ1, gemcitabine or the combination in a 1,000:1 ratio for 96 hours. At the end of drug treatment, alamarBlue was added and cell viability was assessed. Cell viability curves represent the mean of two independent experiments  $\pm$  SD for each dose. GraphPad Prism 7 was used to generate each graph. B) Combination index (CI) values were plotted against the fraction of cells affected. CI values less than 1 indicate drug synergy between JQ1 and gemcitabine at a 1,000:1 ratio in both cell models.**

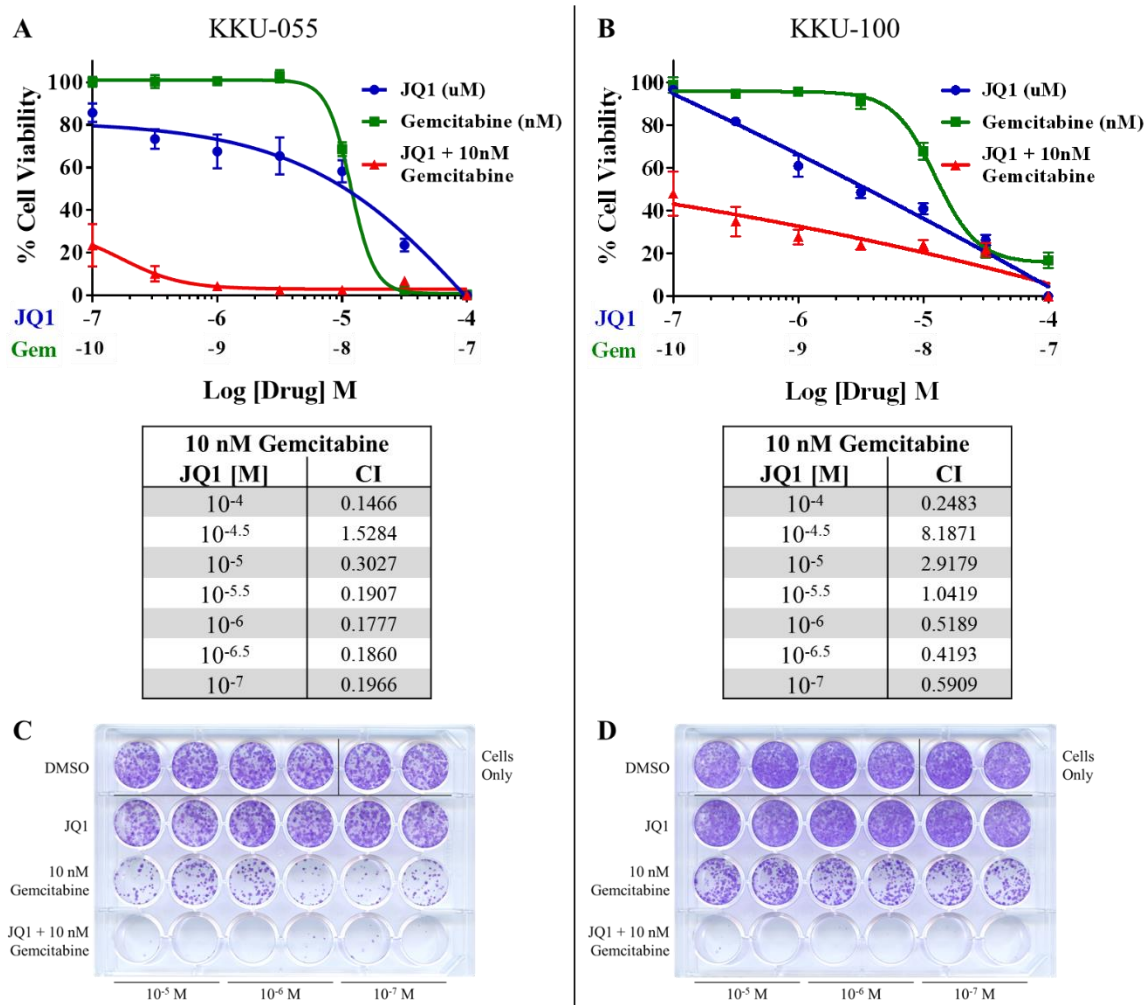


**Figure 3-6. The combination of JQ1 with 10 nM gemcitabine is synergistic in CCA *in vitro* models.** **A)** KKU-055 and **B)** KKU-100 cells were treated with the indicated concentrations of JQ1, gemcitabine or the combination of JQ1 with 10 nM gemcitabine for 96 hours. At the end of drug treatment, alamarBlue was added and cell viability was assessed. Cell viability curves represent the mean of two independent experiments  $\pm$  S.E.M. for each dose. GraphPad Prism 7 was used to generate each graph. **B)** Combination index (CI) values were plotted against the fraction of cells affected. CI values less than 1 indicate drug synergy between JQ1 and 10nM gemcitabine in both cell models. Clonogenic assays for **C)** KKU-055 and **D)** KKU-100 were performed. Both cells models were treated with JQ1 ( $10^{-5}$ ,  $10^{-6}$  or  $10^{-7}$  M), 10 nM gemcitabine or the combination of JQ1 with 10 nM gemcitabine for 72 hours. Cells were then washed with PBS and grown in drug-free media for an additional week.

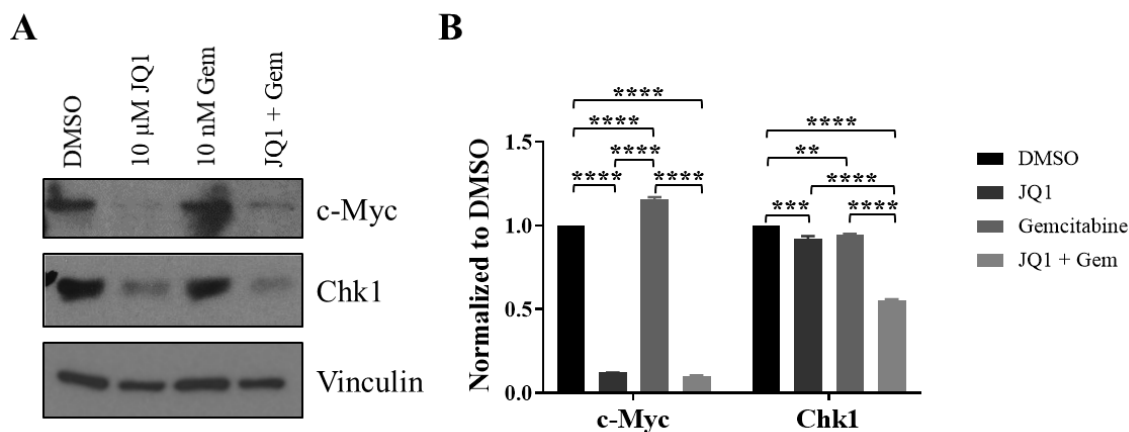


**Figure 3-7. The combination of JQ1 with 10 nM gemcitabine decreases the expression of c-Myc and Chk1 in CCA *in vitro* model, KKU-055.** **A)** KKU-055 was treated with DMSO, 10  $\mu$ M JQ1, 10nM gemcitabine or the combination of 10  $\mu$ M JQ1 with 10nM gemcitabine for 72 hours. Treatment with 10  $\mu$ M JQ1 inhibited expression of c-Myc and Chk1 protein in both model systems. **B)** Immunoblot data were quantitated and presented as percent DMSO using ImageStudio Lite and reported as bar graphs mean  $\pm$  S.E.M.

*Knockdown of BRD2 or BRD4 in KKU-055 does not increase gemcitabine sensitivity*

JQ1 inhibits the binding of the BET family of proteins with K-Ac residues on histones tails and other nuclear proteins. As drug synergy was observed in both KKU-055 and KKU-100 *in vitro* when exposed to JQ1 with 10 nM gemcitabine in addition to the combination of JQ1 with gemcitabine in a 1,000:1 ratio (**Figure 3-5 & 3-6**), we hypothesized that our established BRD2 and BRD4 knockdown (KD) models of KKU-055 (**Figure 4A & 4B**) would display increased gemcitabine sensitivity, similar to the effect of JQ1 in combination with gemcitabine in parental KKU-055. To address this hypothesis, we exposed control (shGFP), BRD2 and BRD4 KD models of KKU-055 to a range of gemcitabine concentrations ( $10^{-7}$  to  $10^{-10}$  M) for 96 hours with cell viability assessed using alamarBlue. Results are depicted in **Figure 3-8** with gemcitabine IC<sub>50</sub>

values displayed to the left of the curve. When combined with gemcitabine, neither BRD2 nor BRD4 KD models recapitulated the synergistic effects observed with JQ1 in combination with gemcitabine in parental KKU-055. BRD2 and BRD4 KD models displayed a 1.19-fold and 1.21-fold increase in gemcitabine sensitivity, respectively, compared to shGFP control.

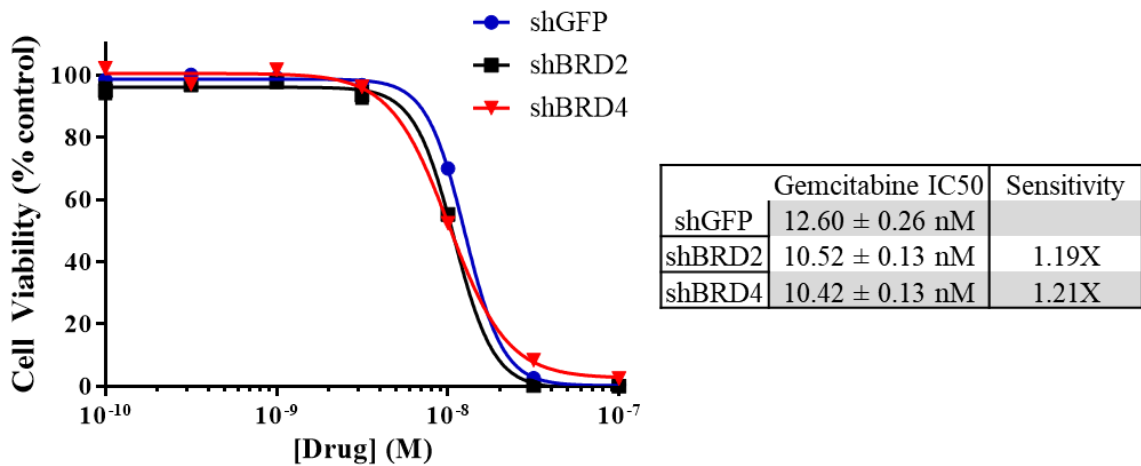


**Figure 3-8. Decreased expression of BRD2 or BRD4 does not increase sensitivity of KKU-055 cells to gemcitabine.** KKU-055 control and KD models were exposed to gemcitabine ( $10^{-7}$  to  $10^{-10}$  M) for 96 hours. Cell viability was assessed using alamarBlue. IC<sub>50</sub> values were calculated utilizing GraphPad Prism 7. Sensitivity was calculated by comparing the respective KD model IC<sub>50</sub> to shGFP control. A minimum of three independent experiments were performed and IC<sub>50</sub> values presented as mean ± S.E.M.

## Summary & Conclusions

The goal of this chapter was to investigate the efficacy of the current standard of care, gemcitabine with cisplatin, utilizing both *in vitro* and *in vivo* model systems and to assess the potency of BET inhibitor, JQ1, in combination with gemcitabine *in vitro*. As the ratio of gemcitabine to cisplatin is given at a 40:1 ratio for patients, we chose ratios of 50:1, 1:50 and 1:10 for *in vitro* cell viability analysis. Gemcitabine with cisplatin displayed drug synergy in both CCA cell lines when exposed to ratios of 50:1 and 1:10, but not when exposed to a ratio of 1:10 (**Figures 3-2 & 3-3**). Following our observation that gemcitabine synergizes with cisplatin in our *in vitro* models, we investigated the efficacy of this combination using our CCA PDX model, CCA1. Tumors bearing CCA1 were administered saline vehicle control, 60 mg/kg gemcitabine, 2.5 mg/kg cisplatin or the combination of gemcitabine with cisplatin once a week for 28 days. Treatment with gemcitabine and cisplatin as single agents displayed a reduction in normalized tumor volume compared to control with the combination seeing a greater decrease in tumor volume which began on day 12 of the study. In addition to the observed decreases in tumor volume over the course of treatment, we assessed the impact of each respective treatment on tumor regrowth. After the 28-day treatment period, mice were removed from treatment and put on observation for an additional 102 days. Gemcitabine treated tumors began growing 32 days after the last day of treatment (day 60 of the study). Further, cisplatin treated tumors began to grow 92 days after the last day of treatment (day 120 of the study). Over the course of the study, up to day 130, tumors treated with gemcitabine in combination with cisplatin did not regrow (**Figure 3-4B**).

Unfortunately, treatment with gemcitabine in combination with cisplatin only prolongs CCA survival by an additional 3-6 months compared to resection alone. Further, most patients experience relapse within 2-3 years. To address these concerns and to develop additional therapeutic strategies for CCA, we investigated the potency of a BET bromodomain inhibitor, JQ1, in combination with gemcitabine. Previous reports indicate that tumors treated with a Chk1 inhibitor displayed increased sensitivity to gemcitabine. Further, we previously reported that BET inhibition decreases Chk1 expression in both *in vitro* (**Figures 2A, 2B, 2C & 2E**) and *in vivo* models of CCA [71]. To investigate whether JQ1-mediated reduction in Chk1 sensitizes CCA cells to gemcitabine, we exposed KKU-055 and KKU-100 to JQ1 in combination with gemcitabine both in a constant ratio of 1,000:1 as well as treatment with their respective gemcitabine IC<sub>50</sub> of 10 nM with a range of JQ1 concentrations (**Figures 3-5 & 3-6**). JQ1 synergized with gemcitabine in both *in vitro* models both at a constant ratio and when exposed to a single dose of gemcitabine with a range of JQ1 concentrations. Further, KKU-055 presented decreased c-Myc and Chk1 protein expression when exposed to 10 μM JQ1 or the combination of 10 μM JQ1 with 10 nM gemcitabine. Of note, the combination of JQ1 with gemcitabine shows more pronounced Chk1 downregulation compared to JQ1 alone (**Figure 3-7**).

As JQ1 is a pan-BET inhibitor, we addressed whether the knockdown of a single BET family member altered sensitivity to gemcitabine. We exposed our shGFP control, BRD2 and BRD4 KD models of KKU-055 (**Figure 4a & 4b**) to a range of gemcitabine concentrations (10<sup>-7</sup> to 10<sup>-10</sup> M) for 96 hours (**Figure 3-8**). Contrary to our hypothesis, no alterations in gemcitabine sensitivity were observed compared to shGFP control. BRD2

and BRD4 KD models displayed a 1.19-fold and 1.21-fold increase in gemcitabine sensitivity, respectively, compared to shGFP control. These data suggest that inhibition of multiple BET family members, not just a single member, may be required for BET inhibitor synergy with gemcitabine in KKKU-055. It is possible that gene KD and therapeutic inhibition via JQ1 are not equivalent due to the established BD independent functions of BRD4. Rather, to address whether the observed increase in BETi sensitivity are through inhibition of K-Ac binding and not loss of BRD4 BD independent functions, the generation of a dominant negative BRD4, which lacks asparagine residues in each bromodomain and would no longer recognize and bind K-Ac residues yet keep non-BD functions intact could be utilized.

## CHAPTER 4

### DEVELOPMENT, CHARACTERIZATION AND TREATMENT OF GEMCITABINE RESISTANT CCA MODELS

#### **Introduction**

CCA remains the second most prevalent primary hepatic malignancy. To date, the most efficacious treatment available for CCA patients is gemcitabine in combination with cisplatin, the current standard of care [12]. Gemcitabine (dFdC) functions as a pyrimidine nucleoside analogue which promotes its cytotoxicity through multiple mechanisms as detailed in Chapter 3 (**Figure 3-1**). Briefly, gemcitabine is imported into the cell by nucleoside transporters (hNTs) where it is then phosphorylated sequentially by dCK, UMP-CMP kinase and NDPK to its monophosphate (dFdCMP), diphosphate (dFdCDP) and triphosphate (dFdCTP) forms, respectively. dFdCTP is incorporated into replicating DNA followed by one additional nucleotide which results in inhibition of DNA synthesis through masked chain termination. Further, dFdCDP covalently binds ribonucleotide reductase (RR) which diminishes the endogenous dNTP pool, thereby increasing the probability of dFdCTP incorporation into replicating DNA [55]. Unfortunately, as



clinical CCA symptoms present at late disease stage, patients experience rampant chemoresistance acquired through extrinsic and intrinsic mechanisms [48, 60, 61].

The majority of CCA cases are enclosed in highly desmoplastic stroma referred to as TRS which contains numerous cell populations including inflammatory cells, endothelial cells, myofibroblasts and mesenchymal stem cells [19, 38, 39]. These cell populations enhance drug resistance through extrinsic mechanisms such as paracrine or endocrine signaling as well as the release of growth factors, cytokines and chemokines [39, 61]. For example, cancer-associated fibroblasts (CAFs) play a major role in chemoresistance through the release of periostin, prostaglandin E2 (PGE2) and sphingosine-1-phosphate which aids CCA resistance to chemotherapeutic agents [38, 61].

In addition to extrinsic chemoresistance mechanisms, normal cholangiocytes display intrinsic resistance to chemotherapeutic agents through activation of farnesoid X receptor (FXR). Exposure to bile acids found in bile and hepatic blood induces FXR activation which leads to upregulation of the ATP-binding cassette (ABC) family of multidrug resistance (MDR) genes as well as downregulation of equilibrative and concentrative nucleoside transporters [6, 61]. Downregulation of nucleoside importers, such as hENT1 and hCNT1, are associated with decreased patient survival and increased gemcitabine resistance (Gem<sup>R</sup>) [55, 165], however, downregulation of these factors does not always correspond with resistance to gemcitabine [62, 165]. In addition to downregulation of hNT, multiple mechanisms of gemcitabine resistance have been reported (**Figure 4-1**). As stated previously, the first step in gemcitabine metabolism is the phosphorylation of dFdC to its monophosphate form, dFdCMP, through the rate limiting reaction performed by dCK. Both *in vitro* and *in vivo* models harboring

deficiencies in dCK have been reported to display increased resistance to gemcitabine [166]. Further, as gemcitabine diphosphate (dFdCDP) covalently binds RR subunit RRM1, thereby decreasing the endogenous dNTP pool, Gem<sup>R</sup> populations have been reported to increase both RR subunits, RRM1 and RRM2, to increase the endogenous dNTP pool and decrease the probability of gemcitabine incorporation into replicating DNA [55, 165, 166]. In addition, inactivation of both gemcitabine (dFdC) and gemcitabine monophosphate (dFdCMP) through deamination by cytidine deaminase (CDA) and deoxycytidylate deaminase (dCMP), respectively, have been linked to gemcitabine resistance [55, 165]. CDA, the main deamination mechanism, converts dFdC to difluorodeoxyuridine (dFdU) whereas dCMP converts dFdCMP to dFdUMP. dFdU is not a substrate for pyrimidine nucleoside phosphorylases, therefore, it is excreted from the cell and is commonly found in the urine of treated patients [166].

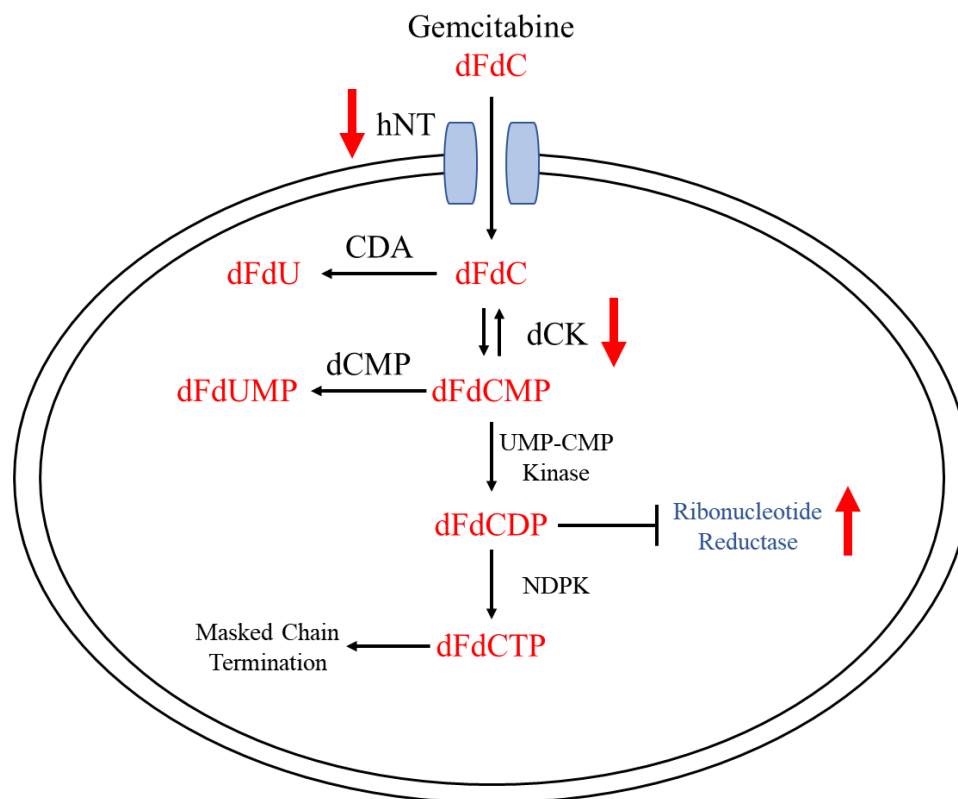


**Figure 4-1. Mechanisms of gemcitabine resistance.** Gemcitabine (dFdC) must be imported into the cell by human nucleoside transporters (hNTs) and metabolized to promote its cytotoxic effect. To decrease gemcitabine-mediated toxicity, cells can downregulate hNTs to decrease the amount of intracellular gemcitabine as well as decrease the expression of dCK, the rate limiting step in gemcitabine metabolism. Inactivation of gemcitabine metabolic products is completed through deamination of gemcitabine (dFdC) and gemcitabine monophosphate (dFdCMP) by cytidine deaminase (CDA) and deoxycytidylate deaminase (dCMP) to form dFdU and dFdUMP, respectively. Further, as gemcitabine diphosphate (dFdCDP) covalently interacts with ribonucleotide reductase (RR) to deplete the endogenous dNTP pool and increase the potential for gemcitabine incorporation during DNA synthesis, upregulation of RR subunits, RRM1 and RRM2, have been shown to decrease gemcitabine sensitivity by increasing the dNTP pool and decreasing the probability of gemcitabine triphosphate (dFdCTP) incorporation into replicating DNA.

Therapeutic inhibition of DNA damage response factor, Chk1, has been reported to increase the sensitivity of colon and pancreatic cancer cell lines to gemcitabine [157, 158, 160]. Chk1 is a Ser/Thr kinase responsible for phosphorylating cell cycle regulator, Cdc25a, leading to its degradation and subsequent slowing or stalling DNA replication

[136]. Further, reports indicate that RRM1-dependent gemcitabine resistant pancreatic, lung and breast cancer cell lines display increased gemcitabine sensitivity when Chk1 is pharmacologically inhibited [167, 168]. Using a CCA PDX model, we reported that once a day treatment with the BET inhibitor, JQ1, lead to significant downregulation of c-Myc and its transcriptional target, Chk1 [71]. Additionally, JQ1 significantly decreased both Chk1 mRNA and protein expression in parental CCA *in vitro* models, K KU-055 and K KU-100 (**Figure 2A, 2B, 2C & 2E**). Therefore, we hypothesized that BET inhibition in CCA may increase the sensitivity of CCA Gem<sup>R</sup> models to gemcitabine through downregulation of Chk1.

In this chapter we first detail the generation of an *in vitro* K KU-055 Gem<sup>R</sup> model through exposure to gradually increasing gemcitabine concentrations. Morphological, cell doubling time and specific *KRAS* mutational status of the established Gem<sup>R</sup> model was then compared to parental K KU-055. Second, we compared the efficacy of the BET bromodomain inhibitor, JQ1, in our K KU-055 Gem<sup>R</sup> model and compare cell viability to the parental line. Poor CCA therapeutic response has been attributed to extensive chemoresistance [169], however, no reports of a gemcitabine resistant CCA PDX model have been described. This more clinically relevant model could provide insight into CCA gemcitabine resistant mechanisms and shed light on potential therapeutic targets for use in the clinic. Therefore, we described the generation of the first established CCA PDX Gem<sup>R</sup> *in vivo* models and compared the histological and molecular characteristics to their respective treatment naïve controls.

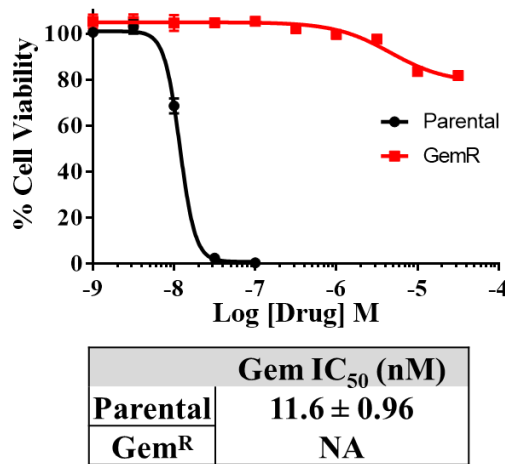
## Results

### *Development of a gemcitabine resistant CCA in vitro model*

In Chapter 3, we demonstrated that the combination of JQ1 with gemcitabine exerted synergistic cytotoxicity in CCA *in vitro* models (**Figures 3-5 & 3-6**). While these observations are important, they were made using gemcitabine-sensitive *in vitro* models whereas the majority of CCA patient tumors display intrinsic chemoresistance or acquire resistance to gemcitabine. To address the rampant chemoresistance observed in CCA patients, we saw fit to develop *in vitro* gemcitabine resistance models which resemble clinical cases and utilize said models to assess drug efficacy. Towards generation of a gemcitabine resistant *in vitro* model, we first assessed the sensitivity of parental KKU-055 cells to gemcitabine. We exposed KKU-055 to a range of gemcitabine concentrations ( $10^{-7}$  to  $10^{-10}$  M) for 96 hours with cell viability and gemcitabine  $IC_{50}$  assessed using alamarBlue and GraphPad Prism, respectively. Once the concentration of gemcitabine required to kill 50% of KKU-055 cells ( $IC_{50}$ ) was determined, we began generation of our gemcitabine resistant (Gem<sup>R</sup>) model. Parental KKU-055 were grown in 10 nM gemcitabine, their  $IC_{50}$ , with fresh drug containing media replenished twice a week on Mondays and Fridays. Once cells grew consistently in media containing 10 nM gemcitabine, the concentration was increased. This process was repeated, and cells were termed gemcitabine resistant (Gem<sup>R</sup>) once they grew consistently in 5  $\mu$ M gemcitabine, 500-fold the parental gemcitabine  $IC_{50}$ .

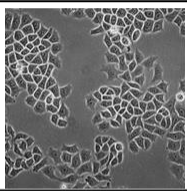
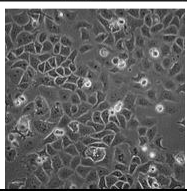
We assessed the difference in gemcitabine sensitivity between the parental and Gem<sup>R</sup> models of KKU-055. Both models were exposed to a range of gemcitabine concentrations ( $10^{-4.5}$  to  $10^{-9}$  M) for 96 hours with cell viability assessed via alamarBlue.

Gemcitabine sensitivity of KKU-055 parental and Gem<sup>R</sup> is displayed in **Figure 4-2**. As expected, the Gem<sup>R</sup> model displayed markedly increased gemcitabine resistance compared to parental KKU-055 and was found to be above maximum concentration of gemcitabine utilized in this assay ( $10^{-4.5}$  M or 31.6  $\mu$ M). Gemcitabine peak plasma concentration for patients treated with 1,000 mg/m<sup>2</sup> is 32  $\mu$ M [170]. As our KKU-055 Gem<sup>R</sup> model displayed ~80% cell viability when exposed to 31.6  $\mu$ M gemcitabine for 96 hours, this indicates our Gem<sup>R</sup> model displays resistance to peak gemcitabine concentrations achievable in the clinic.



**Figure 4-2. KKU-055 gemcitabine resistant (Gem<sup>R</sup>) model displays over 500-fold increase in gemcitabine resistance compared to parental.** Parental KKU-055 were treated with gemcitabine IC<sub>50</sub> of 10 nM. Media, containing gemcitabine, was replenished every three days. Cells were monitored for growth once a day and were considered resistant to the administered gemcitabine dose once cells appeared to grow normally. Gemcitabine concentration was gradually escalated as cells grew normally in increasing concentrations of gemcitabine. To assess the fold increase in gemcitabine resistance over parental KKU-055, both parental and Gem<sup>R</sup> models were exposed to a range of gemcitabine concentrations ( $10^{-4.5}$  to  $10^{-9}$  M) for 96 hours. At the end of drug treatment, alamarBlue was added and cell viability was assessed. Parental data represents the mean of three technical replicates  $\pm$  SEM for each dose. Gem<sup>R</sup> data represent the mean of quadruplet wells  $\pm$  SD for each dose. GraphPad Prism 7 was used to generate each graph and IC<sub>50</sub> value.

As Gem<sup>R</sup> displayed markedly increased resistance to gemcitabine, we assessed whether cellular and molecular alterations exist between parental and Gem<sup>R</sup>. No distinct alterations in cell morphology, cell doubling time or *KRAS* codon 12 mutational status were found to exist between KKU-055 parental and Gem<sup>R</sup> (**Figure 4-3**).

	Morphology (20X)	Cell-Doubling Time (h)	KRAS Status (Codon 12)
KKU-055 JCRB1551		23.6 ± 5.1	WT (GGT) T GGT G GC
KKU-055 Gem <sup>R</sup>		27.16	WT (GGT) T GGT G GC

**Figure 4-3. KKU-055 Gem<sup>R</sup> displays no alterations in morphology, cell doubling time nor specific *KRAS* mutational status compared to parental.** KKU-055 parental and Gem<sup>R</sup> display epithelial-like morphology and proliferate *in vitro* in discrete patches. Cell doubling time was ~24 hours and ~27 hours for parental and Gem<sup>R</sup> cells, respectively. Both models express wild type *KRAS*.

*Gemcitabine resistant CCA in vitro model displays increased JQ1 sensitivity*

Therapeutic resistant *in vitro* models of pancreatic cancer, TNBC and lung adenocarcinoma which display resistance to gemcitabine, doxorubicin, and β-catenin inhibition, respectively, show elevated c-Myc expression. Further, RNAi-mediated downregulation of c-Myc in these models increases their sensitivity to their respective therapeutic agent [161, 171, 172]. Though we have not addressed the expression status of c-Myc in our Gem<sup>R</sup> model, we did assess the efficacy of JQ1 as a single agent in KKU-055 Gem<sup>R</sup>. Having observed that JQ1 decreased cell viability and downregulated the

expression of c-Myc in parental KKU-055, we asked whether KKU-055 Gem<sup>R</sup> exhibited increased BET inhibition sensitivity compared to control. To address this question, we exposed both parental and Gem<sup>R</sup> models to a range of JQ1 concentrations ( $10^{-4}$  to  $10^{-7}$  M) for 96 hours with cell viability assessed via alamarBlue. The sensitivity of KKU-055 parental and Gem<sup>R</sup> to JQ1 is displayed in **Figure 4-4** with JQ1 IC<sub>50</sub> displayed below the graph. KKU-055 Gem<sup>R</sup> displayed a 3.32-fold increase in JQ1 sensitivity compared to parental.

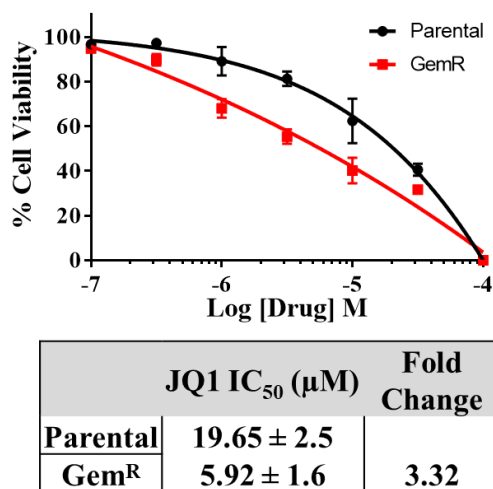


**Figure 4-4. KKU-055 Gem<sup>R</sup> is more sensitive to JQ1.** To assess the potency of JQ1 *in vitro*, we exposed CCA cell lines to a range of concentrations of JQ1 for 96 hours and assessed cell viability using alamarBlue assays. JQ1 decreased cell viability in a dose-dependent manner. Gem<sup>R</sup> model displayed 3.32-fold increase in JQ1 sensitivity compared to parental KKU-055.

#### *Development of gemcitabine resistant CCA in vivo models*

While *in vitro* models are imperative to evaluate mechanisms of drug resistance and therapeutic efficacy, these model systems lack components integral to clinical CCA such as stroma and extracellular matrix (ECM). As discussed previously, PDX models



retain histological features of the patient disease while also comprising these important components. However, there are no reports regarding the generation of gemcitabine CCA PDX models in the literature. Therefore, we set out to develop the first gemcitabine resistant CCA PDX models. We utilized two CCA PDX models, CCA1 and CCA2. In Chapter 3, we implanted CCA PDX model, CCA1, into the flank of SCID mice and treated with 60 mg/kg gemcitabine for 28-days (**Figure 3-4A**). Decrease in CCA1 tumor volume was observed on day 12 of the 28-day treatment. We had not previously assessed the efficacy of gemcitabine in CCA PDX model, CCA2.

To generate *in vivo* Gem<sup>R</sup> PDX models, CCA1 or CCA2 were implanted subcutaneously into SCID mice and allowed to grow until 250-350 mm<sup>3</sup> or 300-500 mm<sup>3</sup>, respectively. Mice bearing CCA1 or CCA2 were randomized into two treatment groups to receive the saline vehicle control (VC) (CCA1 n=6, CCA2 n=9) or 100 mg/kg gemcitabine (CCA1 n=8, CCA2 n=6). Gemcitabine was administered via intraperitoneal (i.p.) injection once a week and tumors were measured every other day over the course of the study. The treatment scheme for CCA1 and CCA2 are outlined in **Figures 4-5A & 4-5B**, respectively. Growth curves for CCA1 and CCA2 over their respective 122-day and 126-day treatment durations are displayed in **Figures 4-6A & 4-6B** and represent tumor volume normalized to Day 0, one day prior to the beginning of treatment. Mice remained on treatment until their tumors grew to their original size or larger than starting volume.

While undergoing treatment, CCA1 and CCA2 experienced their greatest decrease in volume on days 50 (34% of starting volume) and 51 (87% of starting volume), respectively. Regrowth of CCA1 and CCA2 was observed on days 50 and 55, respectively. While receiving gemcitabine treatment, tumor volumes of CCA1 and CCA2

were 2.95-fold and 2.72-fold larger than their respective Day 0 tumor volumes (**Figures 4-6A & 4-6B**). Within 24 hours of final treatment, mice harboring CCA1 or CCA2 treated with gemcitabine were euthanized on days 122 and 126, respectively, tumors were harvested, samples were implanted into mice to develop the next generation Gem<sup>R</sup> PDX and others were formalin-fixed, and paraffin embedded (FFPE) for histological and molecular analysis.

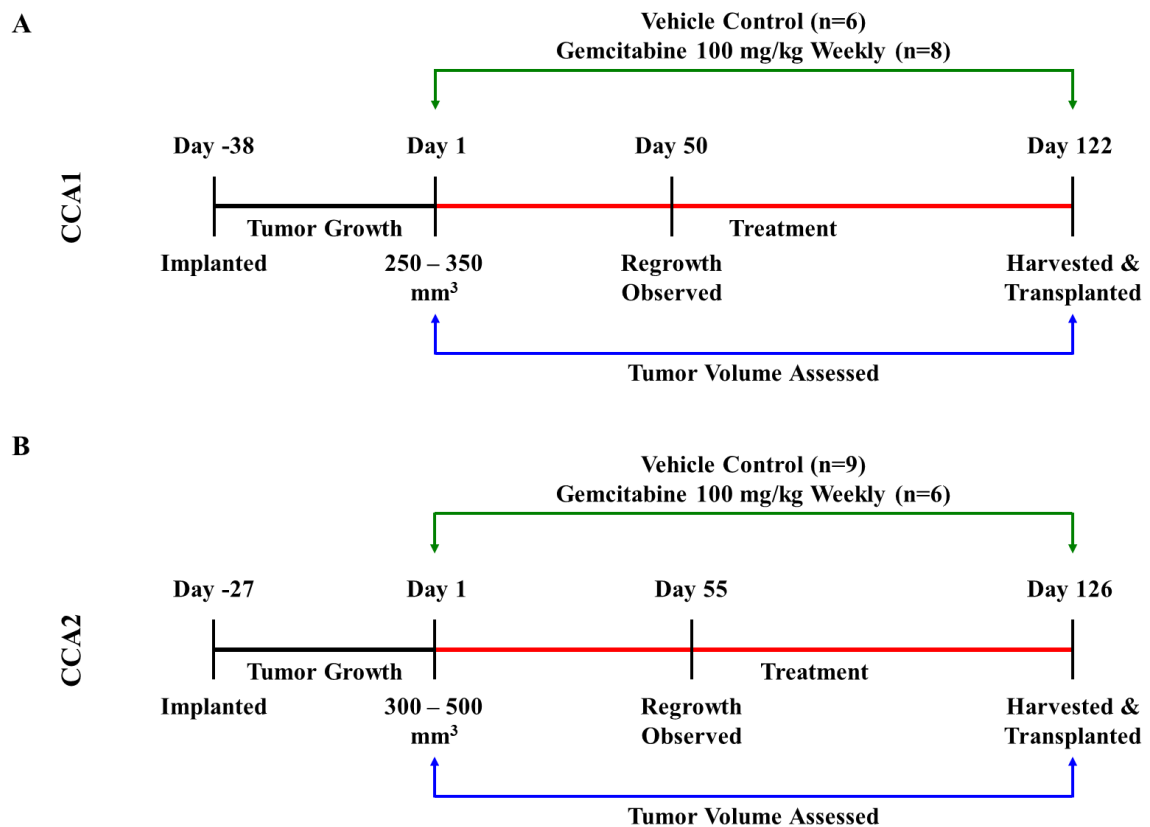


**Figure 4-5. Implantation, treatment and dosing timeline for the development of gemcitabine resistant CCA PDX models.** Mice bearing A) CCA1 or B) CCA2 tumors were administered vehicle control or 100 mg/kg gemcitabine once a week. Tumor volumes were assessed three times a week for growth. CCA1 and CCA2 displayed tumor regrowth on days 50 and 55, respectively, while undergoing gemcitabine treatment. Following tumor regrowth, tumors were harvested for analysis or implanted into the next generation of mice to continue gemcitabine treatment.

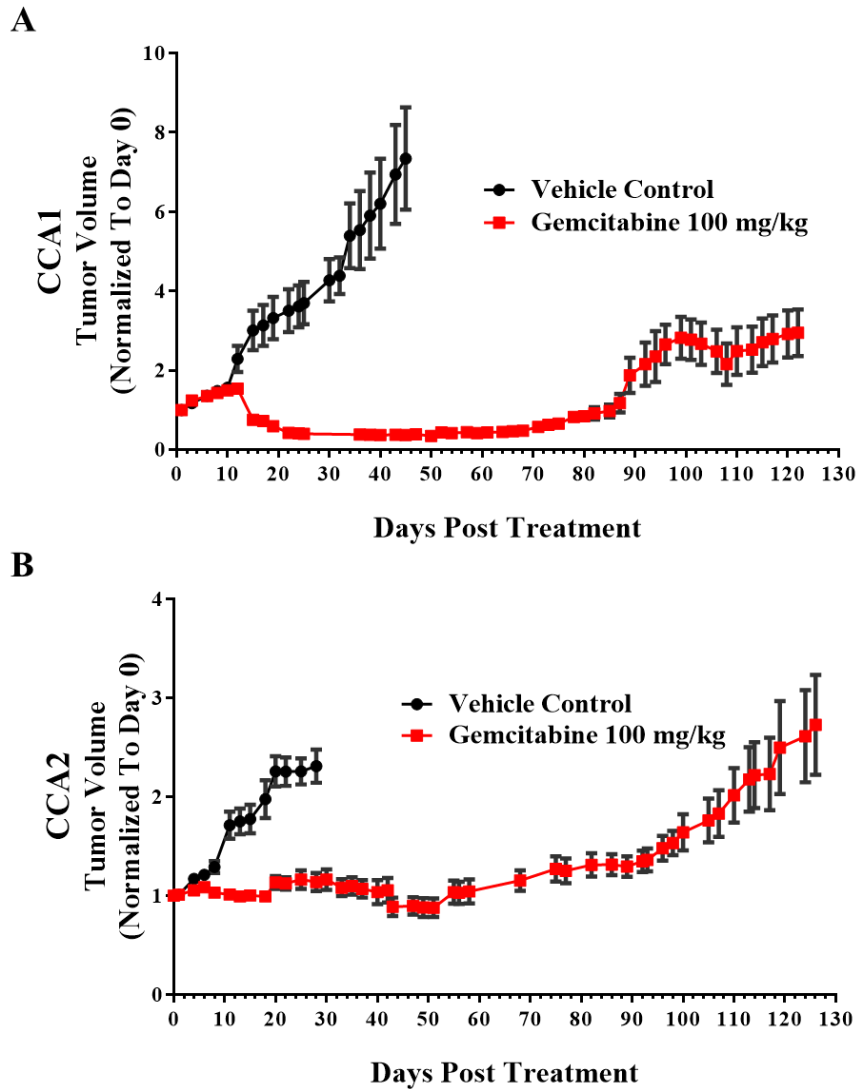


**Figure 4-6. Generation of CCA1 and CCA2 gemcitabine resistant models.** Mice bearing CCA1 or CCA2 tumors were implanted subcutaneously into SCID mice and administered with vehicle control or 100 mg/kg gemcitabine once a week. Tumor volumes were assessed three times a week for growth. CCA1 and CCA2 displayed tumor regrowth on days 50 and 55, respectively, while undergoing gemcitabine treatment. Following tumor regrowth, tumors were harvested for analysis or implanted into the next generation of mice to continue gemcitabine treatment. Harvested tissue was collected 24 hours after the last treatment.

### *Characterization of gemcitabine resistant CCA PDX models*

To date, no reports demonstrate the development nor characterization of a Gem<sup>R</sup> CCA PDX model. As rampant chemoresistance is experienced by the majority of CCA patients, development and characterization of a Gem<sup>R</sup> CCA PDX model would prove an invaluable research tool. As CCA1 and CCA2 Gem<sup>R</sup> models were observed to grow while receiving gemcitabine treatment, we first determined whether this increase in tumor volume was due to tumor cell proliferation and not an increase in stroma. We performed immunohistochemistry (IHC) on tissues collected within 24-hours after final treatment and stained for proliferative marker, Ki-67, across CCA1 and CCA2 vehicle control and Gem<sup>R</sup> tissues. Results were quantified by taking 5 photomicrographs at 40X magnification and counting every cell per field. Those stained brown were interpreted as Ki-67 positive. The percentage of Ki-67 positive cells is displayed in **Figure 4-7** and graphed below the representative images. CCA1 Gem<sup>R</sup> displayed a 3.23-fold increase in Ki-67 positive cells ( $p < 0.0001$ ) over control while CCA2 Gem<sup>R</sup> displayed a 2.61-fold increase ( $p < 0.0006$ ) over control.

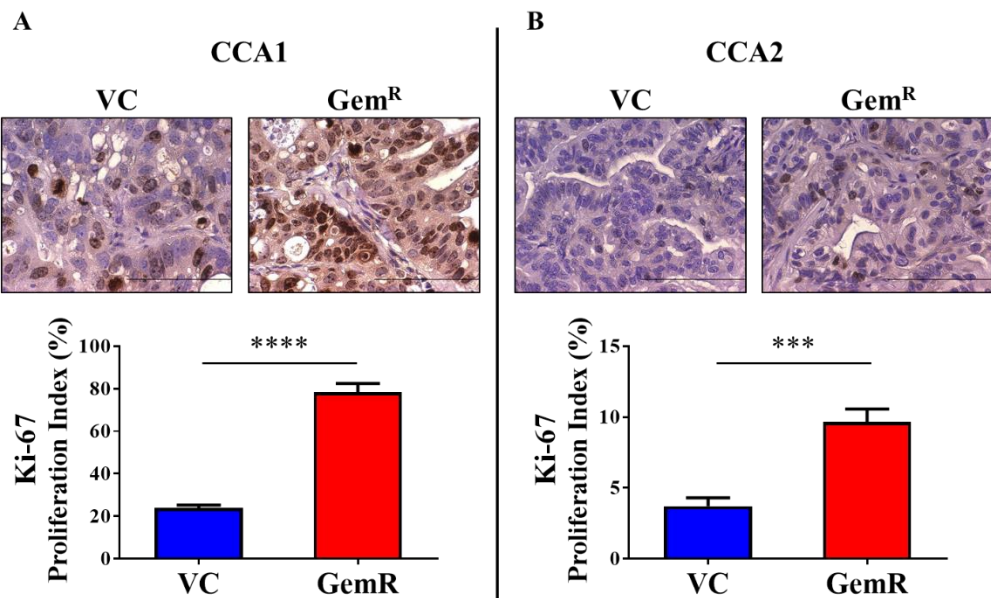


**Figure 4-7. CCA1 and CCA2 Gem<sup>R</sup> models display increased cell proliferation *in vivo*.** Tumor tissue samples were collected within 24-hours after final treatment and stained for proliferative marker, Ki-67, across **A)** CCA1 and **B)** CCA2 vehicle control and Gem<sup>R</sup> tissues. Results were quantified by averaging the percentage of Ki-67 positive cells across 5 photomicrographs at 40X magnification. Cells with nucleus stained brown were interpreted as Ki-67 positive. The percentage of Ki-67 positive cells is displayed below each representative image. CCA1 Gem<sup>R</sup> displayed a 3.23-fold increase in Ki-67 positive cells ( $p < 0.0001$ ) over control while CCA2 Gem<sup>R</sup> displayed a 2.61-fold increase ( $p < 0.0006$ ) over control. Student t-test was utilized for statistical analysis.

Based on the literature, mechanisms of *in vitro* gemcitabine resistance are often the result of altered gemcitabine metabolism including genes involved in drug import, phosphorylation and/or inactivation. To determine whether these mechanisms of resistance are observed in our *in vivo* models, we compared the expression of hCNT1, hENT1, dCK, cytidine deaminase (CDA) and RRM1 between control and Gem<sup>R</sup> CCA PDX models. Representative photomicrographs with expression index quantification are displayed in **Figures 4-8A** and **4-8B**. Expression indices were calculated for each sample

by multiplying the staining intensity (0, 1, 2 or 3) by the percentage of cells expressing the protein of interest.

Normal cholangiocytes display intrinsic chemoresistance through activation of FXR by bile acids. FXR activation induces downregulation of equilibrative and concentrative nucleoside transporters, such as hENT1 and hCNT1, which are associated with increased gemcitabine resistance [6, 55, 61, 165]. CCA1 displayed a 1.18-fold decrease in hCNT1 and a 1.41-fold increase in hENT1 compared to control while CCA2 displayed a 1.29-fold increase and 3.55-fold increase in hCNT1 and hENT1, respectively. Of note, downregulation of nucleoside transporters, including hCNT1 and hENT1, does not strictly correspond with gemcitabine resistance [62, 165]. It has been reported that Gem<sup>R</sup> models harboring deficiencies in dCK, the first step and the rate limiting enzyme in gemcitabine metabolism which converts gemcitabine to its monophosphate form, display increased resistance to gemcitabine [166]. CCA1 displays a 1.79-fold decrease in dCK expression while CCA2 displays a 1.15-fold increase in dCK. Further, gemcitabine metabolic product, gemcitabine diphosphate (dFdCDP), covalently binds the active site of ribonucleotide reductase (RR). RR replenishes the endogenous dNTP pool and upregulation of RR components, including RRM1, are associated with gemcitabine resistance. CCA1 displayed no alterations in RRM1 protein expression whereas CCA2 displayed a 1.36-fold increase in RRM1. Inactivation of gemcitabine is an additional mechanism through which resistance can arise. CDA, which converts dFdC to difluorodeoxyuridine (dFdU) for urine excretion, has been linked to gemcitabine resistance [166]. We observed a 1.1-fold decrease in CDA in CCA1 and a 1.25-fold increase in CCA2.

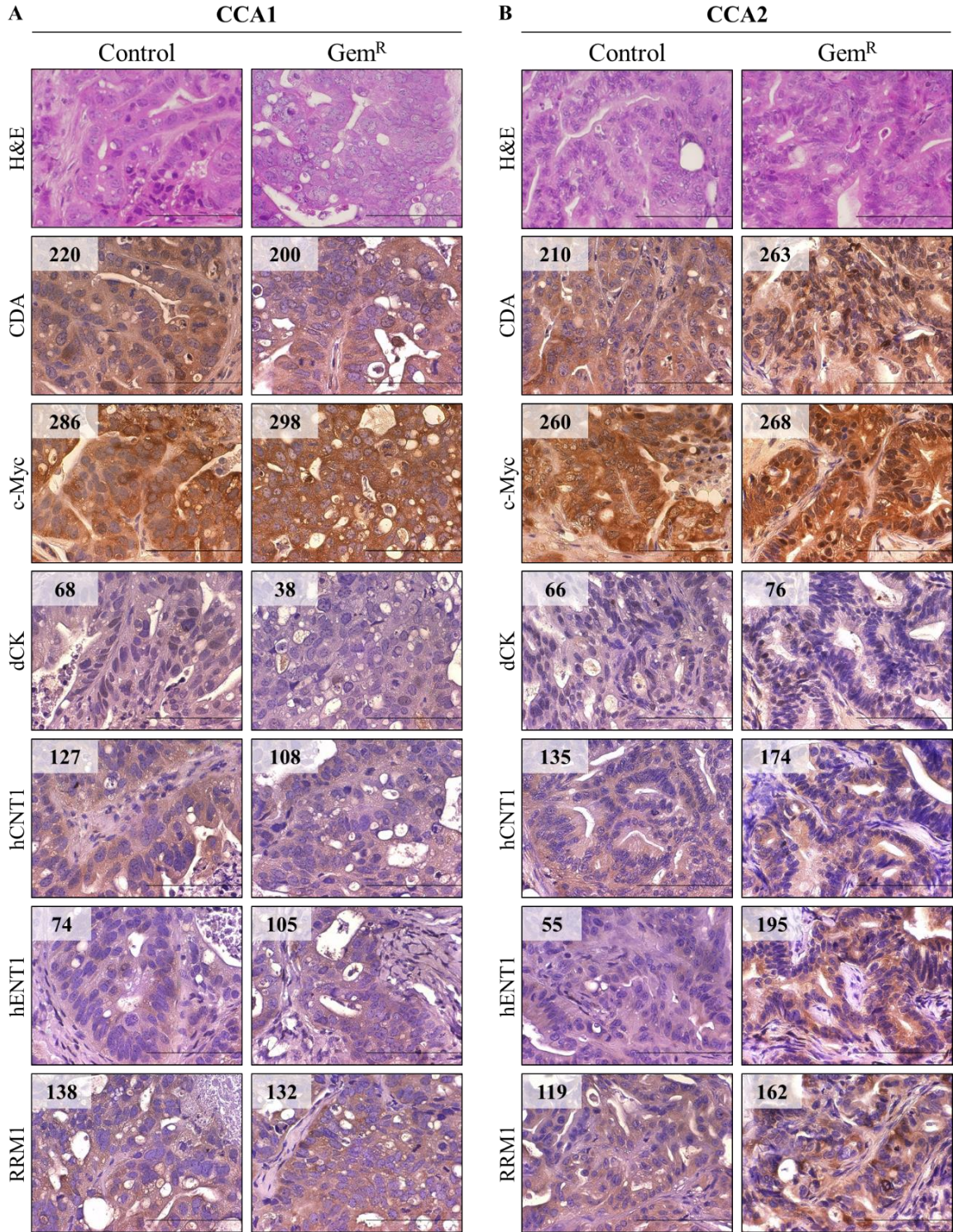


**Figure 4-8. Gemcitabine resistant models of CCA1 & CCA2 display altered expression of gemcitabine metabolic products.** IHC was performed on FFPE tumors harvested from **A)** CCA1 or **B)** CCA2 control or gemcitabine treated mice. Slides were stained for CDA, c-Myc, dCK, hCNT1, hENT1 or RRM1. Image insets indicate the calculated expression index. Expression indices were calculated for each sample by multiplying the staining intensity (0, 1, 2 or 3) by the percentage of cells expressing the protein of interest. Images were taken at 40X magnification.

As upregulation of proto oncogene, c-Myc, has been shown to promote resistance to gemcitabine, doxorubicin, and  $\beta$ -catenin inhibition in pancreatic cancer, TNBC and lung adenocarcinoma *in vitro* models, respectively [161, 171, 172], we chose to assess c-Myc expression in our CCA1 and CCA2 Gem<sup>R</sup> *in vivo* models. However, neither CCA1 nor CCA2 Gem<sup>R</sup> model displayed alterations in c-Myc expression when grown under gemcitabine treatment. Seemingly, CCA1 may be more resistant to gemcitabine through downregulation of gemcitabine metabolic component dCK while CCA2 may be gemcitabine resistant through alterations in gemcitabine metabolic component, RRM1, and inactivation enzyme, CDA. Taken together, our CCA1 and CCA2 Gem<sup>R</sup> models represent two distinct gemcitabine resistant mechanisms. However, this is a preliminary analysis and the expression of additional factors, including the involvement of RRM2, deoxycytidylate deaminase (dCMP), the BET family of proteins and DDR factors such as Chk1 must be assessed.



## Summary & Conclusions

In this study, we described the development of *in vitro* and *in vivo* gemcitabine resistant models. We identified that JQ1 synergized with gemcitabine in Chapter 3 using gemcitabine sensitive models. Unfortunately, the majority of CCA cases display intrinsic and/or acquired resistance. To better model patient disease, it is imperative that we develop gemcitabine resistant models to assess therapeutic efficacy. We first developed a gemcitabine resistant model of KKU-055. Parental cells were exposed to gradually increasing concentration of gemcitabine until cells grew normally at the administered concentration. Gemcitabine resistance was confirmed utilizing alamarBlue cell viability assay (**Figure 4-2**). Photomicrographs indicate no alterations in morphology, and we observed no alterations in cell doubling time nor *KRAS* codon 12 status (**Figure 4-3**).

Elevated c-Myc protein has been reported in therapeutic resistant *in vitro* models of pancreatic cancer, TNBC and lung adenocarcinoma which display resistance to gemcitabine, doxorubicin, and  $\beta$ -catenin inhibition, respectively. Though we have not addressed c-Myc expression in our Gem<sup>R</sup> model compared to parental, we investigated the impact of JQ1 on cell viability. KKU-055 Gem<sup>R</sup> displayed a 3.32-fold increase in JQ1 sensitivity compared to parental cells (**Figure 4-4**). While *in vitro* models are invaluable tools to assess the role of cellular and molecular alterations in the development, progression and treatment of cancer, they do not fully represent the disease. *In vitro* models lack components integral to CCA including stroma and ECM. We and others have established that PDX models recapitulate histology and molecular characteristics of the primary patient tumor. We surmise that development of gemcitabine resistant CCA PDX models will provide a more clinically relevant model system to study gemcitabine

resistance. Utilizing previously established CCA PDX models, CCA1 and CCA2, we developed and characterized gemcitabine resistant CCA PDX models. Tumor bearing mice were treated with 100 mg/kg gemcitabine once a week until tumors no longer responded to therapy (**Figure 4-5A & 4-5B**). Regrowth of CCA1 and CCA2 was observed on days 50 and 55 of treatment, respectively (**Figure 4-6A & 4-6B**). We then assessed histological and molecular differences between control and Gem<sup>R</sup> models. While no distinct morphological differences were observed, both Gem<sup>R</sup> models displayed increased proliferation as indicated by staining for Ki-67 in FFPE tissues. CCA1 Gem<sup>R</sup> and CCA2 Gem<sup>R</sup> displayed a 3.23-fold increase ( $p < 0.0001$ ) and a 2.61-fold increase ( $p < 0.0006$ ) over their respective Day 0 tumor volume (**Figure 4-7A & 4-7B**).

Immunohistochemical analysis suggest CCA1 and CCA2 developed resistance to gemcitabine through independent mechanisms. CCA1 displayed a 1.18-fold decrease in hCNT1, 1.41-fold increase in hENT1, 1.79-fold decrease in dCK, 1.1-fold decrease in CDA and no alterations in RRM1 (**Figure 4-8A**). CCA2 displayed a 1.29-fold increase in hCNT1, 3.55-fold increase in hENT1, 1.15-fold increase in dCK, 1.25-fold increase in CDA and a 1.36-fold increase in RRM1 (**Figure 4-8B**). Neither CCA1 nor CCA2 Gem<sup>R</sup> models displayed alterations in c-Myc protein expression (**Figure 4-8A & 4-8B**).

Based on our preliminary analysis, our data suggest CCA1 may be resistant to gemcitabine in part through downregulation of gemcitabine metabolic component dCK while CCA2 may be gemcitabine resistant through alterations in gemcitabine metabolic component, RRM1, and inactivation enzyme, CDA. Neither model displays markedly reduced expression of nucleoside transporters. This is consistent with the literature where downregulation of hNTs does not always correspond with gemcitabine resistance [62,

165]. Regarding upregulation of RRM1 in CCA2 Gem<sup>R</sup>, this is consistent with previous reports [55, 165, 166]. RR replenishes the dNTP pool and upregulation of RR components, including RRM1 and RRM2, is associated with gemcitabine resistance. Taken together, our CCA1 and CCA2 Gem<sup>R</sup> models represent two distinct gemcitabine resistant mechanisms. However, this is a preliminary analysis and the expression of additional factors, including the involvement of RRM2, deoxycytidylate deaminase (dCMP), the BET family of proteins and DDR factors such as Chk1 must be assessed. Taken together, these data support the use of gemcitabine resistant *in vitro* and *in vivo* model systems of CCA to evaluate the therapeutic efficacy and drug mechanism of action.

## CHAPTER 5

### DISCUSSION

#### **Introduction**

Cholangiocarcinoma (CCA) is the second most common primary hepatic malignancy and is characterized by late disease presentation, dismal prognosis, limited treatment options and poor clinical outcome. Primary hepatic malignancies, including iCCA and HCC, are predicted to become the second leading cause of cancer related death by 2030. While advances in CCA treatment options such as targeted and radiation therapy do improve overall survival, the most effective treatment regimen remains gemcitabine with cisplatin. However, this combination only prolongs survival by an additional 3-6 months over resection alone. Taken together, this paints a dismal picture for those diagnosed with CCA and demonstrates the imperative need to develop safe and effective therapeutic options for patients.

Within the last 10 years, BET bromodomain inhibitors, a class of small molecule and cell-permeable inhibitors has been explored for their anti-cancer properties across models of hematological and solid malignancies. The BET bromodomain and extraterminal domain family of proteins are transcriptional regulators which bind K-Ac

residues on histone tails and other nuclear proteins where they promote transcription elongation. Initial reports displayed BET inhibitor efficacy across a range of hematological malignancies driven by the BET-dependent oncogene, c-Myc. Upregulation of c-Myc has been identified in up to 94% of CCA cases with no observed expression differences existing between CCA subtypes. Together, these data suggest c-Myc downregulation by BET inhibition could benefit the majority of CCA patients irrespective of subtype diagnosis. This dissertation details the use of CCA *in vitro* and *in vivo* model systems to evaluate the mechanism and therapeutic efficacy of BET inhibition as a single agent as well as its use to enhance the efficacy of additional chemotherapeutics for the treatment of CCA.

This chapter will discuss the findings presented in this dissertation. We will describe our interpretation of the data, the importance of the presented results and overall scientific significance. The first chapter will highlight the novel observation that JQ1 inhibited cell viability and tumor growth which coincides with c-Myc inhibition. We will also discuss the novel combination of BETi with PARPi in our *in vitro* and *in vivo* models of CCA. The second chapter will cover the combination of gemcitabine with cisplatin as well as the combination of JQ1 with gemcitabine. And the third chapter will explore the development of novel CCA *in vitro* and *in vivo* gemcitabine resistance models. The final section will detail suggestions and predictions for future aspects of this work.

### *JQ1 in CCA in vitro models*

The first sign that BET proteins were involved in cancer was the identification of BET proteins, BRD3 or BRD4, fused with nuclear protein in testis (NUT) in NUT midline carcinoma (NMC) [81, 102]. BRD4-dependent NMC cells experienced both growth and cell cycle arrest upon treatment with BET inhibitor, JQ1 [81]. One of the most striking impacts of BET inhibition was the downregulation of proto-oncogene, c-Myc. Further, this decrease in c-Myc expression was found to coincide with decreased tumor growth in xenograft models of leukemia and lymphoma by BETi treatment [96, 108]. This was a monumental observation as, up until this point, direct c-Myc therapeutic inhibition had proven difficult [124]. The vast majority (94%) of CCA cases, irrespective of subtype, express elevated levels of c-Myc protein, however, the mechanism through which c-Myc expression is elevated in CCA has not yet been established [117]. In 2011, Li et al. reported that downregulation of c-Myc by RNA interference (RNAi) lead to a significant decrease in CCA invasiveness *in vitro*. However, the impact on cellular viability was not assessed [123]. CCA TCGA data suggest high c-Myc protein expression (z-score threshold =  $\pm 2$ ) correlates with significantly shorter overall patient survival (30.3 months vs. 5.58 months) [122].

Our lab first investigated the use of BET inhibition using two CCA PDX models generated in our lab, CCA1 and CCA2. Both preclinical models expressed comparable levels of c-Myc protein. Mice harboring CCA1 or CCA2 were administered 50 mg/kg JQ1 administered once a day for 20 days [71]. Following treatment, we observed a significant decrease in CCA2 tumor volume, however, this effect was not observed in mice harboring CCA1. Assessing the molecular impact of JQ1 treatment in CCA2, we

observed that c-Myc protein was significantly downregulated and this reduction in c-Myc coincided with the significant reduction of Ki-67 positive cells. While JQ1-mediated downregulation of c-Myc was not surprising and has been reported previously in other malignancies, this was the first report of JQ1-mediated reduction of c-Myc in CCA [96, 107, 173-175].

To elucidate the mechanism and determine if a dose-dependent relationship existed between the concentration of JQ1 and c-Myc downregulation, we utilized *in vitro* CCA models, KKU-055 and KKU-100, and alamarBlue cell viability assays (**Figure 1B-1D**). JQ1 significantly decreased the expression of c-Myc in a dose-dependent manner in both cell lines at both the mRNA and protein level (**Figure 2A-2F**). These results correspond with decreased in cell viability (**Figure 1B-1D**) and colony forming potential (**Figure 1E-1I**) observed in both cell models. JQ1 *in vitro* potency has been reported in the nanomolar range for hematological malignancies with micromolar values reported in osteosarcoma (7.35  $\mu\text{M}$ ), pancreatic cancer (3.5  $\mu\text{M}$ ) and leukemia (> 5  $\mu\text{M}$ ) [110, 176, 177]. Further, pharmacokinetic analysis determined that the peak plasma concentration of the *in vivo* dose of 50 mg/kg JQ1 was 11,000 ng/mL, which is equivalent to 24  $\mu\text{M}$  [178]. JQ1  $\text{IC}_{50}$  values attained in KKU-055 and KKU-100 *in vitro* assays are achievable *in vivo* which indicate these doses are relevant.

Of the two CCA *in vitro* models, KKU-100 displayed greater JQ1 sensitivity compared to KKU-055 (6.3-fold at the 96-hour time point). While both models are derived from patients with *Opisthorchis viverrini* infection [32, 179], alterations in the status of p53 and IDH1/2 have been reported to contribute to BET inhibitor sensitivity. *In vitro* acute myelogenous leukemia (AML) cell models harboring wild type p53 showed

increased sensitivity to JQ1 [180]. Hematulin et al. reported that in response to radiation, p53 phosphorylation on Ser-15, which is necessary for activation, was undetectable in KKU-055. Further analysis indicated that KKU-055 expresses truncated and not full length p53 protein [181, 182]. The p53 status of KKU-100 is inconclusive. The original publication detailing the development of KKU-100 states the primary tumor and subsequent cell line do not express p53, yet studies utilizing KKU-100 *in vitro* specify that p53 is expressed [32, 183-185]. No literature documents the specific mutational status or lack thereof.

In a 2018 report, Fujiwara et al. established a link between CCA *in vitro* models harboring an IDH1 mutation and increased sensitivity to BET inhibitor, JQ1 [128]. In this study, iCCA *in vitro* model RBE, which harbors an *IDH1* mutation (*IDH1*<sup>R132S</sup>), was more sensitive to JQ1 than *IDH1* wild type iCCA cells, HuH28 and HuCCT1 [128]. Forced expression of mutant *IDH1* (*IDH1*<sup>R132S</sup>) in HuCCT1 cells increased JQ1 sensitivity compared to control. However, even with mutant *IDH1* (*IDH1*<sup>R132S</sup>) in HuCCT1, RBE still displayed the greatest JQ1 sensitivity. Interestingly, both HuH28 and HuCCT1 models contain mutations in p53 (p.E271L and R175H, respectively) while RBE contains wild type p53. While not explored by Fujiwara et al, it is possible that RBE displayed the greatest JQ1 sensitivity due to IDH1 mutation in addition to wild type p53.

Comparing results from Fujiwara et al. to the work presented in this dissertation, it is important to indicate that RBE, HuH28 and HuCCT1 *in vitro* models were all derived from metastatic site ascites while *in vitro* models utilized in this dissertation are derived from patients with *O. viverrini* parasitic infection. Mutational profiles differ between *O. viverrini*-associated and non-*O. viverrini*-associated CCA cases. Mutations in



*TP53* are more ubiquitous in *O. viverrini*-associated CCA while mutations in *IDH1* are more prevalent in non-*O. viverrini*-associated CCA [12, 31]. *KRAS* is commonly mutated in both (17%) [16, 31]. Further, CCA cell lines KKU-055 and KKU-100 represent the CCA subtypes iCCA and pCCA, respectively [147]. As *IDH1* mutation occurs primarily in iCCA (20% of iCCA cases), the likelihood of KKU-100 harboring an *IDH1* mutation could be minimal. To date, the status of *IDH1* in KKU-055 and KKU-100 have not been reported.

As indicated, *KRAS* is commonly mutated in both *O. viverrini*-associated CCA and non-*O. viverrini*-associated CCA [12, 31]. Non-small lung cancer (NSLC) harboring a *KRAS* oncogene were reportedly more sensitive to JQ1 [186]. In our initial CCA PDX study utilizing JQ1, we observed that CCA2, which harbors an oncogenic *KRAS*<sup>G12D</sup> mutation, responded to JQ1 treatment *in vivo* while CCA1, which is wild type *KRAS*, did not [71]. In addition, previous reports indicate, and we confirmed that KKU-100 contains an oncogenic *KRAS*<sup>G12D</sup> mutation whereas KKU-055 harbors wild type *KRAS* (**Figure 1A**). It is possible that specific genetic alterations exist which could confer greater sensitivity to BET inhibition between these two model systems. Further genetic analysis and genetic manipulations are necessary to determine the impacts of these mutations in BET inhibitor sensitivity in CCA.

#### *JQ1 reduces the expression of two gene products*

JQ1 has shown efficacy in multiple solid tumor models including pancreatic cancer [109, 110], thyroid cancer [111] and renal cell carcinoma [112]. However, BET-

dependent protein expression reportedly varies among tumor types [78, 81, 93, 113]. As such, BETi mechanism of action and subsequent therapeutic efficacy may be cancer or cell type dependent as treatment with BETi has shown therapeutic efficacy via downregulation of c-Myc, *CDC25B* (by NanoString nCounter analysis) and *FOSL1* in multiple myeloma (MM), pancreatic ductal adenocarcinoma (PDAC) and non-small lung cancers (NSLC), respectively [85, 110, 114, 115]. As c-Myc was observed to be downregulated by JQ1 in CCA2, we next assessed the impact of additional molecular targets by JQ1 in our CCA PDX models. We compared the gene expression patterns of CCA1 and CCA2 vehicle control (VC) treated mice to their respective JQ1 treated counterparts through NanoString nCounter analysis which assessed 230 pan cancer genes. We identified that, in addition to c-Myc, its transcriptional target, Chk1 was also downregulated 2.6-fold by JQ1 in CCA2 but not CCA1. These results were corroborated by immunohistochemistry (IHC) [71] and also observed in our *in vitro* models post JQ1 treatment (**Figures 2A-2F**). Chk1 is both a direct and indirect c-Myc transcriptional target [150, 164] and JQ1-mediated downregulation of Chk1 is consistent with the literature [187]. Further, no significant alterations were observed in *CDC25B* nor *FOSL1* mRNA expression in CCA2 which suggests downregulation of c-Myc by JQ1 contributed to the reduction in tumor volume. Using an *in vitro* CCA model, Li et al. identified that RNAi-mediated downregulation of c-Myc significantly decreased invasiveness, however, the impact on cell viability was not addressed [123]. For these reasons, we focused on BET-dependent downregulation of c-Myc and its transcriptional target, Chk1, in CCA.

## Targeting c-Myc in CCA

### *Knockdown of BRD2 and BRD4 reduces c-Myc protein expression in vitro*

The mechanism through which c-Myc protein expression is elevated in CCA is not known. Literature indicates that BRD2 and BRD4 contribute to the regulation of c-Myc expression in multiple cancer types including lung cancer cells, acute leukemia cells, acute myelogenous leukemia and multiple myeloma cells [91, 96, 107, 153, 188]. Further, knockdown of BRD4 in bladder cancer decreases the expression of c-Myc protein and knockdown of BRD2 or BRD4 in renal cell carcinoma (RCC) reduces c-Myc expression with knockdown of both BRD2 and BRD4 yielding the greatest c-Myc reduction [189, 190]. Alongside BRD2 and BRD4 KD-mediated downregulation of c-Myc in RCC, Chen et al. identified strong anti-proliferative effects in knockdown of BRD2 or BRD4 individually and even greater effects when knocked down together [189].

In Chapter 2, we hypothesized that downregulation of either BRD2 or BRD4 individually would decrease c-Myc expression in CCA. To downregulate the expression of these BET proteins, we transfected *in vitro* CCA model, K KU-055, with shRNA plasmid targeting GFP (negative control), BRD2 or BRD4. When BRD2 expression was decreased by >95%, we observed a concurrent >95% decrease in c-Myc expression (**Figure 4A**). Further, when BRD4 expression was decreased by >98%, c-Myc expression was concomitantly decreased by ~50% (**Figure 4b**). These data suggest that c-Myc expression is BET-dependent in CCA *in vitro* model, K KU-055. Interestingly, while our BRD2 and BRD4 KD models of K KU-055 did display reduced c-Myc protein expression (**Figure 4**), we did not observe alterations in cell doubling time as reported by Chen et al.

in a RCC KD model (data not shown) [189]. Further, we made the novel observation that BRD2 KD model displayed a >95% reduction in c-Myc expression whereas KD of BRD4 displays a ~50% reduction. With the greatest reduction of c-Myc observed in the BRD2 KD model, it is possible that BRD2 primarily drives c-Myc expression in KKU-055. However, if that were the case, KD of BRD4 would not be expected to alter c-Myc expression as BRD2 expression should remain unchanged. Instead, BRD4 KD displays a ~50% reduction in c-Myc expression. This suggests BRD2 is not the sole driver of c-Myc and that BRD4 drives a proportion of c-Myc expression in KKU-055. However, if BRD4 drives a proportion of c-Myc expression, you would expect BRD2 KD model would display a greater proportion of c-Myc than the <10% c-Myc it expresses (**Figure 4A**).

Delmore et al. identified that JQ1 downregulates the expression of c-Myc in multiple myeloma (MM) *in vitro* and that this effect was due to reduced BRD4 association at the *MYC* transcriptional start site (TSS). Interestingly, they also reported that E2F1-dependent genes were downregulated by treatment post JQ1. While c-Myc transcribes E2F1, no reduction in E2F1 protein nor mRNA was observed [96]. E2F is a family of transcription factors encompassing activators (E2F1, E2F2 and E2F3A) and repressors (E2F3B, E2F4, E2F5 and E2F6) [191]. High E2F transcription is detected in nearly all cancers and is the result of alterations in the CDK-RB-E2F axis. Briefly, mitogens signal proliferation leading to inactivation of pocket protein, retinoblastoma (RB), the repressive factor binding to and governing E2F1 [191]. Upon RB inactivation, E2F1 is released where it subsequently promotes the expression of gene targets, particularly those expressed during G1 of the cell cycle [191]. As the expression of c-

Myc is tightly regulated in normal proliferating cells undergoing cell division, it is not a surprise that c-Myc is an E2F1 transcriptional target [192, 193].

Delmore et al. reported JQ1-mediated downregulation of E2F1 gene targets, including c-Myc, in their model of MM. However, as E2F1 is a transcriptional target of c-Myc, the observation that E2F1 itself was not downregulated at the transcriptional or transcriptional level was puzzling. They hypothesized that an unrecognized association between BET proteins and E2F1 transcription exists in MM. However, Delmore et al. were not the only ones to observe this phenomenon. Using an *in vitro* model of medulloblastoma, Venkataraman et al. identified that JQ1 downregulated c-Myc expression and induced senescence through inhibition of E2F1 activity [194]. Previous work documents the protein-protein interaction between BET protein, BRD2, and E2F1 [91, 195-197]. It has been proposed that BRD2 functions as a scaffold and recruits E2F1 to chromatin to promote gene transcription [91, 196, 198]. Additionally, BRD4 interacts with acetylated E2F1 (K117ac/K120ac) through the BD1 domain, however, scaffold function has not been reported [199].

It is possible that, in our model of KKKU-055, c-Myc is primarily driven by BRD2. In parental cells, BRD2 may recognize and bind K-Ac residues along the *MYC* locus, recruit E2F1, and BRD4 binds acetylated E2F1 to promote transcription as a complex. It is also possible that association of BRD4 to acetylated E2F1 may play a role in timing and/or amplitude of c-Myc expression but is not required. This would account for the low (<10%) expression of c-Myc in our BRD2 KD model (**Figure 4a**) yet indicate how KD of BRD4 leads to ~50% reduction in c-Myc expression (**Figure 4b**). However, this is all speculation and would require additional analysis to properly address this hypothesis.

The proposed hypothesis relies upon assumptions which have not been determined experimentally. For example, while overlap exists between histone K-Ac binding of BRD2 and BRD4 (common residues include H3K14, H4K5, H4K8 and H4K12), it is not known whether BRD2 and BRD4 associate with the same region along the *MYC* locus [83]. To address this, CHIP-Seq can be performed in which we pull down BRD2 and BRD4 using CHIP grade antibodies in untreated parental KKU-055 and assess their location along the *MYC* locus. Further, BRD2 and BRD4 have not been reported to associate together in CCA. Immunoprecipitation with BRD2 and BRD4 can be performed to assess whether they, as well as E2F1, pull down together via immunoblot (IB). Further, with generation of stable BRD2/BRD4 KD models, it is possible that genome-wide acetylation changes have occurred in KD cells and other methods have been acquired to express BET-dependent genes. Potentially, downregulation of BRD2 and subsequent c-Myc downregulation could indicate that c-Myc is no longer necessary for survival in this population and the mechanism of survival has shifted. CHIP-Seq of the residual BRD2, as well as endogenous BRD3 and BRD4 could be performed and may indicate increased association to known BET binding sites or identification of new and novel genes regulated by the BET family.

*Knockdown of BRD2 or BRD4 in KKU-055 increased sensitivity to BET inhibition*

This is the first report in which BRD2 or BRD4 KD models were exposed to BET inhibition. Unexpectedly, KD of BRD2 and BRD4 in KKU-055 displayed increased sensitivity to both JQ1 and I-BET. BRD2 KD displayed a 29.3-fold and 21.4-fold increase in sensitivity to JQ1 and I-BET, respectively, and BRD4 KD displayed an 18.3-

fold and 12.4-fold increase in JQ1 and I-BET, respectively. The BET family of proteins canonically recognize and bind K-Ac residues on histone tails and other nuclear proteins [78] which pharmacological BET inhibition has been reported to perturb [81, 85, 96, 105, 106]. BET inhibitor mechanism of action and subsequent therapeutic efficacy may be cancer or cell type dependent as treatment with BETi has shown therapeutic efficacy via downregulation of c-Myc, CDC25B and n-Myc in multiple myeloma (MM), pancreatic ductal adenocarcinoma (PDAC) and neuroblastoma, respectively [85, 110, 114]. To date, the role of BET family member BRD2 in cancer has not been well defined and has not been assessed in cholangiocarcinoma. Previous work investigating BRD2 details its role in the production of proinflammatory cytokines [84], however, BRD2 has been reported to associate with the *MYC* locus in human non-small cell lung cancer cell line, H23 [91]. In contrast, the well-studied BET protein, BRD4, was initially shown to regulate gene expression through interacting with K-Ac residues on histone tails [93-95], however, noncanonical functions have emerged. BRD4 insulates chromatin from DNA damage signaling [98], is involved in telomere maintenance [93] as well as containing an extraterminal domain which is involved in transcriptional regulation through interactions with many proteins such as lysine methyltransferase NSD3 and the chromosome remodeling complex SWIF/SNF [93]. Additionally, BRD4 has been reported to associate with numerous transcription factors (TFs) including p53, YY1, AP2, c-JUN, C/EBP $\alpha/\beta$  and the heterodimer c-MYC/MAX in a bromodomain (BD) independent manner [93]. Further, BRD4 has been shown to contain a histone acetyltransferase (HAT) domain which acetylates histones H3 and H4 in patterns distinct from established HATs [99]. BRD4 acetylates H3K122 which promotes nucleosome eviction, chromatin

decompaction and increased transcription [93]. It is possible that gene KD and therapeutic inhibition, via JQ1 or I-BET, are not equivalent due to the established BD independent functions of BRD4. Rather, to address whether the observed increase in BETi sensitivity are through inhibition of K-Ac binding and not loss of BRD4 BD independent functions, the generation of a dominant negative BRD4, which lacks asparagine residues in each bromodomain and would no longer recognize and bind K-Ac residues yet keep non-BD functions intact could be utilized.

In addition, BET inhibitors are not specific to a single BET protein. Instead, BETi inhibit the entire BET family including BRD2, BRD3, BRD4 and BRDT, with varying binding affinities. It is likely that each BET protein likely contributes to the expression of a different subset of genes. When one BET protein is downregulated, the others are still molecular targets for BET inhibitors. It is possible that cells with low level BET protein expression are more sensitive to BET inhibitors than cells with high level BET expression.

### **Practicality & limitations of BET inhibition for use in cancer**

#### *Long term exposure to BETi in vivo*

Although BET inhibitors specifically target the BET family of proteins and display therapeutic efficacy in multiple cancer models, they are not specific to a single BET protein [81, 103]. With the exception of BRDT which is expressed in the testis [178], the BET family of proteins, BRD2, BRD3 and BRD4, are ubiquitously expressed in all mammalian tissues and are required for transcription of BET-dependent genes in



normal, nonmalignant cells [84, 85]. For example, BRD4 is required for and controls cellular identity during adipogenesis [200]. Moreover, BRD2 and BRD4 are required for mouse embryogenesis [88, 92]. Taken together, systemic BET inhibition could pose potential side effects.

Previous research indicates that KD of BRD4 *in vitro* recapitulates pharmacological BET inhibition in these models [96, 189, 201]. These data indicate the observed phenotypes were due to on-target effects. The studies, experiments and results put forth in this dissertation addressed the impact of BET inhibition over a multi-day exposure *in vitro* and administration of 50 mg/kg JQ1 daily for 21-days *in vivo*. In our *in vivo* model system, we did not observe any adverse side effects such as lethargy or weight gain/loss over the course of treatment. This dose and schedule of JQ1 has been previously established for use in mice with no reported side effects [71, 105]. However, no maximum tolerated dose of JQ1 has been reported for use *in vivo*. To date, the greatest administered dose of JQ1 was performed by Matzuk et al. in which mice were administered 100 mg/kg JQ1 once a day for three months with no reported side effects [178]. Bolden et al. assessed long term BRD4 suppression using a doxycycline inducible and reversible transgenic RNAi mouse model [202]. They observed that strong suppression of BRD4 prompted alopecia, decreased cellular diversity, disrupted tissue homeostasis, depleted the stem cell population in the small intestine and sensitized organs to irradiation. Interestingly, these effects were reversed upon re-expression of BRD4 [202]. While toxic side effects may result from administration of BET inhibition, these data suggest that appropriate dosing and timing of these compounds could be efficacious while managing potential toxicities.

While these studies are paramount, those by Bolden et al. were performed using a transgenic murine model. Human clinical trials can shed light on safety and therapeutic efficacy of BETi for use in cancer therapy. There are currently 17 BET inhibitors in clinical trials across hematological and solid malignancies with the majority currently in phase 1 [203]. JQ1 will not be pursued as a clinical agent due to its short half-life [203]. In the first-in-human clinical trial to determine the safety and pharmacokinetics of BETi ABBV-075 in patients with refractory solid tumors, 98.6% of patients presented with >1 treatment-emergent adverse events (TEAEs) including thrombocytopenia (56.9%), dysgeusia (48.6%), fatigue (43.1%) and nausea (34.7%) [203]. In the same clinical trial, preliminary results displayed antileukemic effects in which bone marrow blast counts were 50% of baseline in 4/10 of evaluable patients and one patient achieved complete remission [203]. There are currently no ongoing clinical trials involving the use of BET inhibition for use in CCA.

#### *BET inhibitor resistance*

The unfortunate reality is that resistance to targeted therapeutics can arise and therapeutic inhibition of BET proteins is no exception. While the first-in-human study of ABBV-075 in solid tumors displayed complete remission in one patient, 35 (57%) of those in the clinical trial experienced progressive disease while undergoing treatment [203, 204]. Understanding and characterizing mechanisms of BETi resistance to optimize clinical efficacy has become an increasing focus. In models of therapeutic resistance, it is not uncommon to see alterations in drug efflux/influx, drug metabolism or development of additional mutations to overcome therapy. However, these events do not appear to

mediate BETi resistance. Instead, mechanisms of resistance appear to be cancer type specific.

In leukemia cells, BET inhibitor resistance induces a global loss of BRD4 binding to DNA. However, the expression of c-Myc remains unaltered, indicating that expression is maintained through another mechanism. Interestingly, they observed no alterations in drug efflux/influx nor alterations in intracellular or extracellular drug concentration. Compared to parental cells, their BETi resistance models were smaller and more homogeneous with increased activation of TGF- $\beta$  and Wnt/ $\beta$ -catenin pathways while NF- $\kappa$ B signaling was reduced [205]. In castration-resistant prostate cancer (CRPC), BRD4 drives transcription of androgen receptor (AR). In a BETi resistant CRPC model, BRD4 was no longer associated with chromatin and reactivation of AR expression was now regulated by CDK9 [206]. In a triple negative breast cancer (TNBC) model of BETi resistance, no new drivers, gatekeeper mutations or drug pump alterations were identified. BRD4 was still found associated with chromatin, however, it was found to promote cell proliferation through a bromodomain-independent mechanism [152]. Interestingly, in all cases, resistant populations were found to be cross resistant to additional BET inhibitors.

### **Combining JQ1 with PARP inhibition for use in CCA**

#### *JQ1 induces DNA damage in CCA models*

As Chk1 plays a role in DNA damage response (DDR), and therapeutic inhibition of Chk1 has been shown to induce DNA damage [207-209], we hypothesized that CCA

models exposed to JQ1 would show signs of DNA damage. Therefore, we utilized the well-established DNA damage marker,  $\gamma$ H2AX, to assess DNA damage. Upon DNA damage, H2AX is phosphorylated on Ser-139 within minutes by ataxia telangiectasia-Rad3-related (ATR), ataxia telangiectasia mutated (ATM) or DNA-dependent protein kinase (DNA-PK), forming  $\gamma$ H2AX [127, 210]. Phosphorylation to  $\gamma$ H2AX plays a vital role in retaining remodeling factors and assembling DDR proteins at sites of SSBs and DSBs [127, 211]. Results from immunohistochemistry (IHC) confirmed that JQ1 induced DNA damage in CCA patient derived xenograft (PDX) model, CCA2, potentially through downregulation of DDR factor, Chk1 [71]. Further, we identified a dose dependent increase in  $\gamma$ H2AX in our CCA *in vitro* models, KKU-055 and KKU-100, by JQ1 using immunoblot (IB) (**Figure 2g & 2i**).

While  $\gamma$ H2AX was primarily observed utilizing IB in this dissertation, other, more sensitive assays are available. The comet assay utilizes a gel electrophoresis-based method to assess DNA damage in individual cells with the added capability of assessing both SSBs and DSBs with protocol modifications [212]. Further, as the phosphorylation of H2AX to  $\gamma$ H2AX spreads 1-2 Mbp along the chromatin, this spread is abundant enough that it can be visualized as discrete foci and utilized as a DNA damage biomarker by immunofluorescence [210, 213]. Individual  $\gamma$ H2AX foci can be quantified and the number then compared between treatment groups [214]. As with many assays,  $\gamma$ H2AX foci quantification is not without limitations.  $\gamma$ H2AX levels increase as cells progress through mitosis due to DNA-PKcs-mediated phosphorylation which does not recruit DDR factors [215]. In addition to  $\gamma$ H2AX foci quantification, immunofluorescence can be utilized to assess homologous recombination-mediate repair through RAD51 foci

[105] or non-homologous end joining (NHEJ)-mediated repair through p53-binding protein 1 (53BP1) or DNA-PKcs foci [216, 217].

Floyd et al. was the first to associate BET protein, BRD4, with response to DNA damage [98]. *BRD4* encodes three splice isoforms (A, B and C) with each isoform comprising two bromodomains (BDs) and one extra-terminal (ET) domain. Of the three isoforms, isoform B recruits the condensin II chromatin remodeling complex to acetylated histones to insulate chromatin from DNA damage signaling. RNAi-mediated downregulation of BRD4 isoform B resulted in relaxed chromatin structure, cell-cycle checkpoint recovery and enhanced survival post radiation therapy *in vitro*. This effect was found to be specific to isoform B [98]. Further, Stanlie et al. established that BRD4 is critical for activation-induced cytidine deaminase (AID) and I-SceI-induced NHEJ repair in B cell IgG class switch recombination (CSR). During B cell CSR, BRD4 is recruited to DNA break sites where it functions as an adapter between chromatin and repair factors such as 53BP1 [100]. Li et al. corroborate this report utilizing an *in vitro* prostate cancer model in which they demonstrate that BRD4 is essential for repair of DSBs through binding of 53BP1 and promoting repair through NHEJ [218]. While the impact of BET proteins, such as BRD4, on DNA damage response has not been reported in CCA *in vitro* models, this dissertation documents the novel observation that JQ1 induces DNA damage in *in vitro* CCA cell line models (**Figure 2g, I, h, & j**). Though this dissertation does not differentiate between the formation of DSBs or SSBs by JQ1, methods discussed above, including comet or immunofluorescence of RAD51, 53BP1 or DNA-PKcs, could be utilized to specify which type of DNA break lesion JQ1 induces in

CCA. It is possible that we can utilize JQ1-induced DNA damage to sensitize cells to additional therapeutics.

*JQ1 sensitizes in vitro and in vivo CCA models to PARP inhibitors*

In response to both single and double strand breaks, PARP1 is rapidly recruited to the break point where it then catalyzes the addition of branched pADPr residues to itself and surrounding histones. These branches recruit hundreds of proteins to the DNA break site which subsequently promotes repair [137]. Tumors harboring deficiencies in DDR factors display PARP inhibitor (PARPi) sensitivity [135, 137]. PARPi inhibit the catalytic function of PARP1 and PARP2 which traps PARP proteins on DNA yet unable to recruit additional DDR proteins [139]. Downregulation or therapeutic inhibition of DDR factors in coordination with PARPi has been shown to induce synthetic lethality [138]. Olaparib was the first FDA-approved PARP1/2 inhibitor to take advantage of breast cancers harboring mutations in *BRCA1* or *BRCA2* to induce synthetic lethality [139-141]. The Cancer Genome Atlas (TCGA) indicates that up to 1.4% and 6% of CCA cases display mutations in *BRCA1* or *BRCA2*, respectively [122]. Mao et al. investigated the use of PARPi to increase the sensitivity of CCA to radiation. They concluded that PARPi in combination with irradiation proved efficacious *in vitro*. However, none of the CCA *in vitro* models utilized for their study harbored *BRCA1* or *BRCA2* mutations. Therefore, whether *BRCA1/2* mutations sensitize CCA *in vitro* models to PARPi was not determined [219]. Interestingly, a single case report from 2018 indicated that treatment with olaparib lead to partial response in a patient diagnosed with iCCA harboring a *BRCA2* mutation [220]. There are currently three ongoing phase 2 clinical trials utilizing

PARPi for use in CCA, however, as two are currently recruiting and the third has not begun recruiting, data are not currently available (ClinicalTrials.gov identifiers: NCT03212274, NCT03207347 and NCT03878095).

Recent evidence across a range of solid tumors indicate that BETi in combination with PARPi pose enhanced efficacy over their use as single agents. These combination therapies describe drug synergy through BETi-mediated downregulation of multiple gene targets including *RAD51*, *XRCC5*, *CDC25B*, *TOPBP1*, *BRCA1* and *WEE1* [105, 156, 221, 222]. Further, cells harboring deficiencies in DDR factors or display increased levels of DNA damage exhibit PARPi sensitivity [129-134]. Further, Mio et al. reported that JQ1 induced a BRCAness phenotype in *BRCA1*-wild type triple negative breast cancer (TNBC) through reduction of *BRCA1* [223]. In our CCA PDX model, CCA2, we observed a significant decrease in *BRCA2* expression but not *BRCA1*. *In vitro* CCA models, KKU-055 and KKU-100 do not harbor mutations in six previously characterized *BRCA1* mutations or in four *BRCA2* mutations (**Figure S1**) [224]. We further identified that JQ1 induced downregulation of *BRCA2* at  $10^{-4.5}$  M and  $10^{-6}$  M in KKU-055 and KKU-100 at a 72-hour time point, respectively (**Figure S2**). As there was no consistent downregulation of *BRCA2* across models, JQ1-mediated downregulation of *BRCA2* was not pursued further. To corroborate the results reported by Mio et al, it will be important to establish whether JQ1 decreases the expression of *BRCA1* in our models. This can be addressed utilizing qRT-PCR as well as IB post JQ1 treatment in our *in vitro* models.

These reports as well as our observation that JQ1 induces DNA damage and decreases Chk1 expression in our CCA PDX model, CCA2 [71], led us to investigate whether PARPi in combination with BETi could prove efficacious in CCA. We first

confirmed downregulation of DDR factor Chk1 by JQ1 *in vitro* (**Figures 2c & 2e**). Next, we explored the potency of BETi in combination with PARPi utilizing *in vitro* models of CCA. KKU-055 and KKU-100 were exposed to a range of BETi + PARPi concentrations as single agents or in a 1:1 ratio. Drug combination indices using CompuSyn (1.0) software were calculated and all four combinations displayed CI values <1 indicating drug synergy in both KKU-055 and KKU-100 *in vitro* models (**Figure 3c & 3d**). In addition to downregulation of c-Myc and Chk1, JQ1 treatment resulted in the accumulation of  $\gamma$ H2AX in both CCA *in vitro* models (**Figures 2g & 2i**). Further, the combination of JQ1 with olaparib promotes greater reduction in tumor volume than either drug alone in an *in vivo* CCA model (**Figure 6a**). While these results were obtained utilizing two cell line models, our *in vitro* and *in vivo* data are promising. This study suggests that the combination of BETi with PARPi warrant further investigation as a therapeutic combination for CCA.

#### *BRD2 and BRD4 knockdown models were more sensitive to BET ± PARPi*

Interestingly, we observed that our KKU-055 BRD2 KD model displayed a 2.74X and 2.89X increase in sensitivity to olaparib and veliparib, respectively, while our KKU-055 BRD4 KD model displayed a 1.22-fold and 1.52-fold increase in sensitivity to olaparib and veliparib, respectively (**Figure 4d & 4f**). However, neither KKU-055 knockdown of BRD2 nor BRD4 recapitulate the synergistic cytotoxicity like phenotype observed in parental KKU-055 when exposed to the combinations of BETi with PARPi. In fact, treatment with BETi in combination with PARPi in these KD models results in drug synergy (CI<1) (**Figure 5a-d**). JQ1 and I-BET762 are both pan-BET inhibitors and



affects all BET proteins simultaneously [104], though with varying binding affinities [81]. Generation of KKU-055 stable KD models provides >95% KD of BRD2 and >98% KD of BRD4 protein. It is reasonable to suggest that either a gene knockout (KO) model of either BET target must be achieved in order to observe increased PARPi sensitivity or that drug synergy observed between BETi and PARPi depends upon inhibition of multiple members of the BET family as opposed to a single member. The generation of a KKU-055 multi-BET knockdown model could address this hypothesis and is an avenue we are currently pursuing. In addition, while c-Myc protein expression was addressed in our BRD2 and BRD4 KD models (**Figure 4a & 4b**), we did not determine the impact KD of BRD2 or BRD4 has on Chk1 protein expression in KKU-055.

### **JQ1 in combination with gemcitabine as a potential therapy for CCA**

#### *Gemcitabine with cisplatin is synergistic in vitro*

Valle et al. were the first to identify that the combination of gemcitabine with cisplatin extended the survival of CCA patients from 8.1 months with gemcitabine alone to 11.7 months with the combination [59]. Due to this observation, gemcitabine in combination with cisplatin became the current standard of care for CCA patients. While this work was initially performed during a phase 2 clinical trial, there are no reports of gemcitabine in combination with cisplatin for CCA *in vitro* models, KKU-055 and KKU-100. Therefore, we utilized these *in vitro* models to assess the potency of this combination. Gemcitabine and cisplatin are administered at 1,000 mg/m<sup>2</sup> vs. 25 mg/m<sup>2</sup>, respectively, to patients in the clinic. Therefore, we assessed the potency of gemcitabine

with cisplatin at ratios including 50:1 as well as 1:50 and 1:10 with cell viability assessed via alamarBlue in K KU-055 (**Figure 3-2A & 2B**) and K KU-100 (**Figure 3-3A & 3-3B**). Both models displayed reduced cell viability in a dose-dependent manner, and both displayed strong drug synergy in gemcitabine to cisplatin ratios of 1:10 and 50:1. K KU-055 did not display synergy when exposed to a ratio of 1:50 whereas K KU-100 displayed synergy at ratios of 1:50 when the fraction of cells affected was less than or equal to 0.2.

As drug synergy between gemcitabine and cisplatin was observed *in vitro*, we assessed the efficacy of this combination in our CCA PDX model, CCA1. Mice were administered gemcitabine (60 mg/kg), cisplatin (2.5 mg/kg) or the combination via intraperitoneal injection (i.p.) once a week for 28-days. Administered doses were consistent with previous reports [163]. Treatment with either gemcitabine or cisplatin alone suppressed tumor volume with the combination displaying a further decrease over the 28-day treatment (**Figure 3-4A**). As gemcitabine with cisplatin is administered for a limited duration in the clinic (every 3 weeks for eight cycles), we assessed regrowth potential of tumors treated with gemcitabine, cisplatin or the combination following a 28-day treatment. Mice were taken off treatment and placed on observation. We observed regrowth of gemcitabine treated tumors on day 60 of the study and cisplatin on day 120 of the study. Over the 130-day study, tumors treated with the combination of gemcitabine with cisplatin did not regrow (**Figure 3-4B**). Our results corroborate those observed in the clinic. Patients treated with the combination experience extended survival over those treated with gemcitabine alone and this corresponds favorably with regrowth observed in CCA1 treated with gemcitabine in combination with cisplatin.

*JQ1 with gemcitabine impairs CCA cell viability in vitro*

Gemcitabine-mediated cytotoxicity relies upon the incorporation of its metabolic products into replicating DNA which results in “masked chain termination”. Previous reports established that tumors which are deficient in DDR factors display increased sensitivity to gemcitabine [157-159]. Further, Langdon et al. displayed increased potency of BET inhibitor JQ1 in combination with gemcitabine in PDAC *in vitro* models [225] and Xie et al. established that the combination of I-BET762 with gemcitabine resulted in decreased tumor volume over either drug alone in a pancreatic xenograft mouse model [226]. As we observed JQ1-mediated reduction of Chk1 in an *in vivo* CCA PDX model [71] as well as in CCA *in vitro* models, KKU-055 and KKU-100 (**Figure 2C & 2E**), we chose to investigate the use of JQ1 in combination with gemcitabine. We hypothesized that JQ1-mediated downregulation of c-Myc and its transcriptional target, Chk1, would sensitize CCA *in vitro* models to gemcitabine. We exposed KKU-055 and KKU-100 to increasing concentrations of JQ1 ( $10^{-4}$  to  $10^{-7}$  M), gemcitabine ( $10^{-7}$  to  $10^{-10}$  M) or the combination in a 1,000:1 ratio for 96 hours and assessed cell viability via alamarBlue (**Figure 3-5A & 3-5B**). Strong drug synergy was calculated when JQ1 was combined with gemcitabine in a ratio of 1,000:1. Additionally, we assessed whether JQ1 increases the sensitivity of KKU-055 and KKU-100 to a single dose of gemcitabine. Both models were exposed to JQ1 ( $10^{-4}$  to  $10^{-7}$  M), gemcitabine ( $10^{-7}$  to  $10^{-10}$  M) or JQ1 in combination with their gemcitabine IC<sub>50</sub> of 10 nM (**Figure 3-6A & 3-6B**). CI values indicated that both high and low concentrations of JQ1 in combination with 10 nM gemcitabine displayed synergy. Clonogenic assays, in which cells were exposed to a range of JQ1 concentrations in combination with 10 nM gemcitabine, confirmed our cell

viability results (**Figures 3-6C & 3-6D**). Our results corroborate those presented by Langdon et al. and suggests JQ1 in combination with gemcitabine may promote additional efficacy over either as a single agent.

*BRD2 and BRD4 knockdown models do not display increased gemcitabine sensitivity*

BET inhibitors, such as JQ1 and I-BET762, are pan-BET inhibitors and affect all three BET proteins simultaneously [104], though with varying binding affinities [81]. We aimed to address whether JQ1 promoted increased sensitivity to gemcitabine through a specific BET protein. We hypothesized that gemcitabine sensitivity would increase in our established KKU-055 BRD2 and BRD4 knockdown (KD) models, similar to the effect of JQ1 in combination with gemcitabine in parental KKU-055. We exposed KKU-055 control, BRD2 and BRD4 KD models to gemcitabine ( $10^{-7}$  to  $10^{-10}$  M) and assessed cell viability using alamarBlue (**Figure 3-8**). Compared to control, BRD2 displayed a 1.19-fold increase in gemcitabine sensitivity while BRD4 KD displayed a 1.21-fold increase in gemcitabine sensitivity suggesting that KD of either of these BET proteins individually does not alter gemcitabine sensitivity. These results mirror those observed in our BRD2 and BRD4 KD models of KKU-055 exposed to PARPi *in vitro* (**Figure 4d & 4f**). As KKU-055 KD models provide >95% KD of BRD2 and >98% KD of BRD4 protein, it is possible that either the generation of a knockout (KO) model of either BET target must be completed to observe increased gemcitabine sensitivity or that drug synergy observed between BETi and gemcitabine depends upon inhibition of more than one BET family member.

As we have established that BRD2 or BRD4 KD results in a ~90% or ~50% reduction in c-Myc expression, respectively (**Figure 4a & 4b**), and that *CHEK1* is a c-Myc transcriptional target [150, 164], we hypothesized that BETi induced gemcitabine sensitivity through downregulation of Chk1. However, we have not determined the impact KD of BRD2 or BRD4 has on Chk1 protein expression in KKU-055. Further, literature suggests that RNAi-mediated reduction of BRD4 does not always correlate with a decrease in Chk1 protein expression [227]. It is possible that, with generation of gene KD models, epigenetic alterations, such as increases or decreases in histone acetylation sites, may have taken place. This may result in alterations in BET protein binding locations or, as there is overlap between K-Ac residue binding amongst the BET family of proteins [83], it is possible that KD of one BET protein leads to the recruitment of another. This further suggests that downregulation or therapeutic inhibition of the entire BET family of proteins is necessary for drug synergy with gemcitabine. We can address these questions by performing ChIP-Seq in our KD models and determining if there are alterations in BET protein binding locations as well as increases or decreases in gene target binding.

### **Gemcitabine resistance models**

#### *Characterization of in vitro and in vivo CCA gemcitabine resistant models*

As the majority of CCA patients display intrinsic chemoresistance or acquired resistance to gemcitabine, we developed one *in vitro* model and two *in vivo* models of gemcitabine resistance to understand mechanisms of resistance. Towards generation of a Gem<sup>R</sup> *in vitro* model, we first determined parental KKU-055 gemcitabine IC<sub>50</sub>, the

gemcitabine concentration required to kill 50% of parental cells. The concentration of gemcitabine was gradually increased as cells continued to grow normally at each administered dose and were termed gemcitabine resistant (Gem<sup>R</sup>) once they grew consistently in 5  $\mu$ M gemcitabine, 500-fold the parental gemcitabine IC<sub>50</sub>. We compared gemcitabine sensitivity between parental and Gem<sup>R</sup> and observed a marked increase in gemcitabine resistance in the Gem<sup>R</sup> model compared to parental. Gem<sup>R</sup> displayed resistance to gemcitabine above the highest utilized *in vitro* assay dose of 31.6  $\mu$ M (**Figure 4-2**). Literature suggests that the peak gemcitabine peak plasma concentration for patients treated with 1,000 mg/m<sup>2</sup> is 32  $\mu$ M [170]. At 31.6  $\mu$ M, KGU-055 Gem<sup>R</sup> displays ~80% cell viability and indicates our Gem<sup>R</sup> model is resistant to clinically relevant gemcitabine plasma concentrations. In addition to assessing the degree of gemcitabine resistance, we determined alterations in cellular morphology, *KRAS* mutational status and molecular alterations between parental and Gem<sup>R</sup>. We did not observe alterations in cell morphology, cell doubling time or *KRAS* codon 12 mutational status in our Gem<sup>R</sup> model compared to parental (**Figure 4-3**).

*In vitro* models are invaluable tools to address drug resistance mechanisms and potential therapeutic options, however, these models lack components which are crucial for clinical CCA including stroma and extracellular matrix (ECM). Preclinical *in vivo* models, such as PDX models, harbor tumor cells as well as the desmoplastic microenvironment of the patient disease. To address these concerns regarding *in vitro* models, we developed the first gemcitabine resistant CCA PDX models, representing CCA1 and CCA2. CCA1 and CCA2 were implanted into the flank of SCID mice and, once tumor volumes reached 250-350 mm<sup>3</sup> or 300-500 mm<sup>3</sup>, respectively, mice were

administered 100 mg/kg gemcitabine weekly (**Figures 4-5A & 4-5B**). Regrowth of CCA1 and CCA2 models undergoing treatment was observed on days 50 and 55, respectively. Final tumor volumes of CCA1 and CCA2 undergoing gemcitabine treatment were 2.95-fold and 2.72-fold larger when normalized to Day 0 tumor volumes (**Figures 4-6A & 4-6B**). To date, this is the first reported generation of CCA PDX Gem<sup>R</sup> models in the literature. We detail the development of the first gemcitabine resistant CCA PDX model to better understand mechanisms of resistance and potentially utilize these models to develop therapeutic strategies. To better understand these models, we began preliminary characterization of control compared to Gem<sup>R</sup>. To do this, we performed IHC staining on tissues collected within 24-hours after final treatment. We first determined whether Gem<sup>R</sup> models displayed increased proliferation compared to control by staining for proliferative marker, Ki-67, across CCA1 and CCA2 vehicle control and Gem<sup>R</sup> tissues. CCA1 Gem<sup>R</sup> and CCA2 Gem<sup>R</sup> displayed a 3.23-fold increase ( $p < 0.0001$ ) and 2.61-fold increase ( $p < 0.0006$ ) in Ki-67 compared to their respective controls (**Figure 4-7**). Further, we assessed whether genes involved in drug import (hCNT1 and hENT1), metabolism (dCK) and/or inactivation (CDA and RRM1) were altered following acquisition of resistance. (**Figures 4-8A and 4-8B**). Neither CCA1 Gem<sup>R</sup> nor CCA2 Gem<sup>R</sup> seem to have acquired resistance through downregulation of nucleoside importers, hCNT1 or hENT1. This is noteworthy as normal cholangiocytes display intrinsic chemoresistance due to bile acid-induced activation of FXR which leads to downregulation of nucleoside transporters including hENT1 and hCNT1. However, it is important to note that downregulation of these transporters is not always correlative with gemcitabine resistance [62, 165]. As we observed drastically decreased c-Myc expression

in our *in vitro* K KU-055 Gem<sup>R</sup> compared to control, we stained for c-Myc in our *in vivo* models. Interestingly, c-Myc protein expression was found to be consistent between both CCA1 and CCA2 Gem<sup>R</sup> compared to their respective vehicle controls.

CCA1 seems to have acquired resistance to gemcitabine through downregulation of gemcitabine metabolic component dCK (1.79-fold decrease) whereas CCA2 may have acquired resistance through alterations in gemcitabine metabolic component, RRM1 (1.36-fold increase), and inactivation enzyme, CDA (1.25-fold increase). Our data suggest that CCA1 and CCA2 Gem<sup>R</sup> models acquired resistance through two independent mechanisms. Though this could be due to underlying mutations, epigenomics and intrinsic characteristics of each respective patient tumor which we have not yet identified, these models allow us the opportunity to study pharmaceutical options utilizing models harboring different resistant mechanisms. As this is a preliminary analysis, it is vital that we assess additional and canonical gemcitabine resistance markers including RRM2, deoxycytidylate deaminase (dCMP), as well as the BET family of proteins and DDR factors such as Chk1.

*In vitro CCA gemcitabine resistant model displays increased JQ1 sensitivity*

We questioned whether K KU-055 Gem<sup>R</sup> displayed increased JQ1 sensitivity. Further, though we have not determined additional mechanisms of gemcitabine resistance, it is possible that our K KU-055 Gem<sup>R</sup> model displayed increased expression of RRM1. Previous reports of RRM1-dependent Gem<sup>R</sup> models, such as pancreatic, lung and breast cancer models, display increased gemcitabine sensitivity when cells are



exposed to a Chk1 inhibitor [167, 168]. We previously reported that CCA PDX model, CCA2, displays reduced Chk1 expression following treatment with JQ1 [71] and here we detail that JQ1 significantly decreases the expression of Chk1 at both the mRNA and protein level *in vitro* (**Figure 2A-2C & 2E**). Further, JQ1 synergized with 10 nM gemcitabine in our K KU-055 gemcitabine-sensitive model (**Figures 3-6**), therefore, we exposed parental and Gem<sup>R</sup> K KU-055 to JQ1 and observed a 3.32-fold increase in JQ1 sensitivity in Gem<sup>R</sup> compared to the parental model (**Figure 4-4**). Next, we assessed whether JQ1 further downregulated the expression of c-Myc and Chk1 in Gem<sup>R</sup> like what we observed in parental K KU-055 (**Figure 2A & 2C**). The same effect is observed when cells are exposed to both JQ1 in combination with 10 nM gemcitabine.

### **Future Directions**

#### *Establish the role of c-Myc in CCA development*

The transcription factor, c-Myc, is highly expressed in up to 94% of CCA cases with no evidence of subtype specificity [36]. To date, no literature documents the role of c-Myc expression in CCA development. We hypothesize that downregulation of c-Myc during CCA development will result in delayed and/or reduced tumor growth. To address whether c-Myc plays a role in CCA development, we will utilize CCA GEM models to generate iCCA-like tumors. Using an established GEM model [69], we will develop two knockout (KO) models utilizing flanked loxP (flox) sites surrounding *SMAD4* (mutated in up to 17% of CCA cases), *PTEN* and/or *MYC* genes. Our goal is to address whether c-Myc expression contributes to iCCA development. Here we will generate two models in

which one expresses endogenous levels of c-Myc while the other model experiences c-Myc KO. Our models will consist of either: 1) *SMAD4*<sup>fl/fl</sup> and *PTEN*<sup>fl/fl</sup> or 2) *SMAD4*<sup>4fl/fl</sup>, *PTEN*<sup>fl/fl</sup> and *MYC*<sup>fl/fl</sup>. Album-Cre will be utilized to generate these KO models. However, as albumin is not cholangiocyte specific and is instead expressed in both hepatocytes and cholangiocytes during embryogenesis, we will be knocking out the expression of *SMAD4*, *PTEN* and/or *MYC* in hepatocytes alongside cholangiocytes. Over the course of the study, mice will be regularly monitored using PET scan. The endpoint of this study is to address the rate at which iCCA develops in our GEM models and assess whether downregulation of c-Myc during CCA development leads to delayed or reduced tumor growth. At the end of the study, tissue will be collected, and gene expression assessed via immunohistochemistry (IHC) for proliferation (Ki-67) as well as mRNA and protein for c-Myc and its transcriptional targets, including Chk1.

As previous reports indicated that generation of this GEM iCCA model requires 4-7 months postnatal [69], we did not see fit to overexpress c-Myc under the albumin promoter. This is again due to lack of a distinct cholangiocyte promoters. Previous reports document that overexpression of c-Myc in hepatocytes, which also utilize the albumin promoter, lead to induced liver fibrosis, alterations in hepatocyte metabolism and enhance hepatocyte cell cycle progression beginning on week 10 postnatal [228].

*Determine whether c-Myc downregulation is required for BETi efficacy*

In Chapter 2, we established that JQ1 inhibits the expression of proto oncogene, c-Myc, both at the mRNA and protein level *in vitro* and at the transcriptional level *in*

*vivo*. JQ1-mediated reduction of *MYC* was found to correspond with a decrease in cell viability *in vitro* and tumor growth *in vivo*. Further, we established that knockdown of BRD2 or BRD4 resulted in reduced c-Myc protein expression. However, these data do not directly assess whether c-Myc downregulation is required for JQ1 efficacy. BRD4 has been reported to bind to the *MYC* promoter, near promoter P2, in multiple myeloma [96]. In **Figure S5**, we corroborated these results and established that BRD4 binds to the *MYC* promoter, P2, in CCA *in vitro* model, KGU-055. In addition, it has been established that BET proteins recognize and bind super enhancers to promote gene transcription [85]. To date, no CCA super enhancers have been reported in the literature. To address the location of BET protein binding in CCA, we will utilize ChIP-Seq to demonstrate the binding of BRD2 and BRD4 to the *MYC* gene locus with or without BETi treatment. Further, we can utilize ChIP-Seq to assess BET binding locations across a host of additional and potentially novel gene targets in the presence or absence of BETi.

To further evaluate whether BETi potency is through downregulation of c-Myc, we will transiently knockdown (KD) c-Myc utilizing polyethylenimine (PEI)-mediated transfection of shRNA and assess cell viability when exposed to BETi. We chose transient c-Myc KD as opposed to the generation of a stable c-Myc KD due to reported alterations associated with long duration c-Myc downregulation. These alterations include examples of reduced cell cycle progression such as reduced cell growth and colony formation [229]. As the development of a stable c-Myc KD model could result in the cells no longer requiring c-Myc for survival, we chose transient c-Myc KD. We hypothesize that BETi potency will be reduced following transient c-Myc downregulation. Conversely, we will exogenously express c-Myc in our *in vitro* models

and expose each to BETi. As the c-Myc expression would no longer be under the control of the BET family of proteins, we hypothesize that exogenous c-Myc expression would abolish BETi potency *in vitro*.

*Elucidate additional mechanisms of JQ1-induced DNA damage*

Our lab has previously reported that JQ1 induces DNA damage in both *in vitro* and *in vivo* models of CCA as well as PDAC (**Figure 2g & 2i**) [71, 105]. We established that this damage was due in part to downregulation of Chk1 in CCA as well as RAD51 and KU80 in PDAC. In Chapter 2, our data suggest JQ1 induces its cytotoxic effect through downregulation of c-Myc. It is important to note that c-Myc regulates the expression of many DDR genes including but not limited to *RAD51*, *RAD51B*, *RAD51C*, *XRCC2*, *RAD50*, *BRCA1*, *BRCA2*, *DNA-PKcs*, *XRCC4*, *KU70*, *CHEK1* and *DNA ligase IV* [150, 164, 230]. It is possible that JQ1-induced downregulation of c-Myc leads to a reduction in additional DDR factors not assessed in this dissertation. We will utilize RNA-Seq in our *in vitro* models with or without JQ1 treatment to determine additional DDR factors downregulated by JQ1. We will confirm these results through immunoblot (IB).

*Evaluate the efficacy of JQ1 ± gemcitabine in gemcitabine resistant in vitro and in vivo models of CCA*

In Chapter 3 of this dissertation, we established that gemcitabine-sensitive CCA *in vitro* models displayed drug synergy when exposed to JQ1 in combination with

gemcitabine. In addition, we detail that K KU-055 shows reduction of both c-Myc and Chk1 protein when exposed to JQ1 or the combination of JQ1 with gemcitabine *in vitro*. In Chapter 4 we document the observation that K KU-055 Gem<sup>R</sup> model shows increased sensitivity to JQ1. Based on these results, we want to address whether JQ1 increases the sensitivity of gemcitabine resistant CCA to gemcitabine using our *in vitro* and *in vivo* Gem<sup>R</sup> models. For *in vitro* analysis, we will expose K KU-055 Gem<sup>R</sup> to JQ1 in combination with gemcitabine in ratios of 1:1, 1:10, 10:1, 1:100, 100:1, 1:1,000 or 1,000:1 with cell viability assessed via alamarBlue. We will determine whether BET inhibition alone results in downregulation of c-Myc and its transcriptional target, Chk1. For analysis of JQ1 in combination with gemcitabine *in vivo*, we will implant parental and gemcitabine resistant models of CCA1 and CCA2 into SCID mice. Mice will then be randomly divided into 4 cohorts to receive either vehicle control (VC), 100 mg/kg gemcitabine once a week, 50 mg/kg JQ1 daily or the combination for at least 21 days. Tumor volume will be assessed three times a week. At the end of the study and within 24 hours of final treatment, tumor tissue will be harvested and either snap frozen for protein and RNA or formalin-fixed and paraffin embedded (FFPE) for analysis. We will assess alterations in proliferation, DNA damage, cell death as well as gene expression alterations of c-Myc and Chk1. We will further compare results between parental CCA1 and CCA2 models to their respective gemcitabine resistant counterparts.

#### *Further characterize in vitro and in vivo Gem<sup>R</sup> models*

In Chapter 4, we described the development of an *in vitro* K KU-055 Gem<sup>R</sup> model. To date, no gemcitabine resistant CCA *in vitro* models have been reported in the

literature. We are currently working to develop a gemcitabine resistant model of KKU-100. While this work is ongoing, we are characterizing KKU-055 Gem<sup>R</sup> compared to parental. Preliminary data suggest this model shows reduced BRD2, c-Myc and Chk1 protein while BRD4 does not seem altered (preliminary data not shown). We are currently working to determine the impact of resistance on canonical gemcitabine resistance markers such as dCK, CDA, RRM1, RRM2 and nucleoside transporters, hCNT1 and hENT1, and aim to confirm the observed reduction of BRD2, c-Myc and Chk1 in this model as well. RNA-Seq will be utilized to identify additional and potentially novel genes involved in CCA gemcitabine resistance. Further and more complete analysis of both KKU-055 and KKU-100 Gem<sup>R</sup> models will be performed.

In addition to development of an *in vitro* Gem<sup>R</sup> model, we have developed two independent CCA PDX Gem<sup>R</sup> models and performed partial characterization compared to control. Preliminary analysis suggests both CCA1 and CCA2 Gem<sup>R</sup> PDX models acquired resistance to gemcitabine through independent mechanisms. In addition to the results shown in Chapter 4, we will perform RNA-Seq to determine additional gene expression changes between control and Gem<sup>R</sup> PDX models with results confirmed by IB, qRT-PCR and IHC. As we assess gene expression alterations, we will identify genes which have been historically altered by JQ1 treatment either identified in the literature or identified in our lab.

## CHAPTER 6

### MATERIALS AND METHODS

#### **Introduction**

This chapter describes the methods and techniques used throughout this dissertation to address the specific question at hand. Antibodies and primers utilized across this dissertation are detailed in Table 6-1 and Table 6-2, respectively. The techniques are described in the order in which they are utilized across this dissertation and each subsection is titled based on the method they detail.

#### *Animal ethics statement*

Studies across this dissertation included the use of vertebrate animals. Animal protocols were approved by the University of Alabama at Birmingham Animal Care and Use Committee (IACUC) and the University of Alabama at Birmingham Institutional Review Board (IRB). Female CB17<sup>-/-</sup> severe-combined immunodeficient (SCID) mice (4-week-old) were purchased from Taconic Farms (Newton, MA, USA) and housed in the AAALAC accredited vivarium at University of Alabama at Birmingham Research Support Building where mice were monitored daily. Mice were given one week to adapt

to their new environment once arriving at our UAB facility before their use for tumorgraft production. If mice appeared to be in discomfort or distress, they were euthanized in accordance with protocol.

#### *Cell culture and compounds*

KKU-055 (JCRB1551) and KKU-100 (JCRB1568) cholangiocarcinoma cell lines were purchased from the Japanese Cancer Research Resources Bank (JCRB) (National Institute of Biomedical Innovation, Japan). Cells were cultured in 1X Dulbecco's Modified Eagle Medium (DMEM) (Fisher Scientific, Waltham, MA, USA) supplemented with 10% heat-inactivated fetal bovine serum (FBS) (Atlanta Biologicals, Flowery Branch, GA, USA) and 2 mM L-glutamine (Thermo Fisher Scientific, Waltham, MA). Cells were grown in a 37°C humidified incubator with 5% CO<sub>2</sub>. Both CCA cell lines were tested for mycoplasma using MycoAlert™ PLUS Mycoplasma Detection Kit (Lonza, Walkersville, MD, USA) and were negative. Cells were passaged by removing media and washing with PBS. Cells were detached from the flask by incubating cells at 37°C in 0.25% Trypsin (Thermo Fisher Scientific, Waltham, MA) until they detached. Cells were passaged 1:7 and seeded in fresh 1X DMEM media. Cells were used at low passage (passage<40) for all experiments.

#### *DNA isolation and gene sequencing*

KKU-055 and KKU-100 cell culture flasks were washed with 1X PBS and cells lifted using 0.25% Trypsin (Thermo Fisher Scientific, Waltham, MA) in a 37°C



incubator. DNA was isolated using Epicentre MasterPure DNA Purification Kit (Illumina, San Diego, CA). Cells were lysed using Tissue and Cell Lysis Solution containing proteinase K and RNA degraded through use of RNase A. Protein was precipitated and debris removed by centrifugation. DNA was subsequently precipitated and washed in 75% ethanol made in DNase/RNase free water. DNA concentration and purity were determined using a NanoDrop 1000 spectrophotometer with Nanodrop 3.0.1 software (Coleman Technologies Inc, Wilmington, DE). Polymerase chain reaction (PCR) was performed using 200 ng DNA combined with PCR-grade water, dNTP mixture, 10X Taq buffer, Ex Taq polymerase and respective primer pairs. dNTP mixture, 10X Taq buffer and Ex Taq polymerase were purchased from Takara (Clontech Laboratories, Mountain View, California). PCR primer sequences are detailed in **Table 6-2**. Once amplification was complete, samples were mixed with 6X loading buffer (New England Biolabs, Ipswich, MA) and run on 2% agarose gel at 100 volts. The correct DNA base pair size was cut from the gel and purified using GeneJET Gel Extraction Kit (Thermo Fisher Scientific, Waltham, MA). Gels containing amplified DNA was dissolved in Binding Buffer, centrifuged in GeneJET purification columns, DNA washed and subsequently eluted from purification columns. DNA concentration and purity were determined using a NanoDrop 1000 spectrophotometer with Nanodrop 3.0.1 software (Coleman Technologies Inc, Wilmington, DE). 30 ng of DNA diluted in PCR-grade water supplemented with the forward primer (**Table 6-2**) was submitted to the University of Alabama at Birmingham (UAB) Heflin Center for Genomic Sciences for sanger sequencing. Sequences were analyzed using the free software Chromas v2.6.6 (Technelysium Pty Ltd, South Brisbane, Australia).

### *Compounds for in vitro drug studies*

JQ1 (HY-13030) was purchased from MedChem Express (Monmouth Junction, NJ, USA) and made as a 110 mM stock solution. I-BET762 (HY-13032) was purchased from MedChem Express (Monmouth Junction, NJ, USA) and was made as a 100 mM stock aliquot. Olaparib (HY-10162) was purchased from MedChem Express (Monmouth Junction, NJ, USA) and was made as a 70 mM stock. Veliparib (ABT-888) was purchased from Enzo Life Sciences (Farmingdale, NY, USA) and prepared as a 10 mM stock solution. Stock solutions for all previously mentioned compounds were dissolved in DMSO (Thermo Fisher Scientific, Waltham, MA) with the final concentrations of DMSO in *in vitro* experiments being <0.3%. Gemcitabine-HCl was purchased from LC Laboratories (Woburn, MA) and was dissolved in 1X PBS and made at 2mM stock solution. Cisplatin (HY-17394) was purchased from MedChem Express (Monmouth Junction, NJ, USA) and made as a 3.3 mM stock solution dissolved in water.

### *In vitro cell viability assay*

Cells were seeded in 96-well plates at densities of 500 to 1,300 cells per well and allowed to adhere for 24-hours at 37°C. Cells were treated for 48 to 120 hours with serial dilutions of BET inhibitors (JQ1 or I-BET762), PARPi (olaparib or veliparib), and/or gemcitabine suspended in culture medium. AlamarBlue (Thermo Fisher Scientific, Waltham, MA) was added in accordance with manufacturer instructions and incubated on cells for ~17 hours. Fluorescence was read on a PerkinElmer Victor X5 microplate reader at 560nm excitation and 590nm emission wavelengths. Cell growth graphs and drug IC<sub>50</sub> values were calculated using GraphPad Prism v7.0 (San Diego, CA, USA). Drug synergy

and subsequent combination indices (CI) were calculated using the free software CompuSyn 1.0. CI values <0.9 indicate synergism, values = 1 are additive and values >1 indicate antagonism [144]. Unless stated otherwise, three independent experiments were performed with quadruplicated wells.

#### *Clonogenic and colony formation assays*

**Survival Fraction:** Cells were plated in a confluency between 50 to 150 cells and 100 to 1,500 cells into 6-well plates for K KU-055 and K KU-100, respectively, and allowed to adhere for 24 hours. Cells were exposed to JQ1 (316.2 nM to 31.62  $\mu$ M) for 72 hours, washed with 1X PBS, given fresh non-drug containing media and allowed to grow for an additional 14 days (total of 18 days in culture). At the end of the study, cells were formalin fixed and stained with 0.025% crystal violet. Colonies containing at least 50 cells were counted. Control (DMSO) plating efficiency (PE) was calculated using the equation ( $PE = \frac{\# \text{ colonies formed}}{\# \text{ of cells seeded}} \times 100$ ) [145]. Percent survival, the number of colonies which grew after treatment is calculated in terms of control PE using the equation

$$(\% \text{ Survival} = \frac{\# \text{ of colonies formed after treatment}}{\# \text{ of cells seeded} \times PE} \times 100) [145].$$

**Colony formation:** 2,000 cells, K KU-055 or K KU-100, were plated per well in 24-well plates and allowed to adhere overnight. Cells were exposed to DMSO (<0.3%) or various concentrations of JQ1 (0.1  $\mu$ M, 1  $\mu$ M or 10  $\mu$ M), olaparib (0.1  $\mu$ M, 1  $\mu$ M or 10  $\mu$ M), or JQ1 + olaparib (1:1) for 72 hours, washed with 1X PBS, and grown in drug-free media for an additional 14 days (total of 18 days in culture). Cells were then formalin fixed and stained using 0.025% crystal violet.

Plates were imaged using Epson scanner. Three independent experiments were performed.

#### *Isolation of total RNA*

Total RNA was isolated from 6-well plates containing KKU-055 or KKU-100 treated with DMSO or JQ1 for 72 hours utilizing Trizol-chloroform extraction. Samples were scraped into Trizol and rotated for 10 minutes. PDX snap frozen tumor tissue was bio-pulverized to a fine powder and added to Trizol. Phase-separation was performed by the addition of chloroform. Samples were centrifuged where the aqueous phase was transferred to a new tube where RNA was then precipitated. RNA was then washed with 75% ethanol containing DNase/RNase free water. Pellet was subsequently air dried, resuspended in PCR-grade water and stored in -80°C. Concentration and purity were determined using a NanoDrop 1000 spectrophotometer with Nanodrop 3.0.1 software (Coleman Technologies Inc, Wilmington, DE).

#### *cDNA synthesis*

Two µg of total RNA was converted to cDNA utilizing Bio-Rad iScript Advanced (BioRad Laboratories, Hercules, CA). Total RNA was added to iScript Advanced Reaction Mix and iScript Advanced Reverse Transcriptase. The mixture was heated to 46°C for 20 minutes, reverse transcriptase inactivated at 95°C for one minute and the solution was then cooled on ice. Samples were stored at -20°C.

#### *qRT-PCR Assay for cDNA and ChIP*

cDNA was first diluted in a 1:5 ratio in PCR-grade water. SsoFast EvaGreen cocktail mix (BioRad Laboratories, Hercules, CA, USA) was diluted in a 1:1 ratio with PCR-grade water and combined with diluted cDNA. Primers (**Table 6-2**) were added to the solution and used at a working concentration of 1  $\mu$ M. 20 ng of cDNA or 2  $\mu$ L of ChIP genomic DNA were utilized per reaction. Twenty  $\mu$ L was added per well into a 96-well qRT-PCR plate (BioRad Laboratories, Hercules, CA, USA). The PCR reaction conditions were denaturation at 95°C for 3 minutes; 40 cycles of denaturation at 95°C for 10 seconds (cDNA) or 15 seconds (ChIP), annealing at 50°C for 10 seconds (cDNA) and extension at 72°C for 10 seconds (cDNA) or annealing/extension at 60°C for 1 minute (ChIP). Reactions were carried out using a CFX96 System and analyzed using Bio-Rad CFX manager software v1.5 (BioRad Laboratories, Hercules, CA, USA). Housekeeping genes for cDNA was GAPDH and 2% input for ChIP, respectively. Three independent experiments were performed unless otherwise stated. Gene expression differences were assessed using  $-2^{\Delta\Delta CT}$  and displayed as percent expression of DMSO with DMSO expression set to 100%.

#### *Cell cycle analysis*

KKU-055 cells were exposed to JQ1 (30  $\mu$ M), olaparib (5  $\mu$ M), veliparib (10  $\mu$ M), JQ1 (30  $\mu$ M) + olaparib (5  $\mu$ M) or JQ1 (30  $\mu$ M) + veliparib (10  $\mu$ M) for 48 hours. Cells were harvested, centrifuged and added drop-wise into ice-cold 70% ethanol while vortexing. The cells were incubated at 4°C overnight. The next day, cells were centrifuged, and the precipitate was incubated with propidium iodide-Triton X-100 resuspension buffer in PBS (0.1% Triton X-100, 200  $\mu$ g/ml RNAase A, and 20  $\mu$ g/ml

propidium iodide) for a minimum of an hour prior to running flow cytometry [146]. Flow cytometry was carried out at the UAB flow cytometry core using a FACSCalibur (BD Biosciences, San Jose, CA, USA) flow cytometry machine. Twenty-thousand cells were analyzed using FlowJo™ (v10.6.1, BD Biosciences) and the Dean-Jett-Fox univariate model.

### *Immunoblot Analysis*

KKU-055 and KKU-100 cells were plated on 6-well plates and allowed to adhere overnight. Cells were treated with concentrations of various compounds and incubated at 37°C for 48 to 72 hours. Media containing floating cells was collected, centrifuged and washed with 1X PBS. Meanwhile, adherent cells were washed with 1X PBS and lysed in NP-40 (Boston BioProducts Inc, Ashland, MA) or RIPA buffer (MilliporeSigma, St. Louis, MO, USA) containing protease inhibitors (Thermo Fisher Scientific, Waltham, MA). Lysates containing adherent cells was then added to centrifuged tubes. Samples were then sonicated on ice to ensure thorough lysis. Following sonication, samples were centrifuged to separate insoluble fraction from soluble fraction. The soluble fraction was then stored in -80°C.

Protein quantification via Bio-Rad protein assay (BioRad Laboratories, Hercules, CA) was performed to assess the amount of protein in each soluble fraction. Unless otherwise specified, 40 µg of protein was combined with sample loading buffer (Thermo Fisher Scientific, Waltham, MA) and were heated to 100°C for 10 minutes to denature the protein. Samples were then loaded on 8% or 12% sodium dodecyl sulfate (SDS) polyacrylamide gel electrophoresis (PAGE) gels to separate proteins based on size.

Samples were run at 150 volts for ~60 minutes then transferred to PVDF membrane (Merck, Millipore, Burlington, MA) by wet transfer at 400 mA for 3 hours. Membranes were blocked using 5% nonfat dry milk made in tris-buffered saline with 0.1% Tween-20 (TBS-T) (Thermo Fisher Scientific, Waltham, MA) to prevent non-specific antibody binding. Membranes were then incubated in diluted primary antibody (**Table 6-1**) overnight at 4°C. The following morning, membranes were washed with TBS-T and incubated in secondary antibody (**Table 6-1**) at room temperature for one hour. Membranes were then washed in TBS-T and proteins detected using Bio-Rad Clarity Western enhanced chemiluminescence (ECL) substrate. Immunoblots were quantitated using ImageStudio Lite 5.2. Data were first normalized to respective loading controls and then to DMSO control.

### *Immunohistochemistry*

Tumor tissue was harvested within 24-hours of the last drug treatment, samples were formalin fixed for 24 hours and paraffin embedded (FFPE) onto glass slides. Slides were heated to 60°C for 20 minutes, deparaffinized and rehydrated in two changes of xylene, xylene with 100% ethanol (1:1 ratio), two changes of 100% ethanol, 95% ethanol, 70% ethanol and washed in deionized water and 1X PBS (pH 7.6). Antigen retrieval was performed by cooking the slides in 1X citrate buffer pH 6.0 in a pressure cooker at 15psi for 5 minutes. Slides were left to cool for 30 to 45 minutes at room temperature. Residual citrate buffer was removed through two changes of 1X PBS and peroxidase activity was blocked using 3% H<sub>2</sub>O<sub>2</sub> (Thermo Fisher Scientific, Waltham, MA) diluted in 100% methanol for 15 minutes and washed in 1X PBS. Slides were

blocked in 10% horse serum (Vector Laboratories, Burlingame, CA) diluted in 1X PBS for 1 hour at room temperature in a humidified chamber. After, slides were incubated with diluted primary antibody of choice (**Table 6-1**) overnight in a humidified chamber at 4°C. The following day, primary antibody was aspirated, and slides washed in 1X PBS. Slides were blocked in 5% horse serum diluted in 1X PBS for 10 minutes at room temperature. Blocking agent was aspirated and the appropriate IMMpress secondary antibody (Vector Laboratories, Burlingame, CA) was added (**Table 6-1**) for one hour at room temperature. Slides were washed in 1X PBS and 0.05% Brij in PBS for one minute. Slides were developed using DAB High Contrast chromogen (Scytek Laboratories, Logan, UT) and counterstained with Harris Hematoxylin (Thermo Fisher Scientific, Waltham, MA). Slides were destained in 0.25% EtOH and rinsed in tap water. Slides were dehydrated in 70% ethanol, 95% ethanol, two washes in 100% ethanol, xylene with 100% ethanol 1:1 and two washes in xylene. Slides were mounted with Permount mounting medium (Thermo Fisher Scientific, Waltham, MA) and images were captured using an Olympus BH-2 microscope, DP71 camera and DPS-BSW v3.1 software.

#### *Generation of stable shRNA-transfected cell lines*

**Optimization:** The optimal ratio of our transfection reagent, polyethylenimine (PEI) (Polysciences Inc., Warrington, PA, USA), to plasmid DNA for use in parental K KU-055 was first determined. PEI was combined with MISSION shRNA targeted for BRD2, BRD4 (MilliporeSigma, Burlington, MA) or the control shRNA (shGFP) (Addgene, Watertown, MA, USA) in ratios of 1:1 to 5:1. Parental K KU-055 were plated into 6-well plates and transfected with the aforementioned PEI to plasmid DNA ratios for 8 hours,



washed with 1X PBS, given fresh media and let grow for an additional 72 hours. Samples were collected and immunoblot (IB) performed to assess knockdown (KD) of target genes. All shRNA plasmids were constructed using the pLKO.1 backbone and contain puromycin N-acetyl-transferase (PAC), resistance to the selection agent, puromycin. The optimal dose of puromycin, necessary to kill 100% of parental, non-transfected cells, was determined by exposing parental cells to a range of puromycin concentrations (1 to 10  $\mu\text{g/ml}$ ) for 72 to 120 hours with cell viability assessed utilizing alamarBlue.

***Generation of stable gene knockdown cell lines:*** A PEI to plasmid DNA ratio of 5:1 and 7.5 $\mu\text{g/ml}$  puromycin were appropriate to generate stable gene KD models utilizing parental KKU-055. Parental KKU-055 cells were plated at low confluency (10%) in 6-well plates and transfected with a 5:1 ratio of PEI (Polysciences Inc., Warrington, PA, USA) to MISSION shRNA targeted for BRD4, BRD2 (MilliporeSigma, Burlington, MA) or the control shRNA for GFP (Addgene, Watertown, MA, USA) for 8 hours. Cells were then washed with 1X PBS, given fresh media and let grow for an additional 72 hours. At the end of the 72-hour period, transfected cell populations were then selected for using puromycin (7.5  $\mu\text{g/ml}$ ) (BML-GR312, Enzo Life). Puromycin-containing media was replenished twice a week. Once colonies formed, cells were passaged as previously described and samples collected for immunoblot (IB) analysis.

*Chromatin immunoprecipitation (ChIP) assay*

Cells were treated with DMSO or JQ1 (30  $\mu\text{M}$ ) for 48 hours. At the end of the study,  $4 \times 10^6$  cells were collected per group and ChIP was performed using the SimpleChIP Plus Kit (Cell Signaling Technology, Danvers, MA). Cells were fixed in 1%

formaldehyde (Thermo Fisher Scientific, Waltham, MA) for 10 minutes to crosslink proteins with bound DNA. Solution was neutralized using glycine. Cells were centrifuged, nuclei pellet collected, and chromatin digested using micrococcal nuclease and sonication on ice to digest DNA to lengths of approximately 150 to 900 base pairs. BRD2 or BRD4 bound DNA was isolated using ChIP grade anti-BRD2 or anti-BRD4 antibodies (**Table 6-1**) and contaminants cleared using magnetic beads. Normal rabbit IgG (**Table 6-1**) was utilized as control. Samples were washed in progressively more stringent salt washes. Chromatin was then isolated, and the cross-links reversed. DNA was purified using spin columns, eluted and stored in -20°C. ChIP qRT data was interpreted by calculating the percent input with results normalized to the 2% of each respective sample. Results were then normalized to the DMSO control. Primers utilized for ChIP are detailed in **Table 6-2**.

*Generation of gemcitabine resistant ( $Gem^R$ ) KKU-055 in vitro model*

Gemcitabine-HCl was purchased from LC laboratories (Woburn, MA). Gemcitabine-HCl was dissolved in 1X PBS to a stock solution of 2 mM and stored in -20°C. Parental KKU-055 were plated into a 96-well plate and allowed to adhere for 24 hours. The following day, cells were treated with a range of gemcitabine concentrations (100 pM to 100 nM) for 96 hours with cell viability assessed through alamarBlue cell viability assay (Thermo Fisher Scientific, Waltham, MA) and  $IC_{50}$  calculated using GraphPad Prism v7.0 (San Diego, CA, USA). Parental cells were plated into T-75 flasks (Thermo Fisher Scientific, Waltham, MA) and allowed to adhere for 24 hours. Cells were treated with gemcitabine  $IC_{50}$  of 10 nM. Media, containing gemcitabine, was replenished

every three days. Cells were monitored for growth once a day and were considered resistant to the administered gemcitabine dose once cells appeared to grow normally. Gemcitabine concentration was gradually escalated as cells grew normally in increasing concentrations of gemcitabine. This process was repeated to as cells grew resistant to elevated doses of gemcitabine.

*Generation of CCA1/2 gemcitabine resistant (Gem<sup>R</sup>) in vivo model*

Gemcitabine-HCl was purchased from LC laboratories (Woburn, MA). Gemcitabine-HCl was dissolved in 0.9% saline to a stock solution of 20 mg/ml and stored in -80°C. CB17<sup>-/-</sup> female SCID mice (4-week-old) were purchased from Taconic Farms (Newton, MA, USA) and housed in the AAALAC accredited vivarium at University of Alabama at Birmingham Research Support Building. Previously established CCA PDX models, CCA1 and CCA2, were implanted into the flank of CB17<sup>-/-</sup> female SCID mice. Once tumors reached 200-300 mm<sup>3</sup>, mice were randomized into two cohorts: vehicle control (CCA1 n=6, CCA2 n=9) and 100 mg/kg gemcitabine (CCA1 n=8, CCA2 n=6). Gemcitabine was administered via i.p. injection once a week. Tumor volumes were measured three times a week using digital calipers, and tumor volume calculated using the formula  $v = (\pi/6) \times d^3$ . Results were normalized to Day 0 of drug treatment, and data are expressed as normalized tumor volume. Models were considered gemcitabine resistant once regrowth was observed while undergoing gemcitabine treatment.

*In vivo JQ1 + olaparib evaluation*

CB17<sup>-/-</sup> female SCID mice (4-week-old) were purchased from Taconic Farms (Newton, MA, USA) and housed in the AAALAC accredited vivarium at University of Alabama at Birmingham Research Support Building. K KU-055 cells ( $5 \times 10^6$ ) in 100  $\mu$ L PBS were injected into each flank via subcutaneous injection. Mice bearing bilateral tumors were randomized into four groups of 5 mice/group when tumors reached  $\sim 200$  mm<sup>3</sup> [105, 110, 143]. Tumor numbers were vehicle control (VC) = 6, JQ1 = 8, olaparib = 7 and JQ1 + olaparib = 9. The JQ1 stock solution was prepared as 50 mg/ml in DMSO and olaparib in stock solution of 50 mg/ml in PBS. Both were stored in 100 $\mu$ L aliquots in -80°C. Drug solutions were quickly thawed in a 37°C water bath and diluted 1:10 in 10%  $\beta$ -cyclodextrin dissolved in sterile water for JQ1 and sterile PBS for olaparib [105]. Intraperitoneal injections of JQ1 (50 mg/kg), olaparib (50 mg/kg) or the combination was administered daily for 21 days with olaparib administered 30 minutes prior to JQ1 [105]. Tumor volumes were measured three times a week using digital calipers, and tumor volume calculated using the formula  $v = (\pi/6) \times d^3$ . Results were normalized to Day 0 of drug treatment, and data are expressed as normalized tumor volume. Average mouse body weight (g) was assessed three times a week using a scale throughout the study. At the end of the study and within 24-hours of final treatment, mice were euthanized by CO<sub>2</sub> and cervical dislocation (CD). Tumor tissue was harvested, collected and snap frozen for RNA extraction.

### *In vivo gemcitabine + cisplatin evaluation*

Cisplatin (HY-17394) was purchased from MedChem Express (Monmouth Junction, NJ, USA), made as a 2.5 mg/ml stock solution dissolved in 0.9% saline and stored in -80°C. CB17<sup>-/-</sup> female SCID mice (4-week-old) were purchased from Taconic Farms (Newton, MA, USA) and housed in the AAALAC accredited vivarium at University of Alabama at Birmingham Research Support Building. CCA PDX model, CCA1, was implanted into each flank via subcutaneous implantation. Mice bearing bilateral CCA1 tumors were randomized into four groups of 5 mice/group when tumors reached ~200 mm<sup>3</sup> [105, 110, 143]. Tumor numbers were vehicle control (VC) = 4, gemcitabine = 8, cisplatin = 8 and gemcitabine + cisplatin = 7. Drug solutions were quickly thawed in a 37°C water bath and cisplatin diluted 1:10 in 10% β-cyclodextrin dissolved in sterile water. Mice were treated with 60 mg/kg gemcitabine, 2.5 mg/kg cisplatin or the combination via i.p. injection once a week for 28 days. Tumor volumes were measured three times a week using digital calipers, and tumor volume calculated using the formula  $v = (\pi/6) \times d^3$ . Results were normalized to Day 0 of drug treatment, and data are expressed as normalized tumor volume. Average mouse body weight (g) was assessed three times a week using a scale throughout the study. At the end of the study and within 24-hours of final treatment, mice were euthanized by CO<sub>2</sub> and cervical dislocation (CD). Tumor tissue was harvested, collected and snap frozen.

### *Statistical analysis*

All statistical analyses were performed using GraphPad Prism 7 software (San Diego, CA, USA) [105, 110]. In Chapter 2, percent clonogenic survival was assessed

amongst JQ1 doses using one-way-ANOVA. Gene expression patterns of *MYC*, *BRCA2* and *CHEK1* were determined via qRT-PCR for mRNA by one-way-ANOVA. Blot densitometry was compared using one-way-ANOVA. Comparison of BRD2 and BRD4 blots was performed using student t test. For *in vivo* studies comparing the drug efficacy of JQ1 with or without olaparib, we utilized two-way-ANOVA test. In Chapter 4, tumor proliferation was determined by staining for Ki-67 and results compared using student t test.  $P < 0.05$  was considered significant for all tests.

Table 6-1. The antibodies used in this dissertation

<b>Antibody</b>	<b>Company</b>	<b>Source</b>	<b>Application</b>
BRD2	Cell Signaling 5848	Rabbit	WB
BRD4	Cell Signaling 13440P	Rabbit	WB
CDA	Abcam 82346	Rabbit	IHC
CDC25B	Abcam 70927	Rabbit	WB
Chk1	Bethyl A300-298AT	Rabbit	WB
Cleaved Caspase-3	Cell Signaling 9661L	Rabbit	WB
Cleaved PARP	Cell Signaling 5625	Rabbit	WB
c-Myc	Cell Signaling 5605S	Rabbit	WB
c-Myc	Invitrogen 132500	Mouse	IHC
dCK	Santa Cruz 393099	Mouse	WB/IHC
GAPDH	Cell Signaling 2118S	Rabbit	WB
hCNT1	Novus NBP2-30857	Rabbit	IHC
hENT1	Sigma SAB5500117	Rabbit	IHC
Ki-67	Abcam 92742	Rabbit	IHC
RRM1	Novus NBP2-49415	Rabbit	IHC
RRM2	Santa Cruz 376973	Mouse	WB
RRM2	Abcam 57653	Mouse	IHC
Vinculin	Sigma V4505	Mouse	WB
$\alpha$ - Tubulin	Cell Signaling 2125	Rabbit	WB
$\alpha$ -mouse 2°	Vector ImmPRESS MP-7402	Horse	IHC
$\alpha$ -mouse 2°	Cell Signaling 7076	Horse	WB
$\alpha$ -rabbit 2°	Vector ImmPRESS MP-7401	Horse	IHC
$\alpha$ -rabbit 2°	Abcam 6721	Goat	WB
$\gamma$ H2AX	Cell Signaling 9272S	Rabbit	WB

Table 6-2. PCR Primers

Gene	Primer Sequence	Product Size
BRCA1 c.68-69delAG	Fwd 5'-GAAGTTGTCATTTTATAAACCTTT-3'	258 bp
	Rev 5'-TGTCTTTTCTTCCCTAGTATGT-3'	
BRCA1 c.4188 (p.Q1396H)	Fwd 5'-CACCAAGTCTTTGAAATGTGCC-3'	540 bp
	Rev 5'-TCTGGATTTTCGCAGGTCCTC-3'	
BRCA1 c.1630 C>G (p.Q544E)	Fwd 5'-ACAAGAGCGTCCCCTCACAA-3'	390 bp
	Rev 5'-AGCGCATGAATATGCCTGGTA-3'	
BRCA1 c.4810 C>T (p.Q1604*)	Fwd 5'-GAGGGAACCCCTTACCTGGA-3'	242 bp
	Rev 5'-AATTCTGGCTTCTCCCTGCTC-3'	
BRCA1 c.4186 C>T (p.Q1396*)	Fwd 5'-CACCAAGTCTTTGAAATGTGCC-3'	540 bp
	Rev 5'-TCTGGATTTTCGCAGGTCCTC-3'	
BRCA1 c.5266 C>T (p.Q1756*)	Fwd 5'-AAATATGACGTGTCTGCTCCACT-3'	259 bp
	Rev 5'-TCTTACAAAATGAAGCGGCC-3'	
BRCA2 c.2808-2811delACAA	Fwd 5'-TGAGCTGTTGCCACCTGAAA-3'	505 bp
	Rev 5'-TGGACCTAAGAGTCCTGCCC-3'	
BRCA2 c.2830 A>T (p.K944*)	Fwd 5'-TGAGCTGTTGCCACCTGAAA-3'	505 bp
	Rev 5'-TGGACCTAAGAGTCCTGCCC-3'	
BRCA2 c.9154 C>T (R3052W)	Fwd 5'-TCAACAACCTACCGGTACAAACCT-3'	337 bp
	Rev 5'-CCAACCTGGTAGCTCCAACCTAAT-3'	
BRCA2 c.9976 A>T (K3326*)	Fwd 5'-ACATTTGTTTCTCCGGCTGC-3'	349 bp
	Rev 5'-ATTCTTCCGTAAGTGGCCTGG-3'	
KRAS	Fwd 5'-GTGTGACATGTTCTAATATAGTCA-3'	214 bp
CHEK1 (qRT)	Fwd 5'-ATATGAAGCGTGCCGTAGACT-3'	183 bp
	Rev 5'-TGCCTATGTCTGGCTCTATTCTG-3'	
BRCA2 (qRT)	Fwd 5'-ACAAGCAACCCAAGTGTCAAT-3'	221 bp
	Rev 5'-TGAAGCTACCTCCAAAACCTGTG-3'	
MYC (qRT)	Fwd 5'-CGACTCTGAGGAGGAACAAG-3'	95 bp
	Rev 5'-GTGATCCAGACTCTGACCTTT-3'	
GAPDH (qRT)	Fwd 5'-AACATCATCCCTGCTTCCAC-3'	234 bp
	Rev 5'-GACCACCTGGTCCCTCAGTGT-3'	
Myc TS1 (ChIP)	Fwd 5'-ACACTAACATCCCACGCTCTG-3'	75 bp
	Rev 5'-GATCAAGAGTCCCAGGGAGA-3'	
Myc Promoter P2 (ChIP)	Fwd 5'-CTTGGCGGGAAAAAGAACGG-3'	99 bp
	Rev 5'-CTGCCTCTCGCTGGAATTACT-3'	



## LIST OF REFERENCES

- [1] Y. Zong, B.Z. Stanger, Molecular mechanisms of bile duct development, *The International Journal of Biochemistry & Cell Biology*, 43 (2011) 257-264.
- [2] F.P. Lemaigre, Development of the biliary tract, *Mechanisms of Development*, 120 (2003) 81-87.
- [3] F.P. Lemaigre, Mechanisms of liver development: concepts for understanding liver disorders and design of novel therapies, *Gastroenterology*, 137 (2009) 62-79.
- [4] M. Squadroni, L. Tondulli, G. Gatta, S. Mosconi, G. Beretta, R. Labianca, Cholangiocarcinoma, *Critical Reviews in Oncology/Hematology*, (2016).
- [5] K.N. Nejak-Bowen, S.P.S. Monga, Chapter 6 - Developmental Pathways in Liver Regeneration-I, in: U. Apte (Ed.) *Liver Regeneration*, Academic Press, Boston, 2015, pp. 77-101.
- [6] G.M. Hirschfield, E.J. Heathcote, M.E. Gershwin, Pathogenesis of Cholestatic Liver Disease and Therapeutic Approaches, *Gastroenterology*, 139 (2010) 1481-1496.
- [7] J.H. Tabibian, A.I. Masyuk, T.V. Masyuk, S.P. O'Hara, N.F. LaRusso, Physiology of cholangiocytes, *Compr Physiol*, 3 (2013) 541-565.
- [8] S. Rizvi, S.A. Khan, C.L. Hallemeier, R.K. Kelley, G.J. Gores, Cholangiocarcinoma - evolving concepts and therapeutic strategies, *Nat Rev Clin Oncol*, 15 (2018) 95-111.

- [9] M. Strazzabosco, L. Fabris, Functional anatomy of normal bile ducts, *Anatomical record* (Hoboken, N.J. : 2007), 291 (2008) 653-660.
- [10] R.B. Schmuck, C.V. de Carvalho-Fischer, C. Neumann, J. Pratschke, M. Bahra, Distal bile duct carcinomas and pancreatic ductal adenocarcinomas: postulating a common tumor entity, *Cancer Med*, 5 (2016) 88-99.
- [11] B. Doherty, V.E. Nambudiri, W.C. Palmer, Update on the Diagnosis and Treatment of Cholangiocarcinoma, *Current Gastroenterology Reports*, 19 (2017) 2.
- [12] B. Blechacz, Cholangiocarcinoma: Current Knowledge and New Developments, *Gut and Liver*, 11 (2017) 13-26.
- [13] G.L. Tyson, H.B. El-Serag, Risk factors for cholangiocarcinoma, *Hepatology*, 54 (2011) 173-184.
- [14] M.J. Olnes, R. Erlich, A review and update on cholangiocarcinoma, *Oncology*, 66 (2004) 167-179.
- [15] C.J. O'Rourke, J. Lafuente-Barquero, J.B. Andersen, Epigenome Remodeling in Cholangiocarcinoma, *Trends in cancer*, 5 (2019) 335-350.
- [16] N. Razumilava, G.J. Gores, Cholangiocarcinoma, *The Lancet*, 383 (2014) 2168-2179.
- [17] S.K. Saha, C.A. Parachoniak, K.S. Ghanta, J. Fitamant, K.N. Ross, M.S. Najem, S. Gurumurthy, E.A. Akbay, D. Sia, H. Cornella, O. Miltiadous, C. Walesky, V. Deshpande, A.X. Zhu, A.F. Hezel, K.E. Yen, K.S. Straley, J. Travins, J. Popovici-Muller, C. Gliser, C.R. Ferrone, U. Apte, J.M. Llovet, K.K. Wong, S. Ramaswamy, N. Bardeesy, Mutant IDH inhibits HNF-4alpha to block hepatocyte differentiation and promote biliary cancer, *Nature*, 513 (2014) 110-114.

- [18] M.J. Borad, G.J. Gores, L.R. Roberts, Fibroblast growth factor receptor 2 fusions as a target for treating cholangiocarcinoma, *Current opinion in gastroenterology*, 31 (2015) 264-268.
- [19] S. Rizvi, G.J. Gores, Pathogenesis, diagnosis, and management of cholangiocarcinoma, *Gastroenterology*, 145 (2013) 1215-1229.
- [20] Y.M. Wu, F. Su, S. Kalyana-Sundaram, N. Khazanov, B. Ateeq, X. Cao, R.J. Lonigro, P. Vats, R. Wang, S.F. Lin, A.J. Cheng, L.P. Kunju, J. Siddiqui, S.A. Tomlins, P. Wyngaard, S. Sadis, S. Roychowdhury, M.H. Hussain, F.Y. Feng, M.M. Zalupski, M. Talpaz, K.J. Pienta, D.R. Rhodes, D.R. Robinson, A.M. Chinnaiyan, Identification of targetable FGFR gene fusions in diverse cancers, *Cancer Discov*, 3 (2013) 636-647.
- [21] Y. Gao, L. Wells, F.I. Comer, G.J. Parker, G.W. Hart, Dynamic O-glycosylation of nuclear and cytosolic proteins: cloning and characterization of a neutral, cytosolic beta-N-acetylglucosaminidase from human brain, *The Journal of biological chemistry*, 276 (2001) 9838-9845.
- [22] F.H. Tan, T.L. Putoczki, S.S. Stylli, R.B. Luwor, Ponatinib: a novel multi-tyrosine kinase inhibitor against human malignancies, *Onco Targets Ther*, 12 (2019) 635-645.
- [23] S. Kongpetch, A. Jusakul, C.K. Ong, W.K. Lim, S.G. Rozen, P. Tan, B.T. Teh, Pathogenesis of cholangiocarcinoma: From genetics to signalling pathways, *Best practice & research. Clinical gastroenterology*, 29 (2015) 233-244.
- [24] M. Javle, M. Lowery, R.T. Shroff, K.H. Weiss, C. Springfield, M.J. Borad, R.K. Ramanathan, L. Goyal, S. Sadeghi, T. Macarulla, A. El-Khoueiry, R.K. Kelley, I. Borbath, S.P. Choo, D.Y. Oh, P.A. Philip, L.T. Chen, T. Reungwetwattana, E. Van Cutsem, K.H. Yeh, K. Ciombor, R.S. Finn, A. Patel, S. Sen, D. Porter, R. Isaacs, A.X. Zhu, G.K. Abou-

Alfa, T. Bekaii-Saab, Phase II Study of BGJ398 in Patients With FGFR-Altered Advanced Cholangiocarcinoma, *Journal of clinical oncology : official journal of the American Society of Clinical Oncology*, 36 (2018) 276-282.

[25] K.K. Farh, A. Marson, J. Zhu, M. Kleinewietfeld, W.J. Housley, S. Beik, N. Shores, H. Whitton, R.J. Ryan, A.A. Shishkin, M. Hatan, M.J. Carrasco-Alfonso, D. Mayer, C.J. Luckey, N.A. Patsopoulos, P.L. De Jager, V.K. Kuchroo, C.B. Epstein, M.J. Daly, D.A. Hafler, B.E. Bernstein, Genetic and epigenetic fine mapping of causal autoimmune disease variants, *Nature*, 518 (2015) 337-343.

[26] S.A. Khan, H.C. Thomas, B.R. Davidson, S.D. Taylor-Robinson, Cholangiocarcinoma, *The Lancet*, 366 (2005) 1303-1314.

[27] T.H. Karlsen, T. Folseraas, D. Thorburn, M. Vesterhus, Primary sclerosing cholangitis - a comprehensive review, *J Hepatol*, 67 (2017) 1298-1323.

[28] T.J. Weismüller, C.P. Strassburg, P.J. Trivedi, G.M. Hirschfield, P.J. Trivedi, A. Bergquist, K. Said, M. Imam, K.N. Lazaridis, B.D. Juran, A. Cheung, K.D. Lindor, T.J. Weismüller, H. Lenzen, M.P. Manns, C.Y. Ponsioen, U. Beuers, K. Holm, S. Naess, T.H. Karlsen, E. Schrumpf, K.M. Boberg, D. Gotthardt, C. Rupp, M.A. Färkkilä, K. Jokelainen, H.U. Marschall, M. Benito de Valle, D. Thorburn, F. Saffioti, R.K. Weersma, J. Fevery, T. Mueller, O. Chazouillères, K. Schulze, C. Schramm, S. Almer, S.P. Pereira, C. Levy, A. Mason, C.L. Bowlus, A. Floreani, E. Halilbasic, M. Trauner, K.K. Yimam, P. Milkiewicz, P. Milkiewicz, D.K. Huynh, A. Pares, C.N. Manser, G.N. Dalekos, B. Eksteen, P. Invernizzi, C.P. Berg, G.I. Kirchner, C. Sarrazin, V. Zimmer, L. Fabris, F. Braun, M. Marzioni, C. Schramm, R.W. Chapman, R.W. Chapman, K.D. Lindor, M. Imam, K.D. Lindor, S. Naess, T.H. Karlsen, E. Schrumpf, K.M. Boberg, B.E. Hansen, B.E. Hansen,

B.E. Hansen, Patient Age, Sex, and Inflammatory Bowel Disease Phenotype Associate With Course of Primary Sclerosing Cholangitis, *Gastroenterology*, 152 (2017) 1975-1984.e1978.

[29] B.K. Chung, T.H. Karlsen, T. Folseraas, Cholangiocytes in the pathogenesis of primary sclerosing cholangitis and development of cholangiocarcinoma, *Biochimica et biophysica acta. Molecular basis of disease*, 1864 (2018) 1390-1400.

[30] P. Fickert, M. Wagner, H.U. Marschall, A. Fuchsbichler, G. Zollner, O. Tsybrovskyy, K. Zatloukal, J. Liu, M.P. Waalkes, C. Cover, H. Denk, A.F. Hofmann, H. Jaeschke, M. Trauner, 24-norUrsodeoxycholic acid is superior to ursodeoxycholic acid in the treatment of sclerosing cholangitis in Mdr2 (Abcb4) knockout mice, *Gastroenterology*, 130 (2006) 465-481.

[31] S. Saensa-Ard, S. Leungwattanawanit, L. Senggunprai, N. Namwat, S. Kongpetch, Y. Chamgramol, W. Loilome, W. Khansaard, A. Jusakul, A. Prawan, C. Pairojkul, N. Khantikeo, P. Yongvanit, V. Kukongviriyapan, Establishment of cholangiocarcinoma cell lines from patients in the endemic area of liver fluke infection in Thailand, *Tumour biology : the journal of the International Society for Oncodevelopmental Biology and Medicine*, 39 (2017) 1010428317725925.

[32] B. Sripa, S. Leungwattanawanit, T. Nitta, C. Wongkham, V. Bhudhisawasdi, A. Puapairoj, C. Sripa, M. Miwa, Establishment and characterization of an opisthorchiasis-associated cholangiocarcinoma cell line (KKU-100), *World Journal of Gastroenterology: WJG*, 11 (2005) 3392.

[33] S. Zheng, Y. Zhu, Z. Zhao, Z. Wu, K. Okanurak, Z. Lv, Liver fluke infection and cholangiocarcinoma: a review, *Parasitology research*, 116 (2017) 11-19.

- [34] R. Liu, K. Cox, S.L. Guthery, L. Book, B. Witt, B. Chadwick, D.G. Adler, Cholangiocarcinoma and high-grade dysplasia in young patients with primary sclerosing cholangitis, *Digestive Diseases and Sciences*, 59 (2014) 2320-2324.
- [35] H. Wehbe, R. Henson, F. Meng, J. Mize-Berge, T. Patel, Interleukin-6 contributes to growth in cholangiocarcinoma cells by aberrant promoter methylation and gene expression, *Cancer Research*, 66 (2006) 10517-10524.
- [36] N. Voravud, C. Foster, J. Gilbertson, K. Sikora, J. Waxman, Oncogene expression in cholangiocarcinoma and in normal hepatic development, *Human Pathology*, 20 (1989) 1163-1168.
- [37] L.E. Vasilieva, S.I. Papadimitriou, S.P. Dourakis, Modern diagnostic approaches to cholangiocarcinoma, *Hepatobiliary & Pancreatic Diseases International*, 11 (2012) 349-359.
- [38] M. Cadamuro, S.D. Morton, M. Strazzabosco, L. Fabris, Unveiling the role of tumor reactive stroma in cholangiocarcinoma: an opportunity for new therapeutic strategies, *Translational Gastrointestinal Cancer*, 2 (2013) 130-144.
- [39] S. Brivio, M. Cadamuro, M. Strazzabosco, L. Fabris, Tumor reactive stroma in cholangiocarcinoma: The fuel behind cancer aggressiveness, *World Journal of Hepatology*, 9 (2017) 455.
- [40] I.S. Oliveira, A. Kilcoyne, J.M. Everett, M. Mino-Kenudson, M.G. Harisinghani, K. Ganesan, Cholangiocarcinoma: classification, diagnosis, staging, imaging features, and management, *Abdominal radiology (New York)*, 42 (2017) 1637-1649.

- [41] H.L. Chen, S.H. Wu, S.H. Hsu, B.Y. Liou, H.L. Chen, M.H. Chang, Jaundice revisited: recent advances in the diagnosis and treatment of inherited cholestatic liver diseases, *Journal of biomedical science*, 25 (2018) 75.
- [42] E. Ghurburrun, I. Borbath, F.P. Lemaigre, P. Jacquemin, Liver and Pancreas: Do Similar Embryonic Development and Tissue Organization Lead to Similar Mechanisms of Tumorigenesis?, *Gene expression*, 18 (2018) 149-155.
- [43] M. Maehle Grimsrud, T. Folseraas, Pathogenesis, diagnosis and treatment of premalignant and malignant stages of cholangiocarcinoma in primary sclerosing cholangitis, *Liver international : official journal of the International Association for the Study of the Liver*, (2019).
- [44] S.B. Edge, C.C. Compton, The American Joint Committee on Cancer: the 7th edition of the AJCC cancer staging manual and the future of TNM, *Annals of surgical oncology*, 17 (2010) 1471-1474.
- [45] Z.-W. Meng, W. Pan, H.-J. Hong, J.-Z. Chen, Y.-L. Chen, Macroscopic types of intrahepatic cholangiocarcinoma and the eighth edition of AJCC/UICC TNM staging system, *Oncotarget*, 8 (2017) 101165-101174.
- [46] M.P. Gaspersz, S. Buettner, J.L.A. van Vugt, J. de Jonge, W.G. Polak, M. Doukas, J.N.M. Ijzermans, B.G. Koerkamp, F. Willemsen, Evaluation of the New American Joint Committee on Cancer Staging Manual 8th Edition for Perihilar Cholangiocarcinoma, *Journal of gastrointestinal surgery : official journal of the Society for Surgery of the Alimentary Tract*, (2019).

- [47] S.-Y. Jun, Y.-N. Sung, J.H. Lee, K.-M. Park, Y.-J. Lee, S.-M. Hong, Validation of the Eighth American Joint Committee on Cancer Staging System for Distal Bile Duct Carcinoma, *Cancer Res Treat*, 51 (2019) 98-111.
- [48] N. Ramírez-Merino, S.P. Aix, H. Cortés-Funes, Chemotherapy for cholangiocarcinoma: an update, *World J Gastrointest Oncol*, 5 (2013) 171-176.
- [49] S.B. Choi, K.S. Kim, J.Y. Choi, S.W. Park, J.S. Choi, W.J. Lee, J.B. Chung, The prognosis and survival outcome of intrahepatic cholangiocarcinoma following surgical resection: association of lymph node metastasis and lymph node dissection with survival, *Annals of surgical oncology*, 16 (2009) 3048-3056.
- [50] I. Endo, M. Gonen, A.C. Yopp, K.M. Dalal, Q. Zhou, D. Klimstra, M. D'Angelica, R.P. DeMatteo, Y. Fong, L. Schwartz, N. Kemeny, E. O'Reilly, G.K. Abou-Alfa, H. Shimada, L.H. Blumgart, W.R. Jarnagin, Intrahepatic cholangiocarcinoma: rising frequency, improved survival, and determinants of outcome after resection, *Annals of surgery*, 248 (2008) 84-96.
- [51] M.L. DeOliveira, S.C. Cunningham, J.L. Cameron, F. Kamangar, J.M. Winter, K.D. Lillemoe, M.A. Choti, C.J. Yeo, R.D. Schulick, Cholangiocarcinoma: thirty-one-year experience with 564 patients at a single institution, *Annals of surgery*, 245 (2007) 755-762.
- [52] W. Marcason, What is the Whipple procedure and what is the appropriate nutrition therapy for it?, *Journal of the Academy of Nutrition and Dietetics*, 115 (2015) 168.
- [53] G. Sapisochin, C. Rodriguez de Lope, M. Gastaca, J. Ortiz de Urbina, M.A. Suarez, J. Santoyo, J.F. Castroagudin, E. Varo, R. Lopez-Andujar, F. Palacios, G. Sanchez Antolin, B. Perez, A. Guiberteau, G. Blanco, M.L. Gonzalez-Dieguez, M. Rodriguez, M.A. Varona, M.A. Barrera, Y. Fundora, J.A. Ferron, E. Ramos, J. Fabregat, R. Ciria, S. Rufian, A. Otero,



M.A. Vazquez, J.A. Pons, P. Parrilla, G. Zozaya, J.I. Herrero, R. Charco, J. Bruix, "Very early" intrahepatic cholangiocarcinoma in cirrhotic patients: should liver transplantation be reconsidered in these patients?, *American journal of transplantation : official journal of the American Society of Transplantation and the American Society of Transplant Surgeons*, 14 (2014) 660-667.

[54] D.B. Brown, J.F. Geschwind, M.C. Soulen, S.F. Millward, D. Sacks, Society of Interventional Radiology position statement on chemoembolization of hepatic malignancies, *Journal of vascular and interventional radiology : JVIR*, 17 (2006) 217-223.

[55] L. de Sousa Cavalcante, G. Monteiro, Gemcitabine: metabolism and molecular mechanisms of action, sensitivity and chemoresistance in pancreatic cancer, *European Journal of Pharmacology*, 741 (2014) 8-16.

[56] R.K. Mehmood, Review of cisplatin and oxaliplatin in current immunogenic and monoclonal antibody treatments, *Oncology Reviews*, 8 (2014).

[57] S. Dasari, P.B. Tchounwou, Cisplatin in cancer therapy: molecular mechanisms of action, *European Journal of Pharmacology*, 740 (2014) 364-378.

[58] A. Basu, S. Krishnamurthy, Cellular responses to Cisplatin-induced DNA damage, *J Nucleic Acids*, 2010 (2010).

[59] J. Valle, H. Wasan, D.H. Palmer, D. Cunningham, A. Anthony, A. Maraveyas, S. Madhusudan, T. Iveson, S. Hughes, S.P. Pereira, Cisplatin plus gemcitabine versus gemcitabine for biliary tract cancer, *New England Journal of Medicine*, 362 (2010) 1273-1281.

- [60] L. Maroni, I. Pierantonelli, J.M. Banales, A. Benedetti, M. Marzioni, The significance of genetics for cholangiocarcinoma development, *Annals of Translational Medicine*, 1 (2013).
- [61] M. Cadamuro, S. Brivio, C. Spirli, R.E. Joplin, M. Strazzabosco, L. Fabris, Autocrine and Paracrine Mechanisms Promoting Chemoresistance in Cholangiocarcinoma, *International Journal of Molecular Sciences*, 18 (2017) 149.
- [62] Y. Nakano, S. Tanno, K. Koizumi, T. Nishikawa, K. Nakamura, M. Minoguchi, T. Izawa, Y. Mizukami, T. Okumura, Y. Kohgo, Gemcitabine chemoresistance and molecular markers associated with gemcitabine transport and metabolism in human pancreatic cancer cells, *British Journal of Cancer*, 96 (2007) 457-463.
- [63] J.C. Mertens, C.D. Fingas, J.D. Christensen, R.L. Smoot, S.F. Bronk, N.W. Werneburg, M.P. Gustafson, A.B. Dietz, L.R. Roberts, A.E. Sirica, G.J. Gores, Therapeutic effects of deleting cancer-associated fibroblasts in cholangiocarcinoma, *Cancer Res*, 73 (2013) 897-907.
- [64] A.Y. Jia, J.X. Wu, Y.T. Zhao, Y.X. Li, Z. Wang, W.Q. Rong, L.M. Wang, J. Jin, S.L. Wang, Y.W. Song, Y.P. Liu, H. Ren, H. Fang, W.Q. Wang, X.F. Liu, Z.H. Yu, W.H. Wang, Intensity-modulated radiotherapy following null-margin resection is associated with improved survival in the treatment of intrahepatic cholangiocarcinoma, *Journal of gastrointestinal oncology*, 6 (2015) 126-133.
- [65] R. Tao, S. Krishnan, P.R. Bhosale, M.M. Javle, T.A. Aloia, R.T. Shroff, A.O. Kaseb, A.J. Bishop, C.W. Swanick, E.J. Koay, H.D. Thames, T.S. Hong, P. Das, C.H. Crane, Ablative Radiotherapy Doses Lead to a Substantial Prolongation of Survival in Patients With Inoperable Intrahepatic Cholangiocarcinoma: A Retrospective Dose Response

Analysis, *Journal of clinical oncology : official journal of the American Society of Clinical Oncology*, 34 (2016) 219-226.

[66] J.L. Wilding, W.F. Bodmer, Cancer cell lines for drug discovery and development, *Cancer Res*, 74 (2014) 2377-2384.

[67] G. Kaur, J.M. Dufour, Cell lines: Valuable tools or useless artifacts, *Spermatogenesis*, 2 (2012) 1-5.

[68] N. Yamaguchi, H. Morioka, H. Ohkura, S. Hirohashi, K. Kawai, Establishment and characterization of the human cholangiocarcinoma cell line HChol-Y1 in a serum-free, chemically defined medium, *J Natl Cancer Inst*, 75 (1985) 29-35.

[69] E. Loeuillard, S.R. Fischbach, G.J. Gores, S. Rizvi, Animal models of cholangiocarcinoma, *Biochimica et biophysica acta*, (2018).

[70] J. Jung, H.S. Seol, S. Chang, The Generation and Application of Patient-Derived Xenograft Model for Cancer Research, *Cancer Res Treat*, 50 (2018) 1-10.

[71] P.L. Garcia, A.L. Miller, T.L. Gamblin, L.N. Council, J.D. Christein, J.P. Arnoletti, M.J. Heslin, S. Reddy, J.H. Richardson, X. Cui, R. van Waardenburg, J.E. Bradner, E.S. Yang, K.J. Yoon, JQ1 Induces DNA Damage and Apoptosis, and Inhibits Tumor Growth in a Patient-Derived Xenograft Model of Cholangiocarcinoma, *Mol Cancer Ther*, 17 (2018) 107-118.

[72] C.D. Allis, T. Jenuwein, The molecular hallmarks of epigenetic control, *Nature Reviews Genetics*, 17 (2016) 487.

[73] Z. Chen, S. Li, S. Subramaniam, J.Y.J. Shyy, S. Chien, Epigenetic Regulation: A New Frontier for Biomedical Engineers, *Annual Review of Biomedical Engineering*, 19 (2017) 195-219.

- [74] R. Marmorstein, M.-M. Zhou, Writers and readers of histone acetylation: structure, mechanism, and inhibition, *Cold Spring Harbor perspectives in biology*, 6 (2014) a018762.
- [75] C. Dhalluin, J.E. Carlson, L. Zeng, C. He, A.K. Aggarwal, M.M. Zhou, Structure and ligand of a histone acetyltransferase bromodomain, *Nature*, 399 (1999) 491-496.
- [76] E. Verdin, M. Ott, 50 years of protein acetylation: from gene regulation to epigenetics, metabolism and beyond, *Nature Reviews Molecular Cell Biology*, 16 (2015) 258-264.
- [77] J.W. Tamkun, R. Deuring, M.P. Scott, M. Kissinger, A.M. Pattatucci, T.C. Kaufman, J.A. Kennison, brahma: a regulator of *Drosophila* homeotic genes structurally related to the yeast transcriptional activator SNF2/SWI2, *Cell*, 68 (1992) 561-572.
- [78] J. Shi, C.R. Vakoc, The mechanisms behind the therapeutic activity of BET bromodomain inhibition, *Molecular Cell*, 54 (2014) 728-736.
- [79] S.-Y. Wu, C.-M. Chiang, The double bromodomain-containing chromatin adaptor Brd4 and transcriptional regulation, *Journal of Biological Chemistry*, 282 (2007) 13141-13145.
- [80] F. Vollmuth, W. Blankenfeldt, M. Geyer, Structures of the dual bromodomains of the P-TEFb-activating protein Brd4 at atomic resolution, *Journal of Biological Chemistry*, 284 (2009) 36547-36556.
- [81] P. Filippakopoulos, J. Qi, S. Picaud, Y. Shen, W.B. Smith, O. Fedorov, E.M. Morse, T. Keates, T.T. Hickman, I. Felletar, Selective inhibition of BET bromodomains, *Nature*, 468 (2010) 1067-1073.
- [82] P. Filippakopoulos, S. Knapp, Targeting bromodomains: epigenetic readers of lysine acetylation, *Nature Reviews Drug Discovery*, 13 (2014) 337-356.

- [83] P. Filippakopoulos, S. Knapp, The bromodomain interaction module, *FEBS Letters*, 586 (2012) 2692-2704.
- [84] A.C. Belkina, B.S. Nikolajczyk, G.V. Denis, BET protein function is required for inflammation: Brd2 genetic disruption and BET inhibitor JQ1 impair mouse macrophage inflammatory responses, *Journal of immunology (Baltimore, Md. : 1950)*, 190 (2013) 3670-3678.
- [85] J. Lovén, H.A. Hoke, C.Y. Lin, A. Lau, D.A. Orlando, C.R. Vakoc, J.E. Bradner, T.I. Lee, R.A. Young, Selective inhibition of tumor oncogenes by disruption of super-enhancers, *Cell*, 153 (2013) 320-334.
- [86] E. Bourova-Flin, F. Chuffart, S. Rousseaux, S. Khochbin, The Role of Bromodomain Testis-Specific Factor, BRDT, in Cancer: A Biomarker and A Possible Therapeutic Target, *Cell journal*, 19 (2017) 1-8.
- [87] T.C. Roberts, U. Etxaniz, A. Dall'Agnes, S.-Y. Wu, C.-M. Chiang, P.E. Brennan, M.J.A. Wood, P.L. Puri, BRD3 and BRD4 BET Bromodomain Proteins Differentially Regulate Skeletal Myogenesis, *Scientific Reports*, 7 (2017) 6153.
- [88] Y. Taniguchi, The Bromodomain and Extra-Terminal Domain (BET) Family: Functional Anatomy of BET Paralogous Proteins, *International Journal of Molecular Sciences*, 17 (2016) 1849.
- [89] J. Dai, S. Zhou, Q. Ge, J. Qin, J. Li, H. Ju, Y. Cao, M. Zheng, C. Li, X. Gao, H. Teng, Q. Jiang, Recruitment of Brd3 and Brd4 to acetylated chromatin is essential for proinflammatory cytokine-induced matrix-degrading enzyme expression, *Journal of orthopaedic surgery and research*, 14 (2019) 59.

- [90] G. LeRoy, B. Rickards, S.J. Flint, The double bromodomain proteins Brd2 and Brd3 couple histone acetylation to transcription, *Molecular Cell*, 30 (2008) 51-60.
- [91] L. Handoko, B. Kaczkowski, C.C. Hon, M. Lizio, M. Wakamori, T. Matsuda, T. Ito, P. Jeyamohan, Y. Sato, K. Sakamoto, S. Yokoyama, H. Kimura, A. Minoda, T. Umehara, JQ1 affects BRD2-dependent and independent transcription regulation without disrupting H4-hyperacetylated chromatin states, *Epigenetics*, (2018) 1-22.
- [92] E. Shang, Q. Cui, X. Wang, C. Beseler, D.A. Greenberg, D.J. Wolgemuth, The bromodomain-containing gene BRD2 is regulated at transcription, splicing, and translation levels, *Journal of cellular biochemistry*, 112 (2011) 2784-2793.
- [93] B. Donati, E. Lorenzini, A. Ciarrocchi, BRD4 and Cancer: going beyond transcriptional regulation, *Mol Cancer*, 17 (2018) 164.
- [94] A. Dey, F. Chitsaz, A. Abbasi, T. Misteli, K. Ozato, The double bromodomain protein Brd4 binds to acetylated chromatin during interphase and mitosis, *Proc Natl Acad Sci U S A*, 100 (2003) 8758-8763.
- [95] C.W. Chung, H. Coste, J.H. White, O. Mirguet, J. Wilde, R.L. Gosmini, C. Delves, S.M. Magny, R. Woodward, S.A. Hughes, E.V. Boursier, H. Flynn, A.M. Bouillot, P. Bamborough, J.M. Brusq, F.J. Gellibert, E.J. Jones, A.M. Riou, P. Homes, S.L. Martin, I.J. Uings, J. Toum, C.A. Clement, A.B. Boullay, R.L. Grimley, F.M. Blandel, R.K. Prinjha, K. Lee, J. Kirilovsky, E. Nicodeme, Discovery and characterization of small molecule inhibitors of the BET family bromodomains, *Journal of medicinal chemistry*, 54 (2011) 3827-3838.

- [96] J.E. Delmore, G.C. Issa, M.E. Lemieux, P.B. Rahl, J. Shi, H.M. Jacobs, E. Kastiris, T. Gilpatrick, R.M. Paranal, J. Qi, BET bromodomain inhibition as a therapeutic strategy to target c-Myc, *Cell*, 146 (2011) 904-917.
- [97] P. Voigt, D. Reinberg, BRD4 jump-starts transcription after mitotic silencing, *Genome Biology*, 12 (2011) 1.
- [98] S.R. Floyd, M.E. Pacold, Q. Huang, S.M. Clarke, F.C. Lam, I.G. Cannell, B.D. Bryson, J. Rameseder, M.J. Lee, E.J. Blake, The bromodomain protein Brd4 insulates chromatin from DNA damage signalling, *Nature*, 498 (2013) 246-250.
- [99] B.N. Devaiah, C. Case-Borden, A. Gegonne, C.H. Hsu, Q. Chen, D. Meerzaman, A. Dey, K. Ozato, D.S. Singer, BRD4 is a histone acetyltransferase that evicts nucleosomes from chromatin, *Nature Structural & Molecular Biology*, 23 (2016) 540-548.
- [100] A. Stanlie, A.S. Yousif, H. Akiyama, T. Honjo, N.A. Begum, Chromatin reader Brd4 functions in Ig class switching as a repair complex adaptor of nonhomologous end-joining, *Molecular Cell*, 55 (2014) 97-110.
- [101] A. Di Costanzo, N. Del Gaudio, A. Migliaccio, L. Altucci, Epigenetic drugs against cancer: an evolving landscape, *Archives of toxicology*, 88 (2014) 1651-1668.
- [102] J.K. Lee, S. Louzada, Y. An, S.Y. Kim, S. Kim, J. Youk, S. Park, S.H. Koo, B. Keam, Y.K. Jeon, J.L. Ku, F. Yang, T.M. Kim, Y.S. Ju, Complex chromosomal rearrangements by single catastrophic pathogenesis in NUT midline carcinoma, *Annals of oncology : official journal of the European Society for Medical Oncology*, 28 (2017) 890-897.
- [103] E. Nicodeme, K.L. Jeffrey, U. Schaefer, S. Beinke, S. Dewell, C.W. Chung, R. Chandwani, I. Marazzi, P. Wilson, H. Coste, J. White, J. Kirilovsky, C.M. Rice, J.M. Lora,

R.K. Prinjha, K. Lee, A. Tarakhovsky, Suppression of inflammation by a synthetic histone mimic, *Nature*, 468 (2010) 1119-1123.

[104] L. Anders, M.G. Guenther, J. Qi, Z.P. Fan, J.J. Marineau, P.B. Rahl, J. Lovén, A.A. Sigova, W.B. Smith, T.I. Lee, Genome-wide localization of small molecules, *Nature Biotechnology*, 32 (2014) 92-96.

[105] A.L. Miller, S.C. Fehling, P.L. Garcia, T.L. Gamblin, L.N. Council, R. van Waardenburg, E.S. Yang, J.E. Bradner, K.J. Yoon, The BET inhibitor JQ1 attenuates double-strand break repair and sensitizes models of pancreatic ductal adenocarcinoma to PARP inhibitors, *EBioMedicine*, (2019).

[106] J.S. Shafran, G.P. Andrieu, B. Gyorffy, G.V. Denis, BRD4 regulates metastatic potential of castration-resistant prostate cancer through AHNAK, *Molecular cancer research : MCR*, (2019).

[107] D. Da Costa, A. Agathangelou, T. Perry, V. Weston, E. Petermann, A. Zlatanou, C. Oldreive, W. Wei, G. Stewart, J. Longman, BET inhibition as a single or combined therapeutic approach in primary paediatric B-precursor acute lymphoblastic leukaemia, *Blood Cancer Journal*, 3 (2013) e126.

[108] J.A. Mertz, A.R. Conery, B.M. Bryant, P. Sandy, S. Balasubramanian, D.A. Mele, L. Bergeron, R.J. Sims, Targeting MYC dependence in cancer by inhibiting BET bromodomains, *Proceedings of the National Academy of Sciences*, 108 (2011) 16669-16674.

[109] A.S. Leal, C.R. Williams, D.B. Royce, P.A. Pioli, M.B. Sporn, K.T. Liby, Bromodomain inhibitors, JQ1 and I-BET 762, as potential therapies for pancreatic cancer, *Cancer Letters*, 394 (2017) 76-87.



- [110] P. Garcia, A. Miller, K. Kreitzburg, L. Council, T. Gamblin, J. Christein, M. Heslin, J. Arnoletti, J. Richardson, D. Chen, The BET bromodomain inhibitor JQ1 suppresses growth of pancreatic ductal adenocarcinoma in patient-derived xenograft models, *Oncogene*, 35 (2016) 833-845.
- [111] K. Enomoto, X. Zhu, S. Park, L. Zhao, Y.J. Zhu, M.C. Willingham, J. Qi, J.A. Copland, P. Meltzer, S.-y. Cheng, Targeting Myc as a therapeutic intervention for anaplastic thyroid cancer, *The Journal of Clinical Endocrinology and Metabolism*, (2017).
- [112] X. Wu, D. Liu, X. Gao, F. Xie, D. Tao, X. Xiao, L. Wang, G. Jiang, F. Zeng, Inhibition of BRD4 Suppresses Cell Proliferation and Induces Apoptosis in Renal Cell Carcinoma, *Cellular Physiology and Biochemistry*, 41 (2017) 1947-1956.
- [113] M.A. Dawson, E.J. Gudgin, S.J. Horton, G. Giotopoulos, E. Meduri, S. Robson, E. Cannizzaro, H. Osaki, M. Wiese, S. Putwain, C.Y. Fong, C. Grove, J. Craig, A. Dittmann, D. Lugo, P. Jeffrey, G. Drewes, K. Lee, L. Bullinger, R.K. Prinjha, T. Kouzarides, G.S. Vassiliou, B.J. Huntly, Recurrent mutations, including NPM1c, activate a BRD4-dependent core transcriptional program in acute myeloid leukemia, *Leukemia*, 28 (2014) 311-320.
- [114] A. Puissant, S.M. Frumm, G. Alexe, C.F. Bassil, J. Qi, Y.H. Chanthery, E.A. Nekritz, R. Zeid, W.C. Gustafson, P. Greninger, Targeting MYCN in neuroblastoma by BET bromodomain inhibition, *Cancer Discovery*, 3 (2013) 308-323.
- [115] W.W. Lockwood, K. Zejnullahu, J.E. Bradner, H. Varmus, Sensitivity of human lung adenocarcinoma cell lines to targeted inhibition of BET epigenetic signaling proteins, *Proc Natl Acad Sci U S A*, 109 (2012) 19408-19413.

- [116] C.J. O'Rourke, P. Munoz-Garrido, E.L. Aguayo, J.B. Andersen, Epigenome dysregulation in cholangiocarcinoma, *Biochimica et Biophysica Acta (BBA) - Molecular Basis of Disease*, 1864 (2018) 1423-1434.
- [117] N. Meyer, L.Z. Penn, Reflecting on 25 years with MYC, *Nature Reviews Cancer*, 8 (2008) 976-990.
- [118] C.V. Dang, c-Myc target genes involved in cell growth, apoptosis, and metabolism, *Molecular and Cellular Biology*, 19 (1999) 1-11.
- [119] C.V. Dang, MYC on the path to cancer, *Cell*, 149 (2012) 22-35.
- [120] E. Laurenti, A. Wilson, A. Trumpp, Myc's other life: stem cells and beyond, *Current Opinion in Cell Biology*, 21 (2009) 844-854.
- [121] K.I. Zeller, X. Zhao, C.W. Lee, K.P. Chiu, F. Yao, J.T. Yustein, H.S. Ooi, Y.L. Orlov, A. Shahab, H.C. Yong, Global mapping of c-Myc binding sites and target gene networks in human B cells, *Proceedings of the National Academy of Sciences*, 103 (2006) 17834-17839.
- [122] E. Cerami, J. Gao, U. Dogrusoz, B.E. Gross, S.O. Sumer, B.A. Aksoy, A. Jacobsen, C.J. Byrne, M.L. Heuer, E. Larsson, The cBio cancer genomics portal: an open platform for exploring multidimensional cancer genomics data, *AACR*, 2012.
- [123] Z.R. Li, Y.F. Wu, C.Y. Ma, S.D. Nie, X.H. Mao, Y.Z. Shi, Down-regulation of c-Myc expression inhibits the invasion of bile duct carcinoma cells, *Cell Biology International*, 35 (2011) 799-802.
- [124] M. Kalkat, J. De Melo, K.A. Hickman, C. Lourenco, C. Redel, D. Resetca, A. Tamachi, W.B. Tu, L.Z. Penn, MYC Deregulation in Primary Human Cancers, *Genes (Basel)*, 8 (2017) 151.

- [125] C.A. French, Small-Molecule Targeting of BET Proteins in Cancer, *Advances in cancer research*, 131 (2016) 21-58.
- [126] M.M. Tomayko, C.P. Reynolds, Determination of subcutaneous tumor size in athymic (nude) mice, *Cancer Chemotherapy and Pharmacology*, 24 (1989) 148-154.
- [127] M. Podhorecka, A. Skladanowski, P. Bozko, H2AX phosphorylation: its role in DNA damage response and cancer therapy, *Journal of Nucleic Acids*, 2010 (2010).
- [128] H. Fujiwara, K. Tateishi, H. Kato, T. Nakatsuka, K. Yamamoto, Y. Tanaka, H. Ijichi, N. Takahara, S. Mizuno, H. Kogure, S. Matsubara, Y. Nakai, K. Koike, Isocitrate dehydrogenase 1 mutation sensitizes intrahepatic cholangiocarcinoma to the BET inhibitor JQ1, *Cancer Sci*, 109 (2018) 3602-3610.
- [129] A.G. Patel, J.N. Sarkaria, S.H. Kaufmann, Nonhomologous end joining drives poly(ADP-ribose) polymerase (PARP) inhibitor lethality in homologous recombination-deficient cells, *Proc Natl Acad Sci U S A*, 108 (2011) 3406-3411.
- [130] A. Min, S.A. Im, Y.K. Yoon, S.H. Song, H.J. Nam, H.S. Hur, H.P. Kim, K.H. Lee, S.W. Han, D.Y. Oh, T.Y. Kim, M.J. O'Connor, W.H. Kim, Y.J. Bang, RAD51C-deficient cancer cells are highly sensitive to the PARP inhibitor olaparib, *Mol Cancer Ther*, 12 (2013) 865-877.
- [131] B. Basu, T.A. Yap, L.R. Molife, J.S. de Bono, Targeting the DNA damage response in oncology: past, present and future perspectives, *Current opinion in oncology*, 24 (2012) 316-324.
- [132] H. Farmer, N. McCabe, C.J. Lord, A.N. Tutt, D.A. Johnson, T.B. Richardson, M. Santarosa, K.J. Dillon, I. Hickson, C. Knights, N.M. Martin, S.P. Jackson, G.C. Smith, A.

Ashworth, Targeting the DNA repair defect in BRCA mutant cells as a therapeutic strategy, *Nature*, 434 (2005) 917-921.

[133] N. McCabe, N.C. Turner, C.J. Lord, K. Kluzek, A. Bialkowska, S. Swift, S. Giavara, M.J. O'Connor, A.N. Tutt, M.Z. Zdzienicka, G.C. Smith, A. Ashworth, Deficiency in the repair of DNA damage by homologous recombination and sensitivity to poly(ADP-ribose) polymerase inhibition, *Cancer Res*, 66 (2006) 8109-8115.

[134] A.G. Patel, K.S. Flatten, P.A. Schneider, N.T. Dai, J.S. McDonald, G.G. Poirier, S.H. Kaufmann, Enhanced killing of cancer cells by poly(ADP-ribose) polymerase inhibitors and topoisomerase I inhibitors reflects poisoning of both enzymes, *The Journal of biological chemistry*, 287 (2012) 4198-4210.

[135] Y. Yin, Q. Shen, P. Zhang, R. Tao, W. Chang, R. Li, G. Xie, W. Liu, L. Zhang, P. Kapoor, Chk1 inhibition potentiates the therapeutic efficacy of PARP inhibitor BMN673 in gastric cancer, *American Journal of Cancer Research*, 7 (2017) 473.

[136] Y. Zhang, T. Hunter, Roles of Chk1 in cell biology and cancer therapy, *Int J Cancer*, 134 (2014) 1013-1023.

[137] M. Rouleau, A. Patel, M.J. Hendzel, S.H. Kaufmann, G.G. Poirier, PARP inhibition: PARP1 and beyond, *Nature Reviews Cancer*, 10 (2010) 293-301.

[138] K.J. Dedes, P.M. Wilkerson, D. Wetterskog, B. Weigelt, A. Ashworth, J.S. Reis-Filho, Synthetic lethality of PARP inhibition in cancers lacking BRCA1 and BRCA2 mutations, *Cell Cycle*, 10 (2011) 1192-1199.

[139] M.J. O'Connor, Targeting the DNA damage response in cancer, *Molecular Cell*, 60 (2015) 547-560.

- [140] C. Underhill, M. Toulmonde, H. Bonnefoi, A review of PARP inhibitors: from bench to bedside, *Annals of Oncology*, 22 (2011) 268-279.
- [141] C.K. Donawho, Y. Luo, Y. Luo, T.D. Penning, J.L. Bauch, J.J. Bouska, V.D. Bontcheva-Diaz, B.F. Cox, T.L. DeWeese, L.E. Dillehay, ABT-888, an orally active poly (ADP-ribose) polymerase inhibitor that potentiates DNA-damaging agents in preclinical tumor models, *Clinical Cancer Research*, 13 (2007) 2728-2737.
- [142] S.C. Fehling, A.L. Miller, P.L. Garcia, R.B. Vance, K.J. Yoon, The combination of BET and PARP inhibitors is synergistic in models of cholangiocarcinoma, *Cancer Letters*, (2019).
- [143] K.M. Kreitzburg, S.C. Fehling, C.N. Landen, T.L. Gamblin, R.B. Vance, R.C. Arend, A.A. Katre, P.G. Oliver, R. van Waardenburg, R.D. Alvarez, K.J. Yoon, FTY720 enhances the anti-tumor activity of carboplatin and tamoxifen in a patient-derived xenograft model of ovarian cancer, *Cancer Lett*, 436 (2018) 75-86.
- [144] T.-C. Chou, Drug combination studies and their synergy quantification using the Chou-Talalay method, *Cancer Research*, 70 (2010) 440-446.
- [145] N.A. Franken, H.M. Rodermond, J. Stap, J. Haveman, C. Van Bree, Clonogenic assay of cells *in vitro*, *Nature Protocols*, 1 (2006) 2315-2319.
- [146] C. Riccardi, I. Nicoletti, Analysis of apoptosis by propidium iodide staining and flow cytometry, *Nature Protocols*, 1 (2006) 1458-1461.
- [147] N. Tepsiri, L. Chaturat, B. Sripa, W. Namwat, S. Wongkham, V. Bhudhisawasdi, W. Tassaneeyakul, Drug sensitivity and drug resistance profiles of human intrahepatic cholangiocarcinoma cell lines, *World journal of gastroenterology*, 11 (2005) 2748-2753.

- [148] J.G. Tate, S. Bamford, H.C. Jubb, Z. Sondka, D.M. Beare, N. Bindal, H. Boutselakis, C.G. Cole, C. Creatore, E. Dawson, P. Fish, B. Harsha, C. Hathaway, S.C. Jupe, C.Y. Kok, K. Noble, L. Ponting, C.C. Ramshaw, C.E. Rye, H.E. Speedy, R. Stefancsik, S.L. Thompson, S. Wang, S. Ward, P.J. Campbell, S.A. Forbes, COSMIC: the Catalogue Of Somatic Mutations In Cancer, *Nucleic Acids Res*, 47 (2019) D941-d947.
- [149] A. Hoglund, L.M. Nilsson, S.V. Muralidharan, L.A. Hasvold, P. Merta, M. Rudelius, V. Nikolova, U. Keller, J.A. Nilsson, Therapeutic implications for the induced levels of Chk1 in Myc-expressing cancer cells, *Clinical cancer research : an official journal of the American Association for Cancer Research*, 17 (2011) 7067-7079.
- [150] W.J. Wang, S.P. Wu, J.B. Liu, Y.S. Shi, X. Huang, Q.B. Zhang, K.T. Yao, MYC regulation of CHK1 and CHK2 promotes radioresistance in a stem cell-like population of nasopharyngeal carcinoma cells, *Cancer Res*, 73 (2013) 1219-1231.
- [151] P. Jelinic, D.A. Levine, New insights into PARP inhibitors' effect on cell cycle and homology-directed DNA damage repair, *Mol Cancer Ther*, 13 (2014) 1645-1654.
- [152] S. Shu, C.Y. Lin, H.H. He, R.M. Witwicki, D.P. Tabassum, J.M. Roberts, M. Janiszewska, S.J. Huh, Y. Liang, J. Ryan, E. Doherty, H. Mohammed, H. Guo, D.G. Stover, M.B. Ekram, J. Brown, C. D'Santos, I.E. Krop, D. Dillon, M. McKeown, C. Ott, J. Qi, M. Ni, P.K. Rao, M. Duarte, S.Y. Wu, C.M. Chiang, L. Anders, R.A. Young, E. Winer, A. Letai, W.T. Barry, J.S. Carroll, H. Long, M. Brown, X.S. Liu, C.A. Meyer, J.E. Bradner, K. Polyak, Response and resistance to BET bromodomain inhibitors in triple-negative breast cancer, *Nature*, 529 (2016) 413-417.
- [153] S. Pinz, S. Unser, A. Rasclé, Signal transducer and activator of transcription STAT5 is recruited to c-Myc super-enhancer, *BMC molecular biology*, 17 (2016) 10.

- [154] C. Mostocotto, M. Carbone, C. Battistelli, A. Ciotti, P. Amati, R. Maione, Poly(ADP-ribose)ylation is required to modulate chromatin changes at c-MYC promoter during emergence from quiescence, *PLoS One*, 9 (2014) e102575.
- [155] C.M. Simbulan-Rosenthal, D.S. Rosenthal, R. Luo, R. Samara, L.A. Espinoza, P.O. Hassa, M.O. Hottiger, M.E. Smulson, PARP-1 binds E2F-1 independently of its DNA binding and catalytic domains, and acts as a novel coactivator of E2F-1-mediated transcription during re-entry of quiescent cells into S phase, *Oncogene*, 22 (2003) 8460-8471.
- [156] S. Karakashev, H. Zhu, Y. Yokoyama, B. Zhao, N. Fatkhutdinov, A.V. Kossenkov, A.J. Wilson, F. Simpkins, D. Speicher, D. Khabele, B.G. Bitler, R. Zhang, BET Bromodomain Inhibition Synergizes with PARP Inhibitor in Epithelial Ovarian Cancer, *Cell Reports*, 21 (2017) 3398-3405.
- [157] L.A. Parsels, M.A. Morgan, D.M. Tanska, J.D. Parsels, B.D. Palmer, R.J. Booth, W.A. Denny, C.E. Canman, A.J. Kraker, T.S. Lawrence, Gemcitabine sensitization by checkpoint kinase 1 inhibition correlates with inhibition of a Rad51 DNA damage response in pancreatic cancer cells, *Molecular Cancer Therapeutics*, 8 (2009) 45-54.
- [158] M.A. Morgan, L.A. Parsels, J.D. Parsels, T.S. Lawrence, J. Maybaum, The relationship of premature mitosis to cytotoxicity in response to checkpoint abrogation and antimetabolite treatment, *Cell Cycle*, 5 (2006) 1983-1988.
- [159] I. Lohse, A. Borgida, P. Cao, M. Cheung, M. Pintilie, T. Bianco, S. Holter, E. Ibrahimov, R. Kumareswaran, R. Bristow, BRCA1 and BRCA2 mutations sensitize to chemotherapy in patient-derived pancreatic cancer xenografts, *British Journal of Cancer*, 113 (2015) 425-432.

- [160] M.A. Morgan, L.A. Parsels, J. Maybaum, T.S. Lawrence, Improving gemcitabine-mediated radiosensitization using molecularly targeted therapy: A review, *Clinical Cancer Research*, 14 (2008) 6744-6750.
- [161] A.S. Farrell, M.M. Joly, B.L. Allen-Petersen, P.J. Worth, C. Lanciault, D. Sauer, J. Link, C. Pelz, L.M. Heiser, J.P. Morton, N. Muthalagu, M.T. Hoffman, S.L. Manning, E.D. Pratt, N.D. Kendsersky, N. Egbukichi, T.S. Amery, M.C. Thoma, Z.P. Jenny, A.D. Rhim, D.J. Murphy, O.J. Sansom, H.C. Crawford, B.C. Sheppard, R.C. Sears, MYC regulates ductal-neuroendocrine lineage plasticity in pancreatic ductal adenocarcinoma associated with poor outcome and chemoresistance, *Nature communications*, 8 (2017) 1728.
- [162] J.O. Park, D.-Y. Oh, C. Hsu, J.-S. Chen, L.-T. Chen, M. Orlando, J.S. Kim, H.Y. Lim, Gemcitabine Plus Cisplatin for Advanced Biliary Tract Cancer: A Systematic Review, *Cancer Res Treat*, 47 (2015) 343-361.
- [163] C.J. van Moorsel, H.M. Pinedo, G. Veerman, J.B. Vermorken, P.E. Postmus, G.J. Peters, Scheduling of gemcitabine and cisplatin in Lewis lung tumour bearing mice, *European journal of cancer (Oxford, England : 1990)*, 35 (1999) 808-814.
- [164] A. Höglund, L.M. Nilsson, S.V. Muralidharan, L.A. Hasvold, P. Merta, M. Rudelius, V. Nikolova, U. Keller, J.A. Nilsson, Therapeutic implications for the induced levels of Chk1 in Myc-expressing cancer cells, *Clinical Cancer Research*, 17 (2011) 7067-7079.
- [165] J. Sato, T. Kimura, T. Saito, T. Anazawa, A. Kenjo, Y. Sato, T. Tsuchiya, M. Gotoh, Gene expression analysis for predicting gemcitabine resistance in human cholangiocarcinoma, *J Hepatobiliary Pancreat Sci*, 18 (2011) 700-711.



- [166] Y. Binenbaum, S. Na'ara, Z. Gil, Gemcitabine resistance in pancreatic ductal adenocarcinoma, *Drug resistance updates : reviews and commentaries in antimicrobial and anticancer chemotherapy*, 23 (2015) 55-68.
- [167] J. Zhou, Z. Chen, A. Malysa, X. Li, P. Oliveira, Y. Zhang, G. Bepler, A kinome screen identifies checkpoint kinase 1 (CHK1) as a sensitizer for RRM1-dependent gemcitabine efficacy, *PloS one*, 8 (2013) e58091-e58091.
- [168] M. Liang, T. Zhao, L. Ma, Y. Guo, CHK1 inhibition sensitizes pancreatic cancer cells to gemcitabine via promoting CDK-dependent DNA damage and ribonucleotide reductase downregulation, *Oncol Rep*, 39 (2018) 1322-1330.
- [169] J.J.G. Marin, E. Lozano, E. Herraiz, M. Asensio, S. Di Giacomo, M.R. Romero, O. Briz, M.A. Serrano, T. Efferth, R.I.R. Macias, Chemoresistance and chemosensitization in cholangiocarcinoma, *Biochimica et biophysica acta. Molecular basis of disease*, 1864 (2018) 1444-1453.
- [170] J. Ciccolini, C. Serdjebi, G.J. Peters, E. Giovannetti, Pharmacokinetics and pharmacogenetics of Gemcitabine as a mainstay in adult and pediatric oncology: an EORTC-PAMM perspective, *Cancer Chemother Pharmacol*, 78 (2016) 1-12.
- [171] C. Xie, Y. Pan, F. Hao, Y. Gao, Z. Liu, X. Zhang, L. Xie, G. Jiang, Q. Li, E. Wang, C-Myc participates in beta-catenin-mediated drug resistance in A549/DDP lung adenocarcinoma cells, *APMIS : acta pathologica, microbiologica, et immunologica Scandinavica*, 122 (2014) 1251-1258.
- [172] C.C. Cheng, L.H. Shi, X.J. Wang, S.X. Wang, X.Q. Wan, S.R. Liu, Y.F. Wang, Z. Lu, L.H. Wang, Y. Ding, Stat3/Oct-4/c-Myc signal circuit for regulating stemness-

mediated doxorubicin resistance of triple-negative breast cancer cells and inhibitory effects of WP1066, *Int J Oncol*, 53 (2018) 339-348.

[173] P.K. Mazur, A. Herner, S.S. Mello, M. Wirth, S. Hausmann, F.J. Sánchez-Rivera, S.M. Lofgren, T. Kuschma, S.A. Hahn, D. Vangala, Combined inhibition of BET family proteins and histone deacetylases as a potential epigenetics-based therapy for pancreatic ductal adenocarcinoma, *Nature Medicine*, (2015).

[174] I.A. Asangani, V.L. Dommeti, X. Wang, R. Malik, M. Cieslik, R. Yang, J. Escara-Wilke, K. Wilder-Romans, S. Dhanireddy, C. Engelke, M.K. Iyer, X. Jing, Y.M. Wu, X. Cao, Z.S. Qin, S. Wang, F.Y. Feng, A.M. Chinnaiyan, Therapeutic targeting of BET bromodomain proteins in castration-resistant prostate cancer, *Nature*, 510 (2014) 278-282.

[175] L.L. da Motta, I. Ledaki, K. Purshouse, S. Haider, M.A. De Bastiani, D. Baban, M. Morotti, G. Steers, S. Wigfield, E. Bridges, The BET inhibitor JQ1 selectively impairs tumour response to hypoxia and downregulates CA9 and angiogenesis in triple negative breast cancer, *Oncogene*, (2016).

[176] D.H. Lee, J. Qi, J.E. Bradner, J.W. Said, N.B. Doan, C. Forscher, H. Yang, H.P. Koeffler, Synergistic effect of JQ1 and rapamycin for treatment of human osteosarcoma, *International Journal of Cancer*, 136 (2015) 2055-2064.

[177] B. Tolani, R. Gopalakrishnan, V. Punj, H. Matta, P.M. Chaudhary, Targeting Myc in KSHV-associated primary effusion lymphoma with BET bromodomain inhibitors, *Oncogene*, 33 (2014) 2928-2937.

[178] M.M. Matzuk, M.R. McKeown, P. Filippakopoulos, Q. Li, L. Ma, J.E. Agno, M.E. Lemieux, S. Picaud, N.Y. Richard, J. Qi, Small-molecule inhibition of BRDT for male contraception, *Cell*, 150 (2012) 673-684.

- [179] J. Khoontawad, C. Pairojkul, R. Rucksaken, P. Pinlaor, C. Wongkham, P. Yongvanit, A. Pugkhem, A. Jones, J. Plieskatt, J. Potriquet, J. Bethony, S. Pinlaor, J. Mulvenna, Differential Protein Expression Marks the Transition From Infection With *Opisthorchis viverrini* to Cholangiocarcinoma, *Mol Cell Proteomics*, 16 (2017) 911-923.
- [180] H.J. Stewart, G.A. Horne, S. Bastow, T.J. Chevassut, BRD4 associates with p53 in DNMT3A-mutated leukemia cells and is implicated in apoptosis by the bromodomain inhibitor JQ1, *Cancer Med*, 2 (2013) 826-835.
- [181] A. Hematulin, S. Meethang, K. Utapom, S. Wongkham, D. Sagan, Etoposide radiosensitizes p53-defective cholangiocarcinoma cell lines independent of their G2 checkpoint efficacies, *Oncology Letters*, 15 (2018) 3895-3903.
- [182] A. Hematulin, D. Sagan, K. Sawanyawisuth, W. Seubwai, S. Wongkham, Association between cellular radiosensitivity and G1/G2 checkpoint proficiencies in human cholangiocarcinoma cell lines, *Int J Oncol*, 45 (2014) 1159-1166.
- [183] C. Hahnvajanawong, S. Ketnimit, K. Pattanapanyasat, N. Anantachoke, B. Sripa, K. Pinmai, W. Seubwai, V. Reutrakul, Involvement of p53 and nuclear factor-kappaB signaling pathway for the induction of G1-phase cell cycle arrest of cholangiocarcinoma cell lines by isomorellin, *Biological & pharmaceutical bulletin*, 35 (2012) 1914-1925.
- [184] S. Saenglee, G. Senawong, S. Jogloy, B. Sripa, T. Senawong, Peanut testa extracts possessing histone deacetylase inhibitory activity induce apoptosis in cholangiocarcinoma cells, *Biomedicine & pharmacotherapy = Biomedecine & pharmacotherapie*, 98 (2018) 233-241.
- [185] W. Boonyanugomol, C. Chomvarin, S.C. Baik, J.Y. Song, C. Hahnvajanawong, K.M. Kim, M.J. Cho, W.K. Lee, H.L. Kang, K.H. Rhee, B. Sripa, Role of cagA-positive

*Helicobacter pylori* on cell proliferation, apoptosis, and inflammation in biliary cells, *Dig Dis Sci*, 56 (2011) 1682-1692.

[186] T. Shimamura, Z. Chen, M. Soucheray, J. Carretero, E. Kikuchi, J.H. Tchaicha, Y. Gao, K.A. Cheng, T.J. Cohoon, J. Qi, Efficacy of BET bromodomain inhibition in Kras-mutant non-small cell lung cancer, *Clinical Cancer Research*, 19 (2013) 6183-6192.

[187] J. Zhang, A.M. Dulak, M.M. Hattersley, B.S. Willis, J. Nikkila, A. Wang, A. Lau, C. Reimer, M. Zinda, S.E. Fawell, G.B. Mills, H. Chen, BRD4 facilitates replication stress-induced DNA damage response, *Oncogene*, (2018).

[188] H. Qiu, J. Li, L.H. Clark, A.L. Jackson, L. Zhang, H. Guo, J.E. Kilgore, P.A. Gehrig, C. Zhou, V.L. Bae-Jump, JQ1 suppresses tumor growth via PTEN/PI3K/AKT pathway in endometrial cancer, *Oncotarget*, 7 (2016) 66809-66821.

[189] W. Chen, H. Zhang, Z. Chen, H. Jiang, L. Liao, S. Fan, J. Xing, Y. Xie, S. Chen, H. Ding, K. Chen, H. Jiang, C. Luo, M. Zheng, Z. Yao, Y. Huang, Y. Zhang, Development and evaluation of a novel series of Nitroxoline-derived BET inhibitors with antitumor activity in renal cell carcinoma, *Oncogenesis*, 7 (2018) 83.

[190] X. Wu, D. Liu, D. Tao, W. Xiang, X. Xiao, M. Wang, L. Wang, G. Luo, Y. Li, F. Zeng, G. Jiang, BRD4 Regulates EZH2 Transcription through Upregulation of C-MYC and Represents a Novel Therapeutic Target in Bladder Cancer, *Mol Cancer Ther*, 15 (2016) 1029-1042.

[191] L.N. Kent, G. Leone, The broken cycle: E2F dysfunction in cancer, *Nature Review Cancer*, 19 (2019) 326-338.

[192] S. Ishida, K. Shudo, S. Takada, K. Koike, A direct role of transcription factor E2F in c-myc gene expression during granulocytic and macrophage-like differentiation of HL60

cells, *Cell growth & differentiation : the molecular biology journal of the American Association for Cancer Research*, 6 (1995) 229-237.

[193] G.R. Brown, V. Hem, K.S. Katz, M. Ovetsky, C. Wallin, O. Ermolaeva, I. Tolstoy, T. Tatusova, K.D. Pruitt, D.R. Maglott, T.D. Murphy, Gene: a gene-centered information resource at NCBI, *Nucleic Acids Res*, 43 (2015) D36-42.

[194] S. Venkataraman, I. Alimova, I. Balakrishnan, P. Harris, D.K. Birks, A. Griesinger, V. Amani, B. Cristiano, M. Remke, M.D. Taylor, M. Handler, N.K. Foreman, R. Vibhakar, Inhibition of BRD4 attenuates tumor cell self-renewal and suppresses stem cell signaling in MYC driven medulloblastoma, *Oncotarget*, 5 (2014) 2355-2371.

[195] G.V. Denis, C. Vaziri, N. Guo, D.V. Faller, RING3 kinase transactivates promoters of cell cycle regulatory genes through E2F, *Cell growth & differentiation : the molecular biology journal of the American Association for Cancer Research*, 11 (2000) 417-424.

[196] J. Peng, W. Dong, L. Chen, T. Zou, Y. Qi, Y. Liu, Brd2 is a TBP-associated protein and recruits TBP into E2F-1 transcriptional complex in response to serum stimulation, *Mol Cell Biochem*, 294 (2007) 45-54.

[197] S. Rahman, M.E. Sowa, M. Ottinger, J.A. Smith, Y. Shi, J.W. Harper, P.M. Howley, The Brd4 extraterminal domain confers transcription activation independent of pTEFb by recruiting multiple proteins, including NSD3, *Molecular and Cellular Biology*, 31 (2011) 2641-2652.

[198] A. Sinha, D.V. Faller, G.V. Denis, Bromodomain analysis of Brd2-dependent transcriptional activation of cyclin A, *The Biochemical journal*, 387 (2005) 257-269.

[199] J.P. Lambert, S. Picaud, T. Fujisawa, H. Hou, P. Savitsky, L. Uuskula-Reimand, G.D. Gupta, H. Abdouni, Z.Y. Lin, M. Tucholska, J.D.R. Knight, B. Gonzalez-Badillo, N.

- St-Denis, J.A. Newman, M. Stucki, L. Pelletier, N. Bandeira, M.D. Wilson, P. Filippakopoulos, A.C. Gingras, Interactome Rewiring Following Pharmacological Targeting of BET Bromodomains, *Mol Cell*, (2018).
- [200] J.-E. Lee, Y.-K. Park, S. Park, Y. Jang, N. Waring, A. Dey, K. Ozato, B. Lai, W. Peng, K. Ge, Brd4 binds to active enhancers to control cell identity gene induction in adipogenesis and myogenesis, *Nature communications*, 8 (2017) 2217.
- [201] J. Zuber, J. Shi, E. Wang, A.R. Rappaport, H. Herrmann, E.A. Sison, D. Magoon, J. Qi, K. Blatt, M. Wunderlich, M.J. Taylor, C. Johns, A. Chicas, J.C. Mulloy, S.C. Kogan, P. Brown, P. Valent, J.E. Bradner, S.W. Lowe, C.R. Vakoc, RNAi screen identifies Brd4 as a therapeutic target in acute myeloid leukaemia, *Nature*, 478 (2011) 524-528.
- [202] J.E. Bolden, N. Tasdemir, L.E. Dow, J.H. van Es, J.E. Wilkinson, Z. Zhao, H. Clevers, S.W. Lowe, Inducible *in vivo* silencing of Brd4 identifies potential toxicities of sustained BET protein inhibition, *Cell reports*, 8 (2014) 1919-1929.
- [203] A. Alqahtani, K. Choucair, M. Ashraf, D.M. Hammouda, A. Alloghbi, T. Khan, N. Senzer, J. Nemunaitis, Bromodomain and extra-terminal motif inhibitors: a review of preclinical and clinical advances in cancer therapy, *Future Sci OA*, 5 (2019) FSO372-FSO372.
- [204] S.A. Piha-Paul, J.C. Sachdev, M. Barve, P. LoRusso, R. Szmulewitz, S.P. Patel, P.N. Lara, Jr., X. Chen, B. Hu, K.J. Freise, D. Modi, A. Sood, J.E. Hutti, J. Wolff, B.H. O'Neil, First-in-Human Study of Mivebresib (ABBV-075), an Oral Pan-Inhibitor of Bromodomain and Extra Terminal Proteins, in Patients with Relapsed/Refractory Solid Tumors, *Clinical cancer research : an official journal of the American Association for Cancer Research*, (2019).

- [205] C.Y. Fong, O. Gilan, E.Y. Lam, A.F. Rubin, S. Ftouni, D. Tyler, K. Stanley, D. Sinha, P. Yeh, J. Morison, BET inhibitor resistance emerges from leukaemia stem cells, *Nature*, 525 (2015) 538-542.
- [206] A. Pawar, P.N. Gollavilli, S. Wang, I.A. Asangani, Resistance to BET Inhibitor Leads to Alternative Therapeutic Vulnerabilities in Castration-Resistant Prostate Cancer, *Cell Rep*, 22 (2018) 2236-2245.
- [207] B.-J. Hwang, G. Adhikary, R.L. Eckert, A.L. Lu, Chk1 inhibition as a novel therapeutic strategy in melanoma, *Oncotarget*, 9 (2018) 30450-30464.
- [208] R.G. Syljuasen, C.S. Sorensen, L.T. Hansen, K. Fugger, C. Lundin, F. Johansson, T. Helleday, M. Sehested, J. Lukas, J. Bartek, Inhibition of human Chk1 causes increased initiation of DNA replication, phosphorylation of ATR targets, and DNA breakage, *Mol Cell Biol*, 25 (2005) 3553-3562.
- [209] J. Wayne, T. Brooks, A.J. Massey, Inhibition of Chk1 with the small molecule inhibitor V158411 induces DNA damage and cell death in an unperturbed S-phase, *Oncotarget*, 7 (2016) 85033-85048.
- [210] L.J. Kuo, L.-X. Yang,  $\gamma$ -H2AX-a novel biomarker for DNA double-strand breaks, *In Vivo*, 22 (2008) 305-309.
- [211] V. Turinetto, C. Giachino, Multiple facets of histone variant H2AX: a DNA double-strand-break marker with several biological functions, *Nucleic Acids Research*, (2015) gkv061.
- [212] P.L. Olive, J.P. Banáth, The comet assay: a method to measure DNA damage in individual cells, *Nature Protocols*, 1 (2006) 23.

- [213] J. Bewersdorf, B.T. Bennett, K.L. Knight, H2AX chromatin structures and their response to DNA damage revealed by 4Pi microscopy, *Proc Natl Acad Sci U S A*, 103 (2006) 18137-18142.
- [214] L.-J. Mah, R.S. Vasireddy, M.M. Tang, G.T. Georgiadis, A. El-Osta, T.C. Karagiannis, Quantification of gammaH2AX foci in response to ionising radiation, *J Vis Exp*, (2010) 1957.
- [215] W.Z. Tu, B. Li, B. Huang, Y. Wang, X.D. Liu, H. Guan, S.M. Zhang, Y. Tang, W.Q. Rang, P.K. Zhou, gammaH2AX foci formation in the absence of DNA damage: mitotic H2AX phosphorylation is mediated by the DNA-PKcs/CHK2 pathway, *FEBS Letters*, 587 (2013) 3437-3443.
- [216] T. Kurashige, M. Shimamura, Y. Nagayama, Differences in quantification of DNA double-strand breaks assessed by 53BP1/ $\gamma$ H2AX focus formation assays and the comet assay in mammalian cells treated with irradiation and N-acetyl-L-cysteine, *Journal of radiation research*, 57 (2016) 312-317.
- [217] M. Shrivastav, C.A. Miller, L.P. De Haro, S.T. Durant, B.P.C. Chen, D.J. Chen, J.A. Nickoloff, DNA-PKcs and ATM co-regulate DNA double-strand break repair, *DNA repair*, 8 (2009) 920-929.
- [218] X. Li, G. Baek, S.G. Ramanand, A. Sharp, Y. Gao, W. Yuan, J. Welti, D.N. Rodrigues, D. Dolling, I. Figueiredo, S. Sumanasuriya, M. Crespo, A. Aslam, R. Li, Y. Yin, B. Mukherjee, M. Kanchwala, A.M. Hughes, W.S. Halsey, C.M. Chiang, C. Xing, G.V. Raj, S. Burma, J. de Bono, R.S. Mani, BRD4 Promotes DNA Repair and Mediates the Formation of Tmprss2-ERG Gene Rearrangements in Prostate Cancer, *Cell Rep*, 22 (2018) 796-808.



- [219] Y. Mao, X. Huang, Z. Shuang, G. Lin, J. Wang, F. Duan, J. Chen, S. Li, PARP inhibitor olaparib sensitizes cholangiocarcinoma cells to radiation, *Cancer Med*, 7 (2018) 1285-1296.
- [220] Y. Cheng, J. Zhang, S.K. Qin, H.Q. Hua, Treatment with olaparib monotherapy for BRCA2-mutated refractory intrahepatic cholangiocarcinoma: a case report, *Onco Targets Ther*, 11 (2018) 5957-5962.
- [221] A.J. Wilson, M. Stubbs, P. Liu, B. Ruggeri, D. Khabele, The BET inhibitor INCB054329 reduces homologous recombination efficiency and augments PARP inhibitor activity in ovarian cancer, *Gynecologic oncology*, (2018).
- [222] L. Yang, Y. Zhang, W. Shan, Z. Hu, J. Yuan, J. Pi, Y. Wang, L. Fan, Z. Tang, C. Li, X. Hu, J.L. Tanyi, Y. Fan, Q. Huang, K. Montone, C.V. Dang, L. Zhang, Repression of BET activity sensitizes homologous recombination-proficient cancers to PARP inhibition, *Science translational medicine*, 9 (2017).
- [223] C. Mio, L. Gerratana, M. Bolis, F. Caponnetto, A. Zanello, M. Barbina, C. Di Loreto, E. Garattini, G. Damante, F. Puglisi, BET proteins regulate homologous recombination-mediated DNA repair: BRCAness and implications for cancer therapy, *Int J Cancer*, 144 (2019) 755-766.
- [224] T. Golan, M. Raitses-Gurevich, R.K. Kelley, A.G. Bocobo, A. Borgida, R.T. Shroff, S. Holter, S. Gallinger, D.H. Ahn, D. Aderka, Overall Survival and Clinical Characteristics of BRCA-Associated Cholangiocarcinoma: A Multicenter Retrospective Study, *The Oncologist*, (2017) theoncologist. 2016-0415.
- [225] C.G. Langdon, J.T. Platt, R.E. Means, P. Iyidogan, R. Mamillapalli, M. Klein, M.A. Held, J.W. Lee, J.S. Koo, C. Hatzis, H.S. Hochster, D.F. Stern, Combinatorial Screening

of Pancreatic Adenocarcinoma Reveals Sensitivity to Drug Combinations Including Bromodomain Inhibitor Plus Neddylation Inhibitor, *Mol Cancer Ther*, 16 (2017) 1041-1053.

[226] F. Xie, M. Huang, X. Lin, C. Liu, Z. Liu, F. Meng, C. Wang, Q. Huang, The BET inhibitor I-BET762 inhibits pancreatic ductal adenocarcinoma cell proliferation and enhances the therapeutic effect of gemcitabine, *Sci Rep*, 8 (2018) 8102.

[227] G. Pongas, M.K. Kim, D.J. Min, C.D. House, E. Jordan, N. Caplen, S. Chakka, J. Ohiri, M.J. Kruhlak, C.M. Annunziata, BRD4 facilitates DNA damage response and represses CBX5/Heterochromatin protein 1 (HP1), *Oncotarget*, 8 (2017) 51402-51415.

[228] Y.A. Nevzorova, W. Hu, F.J. Cubero, U. Haas, J. Freimuth, F. Tacke, C. Trautwein, C. Liedtke, Overexpression of c-myc in hepatocytes promotes activation of hepatic stellate cells and facilitates the onset of liver fibrosis, *Biochimica et biophysica acta*, 1832 (2013) 1765-1775.

[229] Z. Niu, H. Liu, M. Zhou, H. Wang, Y. Liu, X. Li, W. Xiong, J. Ma, X. Li, G. Li, Knockdown of c-Myc inhibits cell proliferation by negatively regulating the Cdk/Rb/E2F pathway in nasopharyngeal carcinoma cells, *Acta biochimica et biophysica Sinica*, 47 (2015) 183-191.

[230] K.R. Luoto, A.X. Meng, A.R. Wasylshen, H. Zhao, C.L. Coackley, L.Z. Penn, R.G. Bristow, Tumor cell kill by c-MYC depletion: role of MYC-regulated genes that control DNA double-strand break repair, *Cancer Research*, 70 (2010) 8748-8759.

**MEMORANDUM**

**DATE:** 26-Sep-2019

**TO:** Yoon, Karina

**FROM:** 

Robert A. Kesterson, Ph.D., Chair

Institutional Animal Care and Use Committee (IACUC)

**SUBJECT: NOTICE OF APPROVAL**

The following application was approved by the University of Alabama at Birmingham Institutional Animal Care and Use Committee (IACUC) on 26-Sep-2019.

**Protocol PI:** Yoon, Karina  
**Title:** Developing therapy for the treatment of solid tumors  
**Sponsor:** National Cancer Institute/NIH/DHHS  
**Animal Project Number (APN):** IACUC-09186

This institution has an Animal Welfare Assurance on file with the Office of Laboratory Animal Welfare (OLAW), is registered as a Research Facility with the USDA, and is accredited by the Association for Assessment and Accreditation of Laboratory Animal Care International (AAALAC).

This protocol is due for full review by 25-Sep-2022.

**Institutional Animal Care and Use Committee (IACUC)**

403 Community Health on 19th | 933 19th Street South

Mailing Address:

CH19 403 | 1720 2nd Ave South | Birmingham AL 35294-2041

phone: 205.934.7692 | fax: 205.934.1188

[www.uab.edu/iacuc](http://www.uab.edu/iacuc) | [iacuc@uab.edu](mailto:iacuc@uab.edu)